NANOSCALE CHARACTERIZATION OF FIBER/MATRIX INTERPHASE AND ITS IMPACT ON THE PERFORMANCE OF NATURAL FIBER REINFORCED POLYMER COMPOSITES

A Dissertation

Presented for the

Doctor of Philosophy Degree

The University of Tennessee, Knoxville

Sandeep Sudhakaran Nair

May 2012

Copyright © by Sandeep Sudhakaran Nair

All Rights Reserved

DEDICATION

This dissertation is dedicated to my wife and son, since I couldn't be successful without their support, love, patience and encouragement.

ACKNOWLEDGEMENT

I would like to thank Dr. Siqun Wang for being a great mentor and sharing his vast knowledge with me. I would like to thank him for providing me an important opportunity to work in this project supporting me financially and for the inspiration, advice and guidance in obtaining my degree. I would like to thank Dr. Donna Hurley for having collaborated with me and providing her valuable opinions and advice on my research. She has been a great teacher and working with her has enabled me to understand the finer points of research and become a better scientist. I wish to thank other members in my committee, Dr. David Harper, Dr. Kevin kit, Dr. Timothy Young for the time and their valuable suggestions throughout my course of study, process of researching and writing this dissertation.

I would also like to express my appreciation to the institutions that have supported my work at various stages, particularly Centre for Renewable Carbon, University of Tennessee and National Institute of Standards and Technology at Boulder, Colorado.

I would like to thank Dr. John Dunlap for his valuable assistance in SEM experiments and Lenzing Company for their supply of lyocell fibers. Special thanks to National Research Initiative of the USDA Co-operative State Research, Education and Extension service, USDA Wood Utilization Research Program and The National Science Foundation of China for funding.

Finally, I would like to thank all graduate students, faculty, and staff with whom I have shared my highs and lows of time here at the University of Tennessee.

ABSTRACT

Contact resonance force microscopy (CR-FM) is a valuable technique for evaluating the interphase of natural fiber-reinforced polymer composites and for characterizing the elastic properties of cell wall layers of natural fibers. The nanoscale spatial resolution of CR-FM, combined with its ability to provide quantitative modulus images, makes it possible to investigate the mechanical properties of interphases as narrow as 30 nm in NFRPCs and thin cell wall layers in natural fibers. The nanoscale characterization of interphase and its effects on the bulk mechanical properties in this study shows that an increased interphase thickness is very essential for the improved tensile strength in lyocell/polypropylene (PP)/maleic anhydride grafted polypropylene (MAPP) composites. An optimum amount of MAPP increase the interphase thickness to the maximum of 100 nm and further addition only decreased the interphase thickness and adversely affected the strength properties. The average impact strength was found to decrease with the increasing concentration of MAPP and our results showed that matrix properties were also a determinant factor on the impact strength. After comparing the results obtained from CR-FM, tensile testing, and dynamic mechanical analysis (DMA), it was quite clear that β transition was not a strong indicator of the filler –matrix interaction within these composites. For lyocell/PP/maleic anhydride grafted styrene-ethylene/butylene-styrene (MA-SEBS) composites, tensile strength was not a direct reflection of interfacial bonding. The impact strength was found to increase with addition of MA-SEBS. Interphase region showed gradient of modulus values that ranged between the modulus values of the fiber and the matrix for both lyocell/PP/MAPP and lyocell/PP/MA-SEBS composites. The interphase region showed a gradient in modulus that could be described to first order by a linear fit, with a gradual decrease in modulus from fiber to

matrix. Also, it was quite evident that the interphase thickness accounts for the majority of property variations within the interphase for different treatments. This result defies the earlier perception of a flexible interphase with low modulus than the matrix formed by the elastomers in composites.

TABLE OF CONTENT

CHAPTER 1. INTRODUCTION ……..……..... 1

1.1. Brief Background……..…….……..2

1.2. Research Objectives …….……. …….…..... 3

1.3. Rational and Significance …….……...….….. 4

CHAPTER 2. LITERATURE REVIEW ……...……..…..... 6

2.1. Abstract ……..….. .....….....7

2.2. Introduction……...…….…..…….....7

2.3. Natural Fibers……... ……..……..…..10

2.3.1. Composition and structure …….….……..….....10

2.3.2. Characterization of natural fibers…….13

2.4. Interphase……..….15

2.4.1. Mechanisms at the interphase ……..…….……....…..16

2.4.2 Characterization of interphase …….....….…..... 18

2.4.3. Interphase impact on the macroscale performance of the composites…...…..20

2.5. Conclusions ……. ……..... 22

2.6. References ……...……. 22

CHAPTER 3. CHARACTERIZATION OF NATURAL FIBERS AND THEIR COMPOSITES USING ADVANCED AFM BASED TECHNIQUE …….……...…..... 32

3.1. Abstract ……..…….. 33

3.2. Introduction …….….……... 34

3.3. Experimental …….……..... 38

3.3.1. Material and sample preparation ……..…... 38

3.3.2. Nanoindentation techniques……..……39

3.3.3. CR–FM techniques ……...…...…….…..…. 40

3.4. Results and Discussion ……..……...……..... 43

3.4.1. Evaluation of interphase in fiber reinforced composites ……..……..... 43

3.4.2. Evaluation of mechanical properties of cell wall layers ……..……..... 51

3.5. Conclusion ……..……....….... 57

3.6. References ……...…..... 58

CHAPTER 4. CHARACTERIZATION OF INTERPHASE NANOSCALE PROPERTY VARIATIONS IN MALEATED POLYPROPYLENE TREATED NATURAL FIBER REINFORCED POLYMER COMPOSITES …….…….…..... 64

4.1. Abstract …….…..... . 65

4.2. Introduction ……..... . 66

4.3. Experimental …….……...….. .. 69

4.3.1. Materials and sample preparation …….……... 69

.

4.3.2. Nanoindentation techniques ……...……..…69

4.3.3. CR–FM techniques …….…..……70

4.3.4. AFM–PI techniques …….....…… . 71

4.4. Results and Discussion …….……... ….....72

4.5. Conclusions ……...……..…….……..... 84

4.6. References …..…….….…….…….…....85

CHAPTER 5. EFFECTS OF MAPP AND MA-SEBS MODIFICATIONS ON THE MACROSCALE PERFORMANCE OF NATURAL FIBER REINFORCED POLYMER COMPOSITES……...……..89

5.1. Abstract …….…….……... 90

5.2. Introduction…….……91

5.3. Experimental……...……93

5.3.1. Materials and sample preparation ……..…. 93

5.3.2. Nanoindentation techniques ……... ...….94

5.3.3. CR - FM techniques ……...…….….….…..... ..95

5.3.4. FTIR and multivariate analysis …….……. ... .96

5.3.5. Tensile testing …….…… ...…. 96

5.3.6. Dynamic mechanical analysis (DMA) ……..…….. .....… 97

5.4. Results and Discussion …….....…….…..... …. 97

5.4.1. MAPP …….……....…. 97

5.4.1.1. Interphase characterization ……. .… 97

5.4.1.1.1. CR-FM ……... …... 97

5.4.1.1.2. FTIR…….……103

5.4.1.2. Bulk mechanical properties ……..….. 109

5.4.1.2.1. Tensile and impact properties ……..... 109

.

5.4.1.2.2. Dynamic mechanical response ……... 116

5.4.2. SEBS ……..……...… 119

5.4.2.1. Interphase characterization …….…….… .. 119

5.4.2.1.1. CR-FM …….… …..… ... 119

5.4.2.1.2. FTIR……..……122

5.4.2.2. Mechanical properties …… 125

5.4.2.2.1. Tensile and impact properties …… …125

5.4.2.2.2. Dynamic mechanical response …… …… 129

5.5. Conclusions …… 131

5.6. References …… … 132

CHAPTER 6. CONCLUSIONS AND RECOMMENDATIONS …… 137

6.1. Conclusions …… 138

6.2. Recommendations for Future Work …… 140

APPENDIXES …… 142

Appendix A. Accomplishments from This Work …… 143

A.1. Publications …… 144

A.2. Awards and Recognitions …… 144

A.3. Conference Presentations …… 144

Appendix B. Qualitative Imaging of Natural Fiber Cell Walls Using Advanced AFM Based Techniques……147

B.1. Abstract ……147

B.2. Introduction ……147

B.3. Experimental ……148

B.3.1. Materials and sample preparation……148

B.3.2. AFM-PI……149

B.3.3. SThM……149

B.4. Results and Discussion ……150

B.5. Conclusions……..……..…….……...……...153

B.6. References ……..…….……..….….....153

Appendix C. Score Maps for Different Treatments…….....….……..….155

.

VITA……..……..….160

LIST OF FIGURES

CHAPTER 2

Figure 2.1. Classification of natural fibers ……. ….…...10

Figure 2.2. Schematic representation of cell wall layers……11

Figure 2.3. Structure of cellulose …….....12

Figure 2.4. Schematic representation of interphase between fiber and matrix (Drzal et al., 1983) ……. …….....15

CHAPTER 3

Figure 3.1. Schematic representation of CR-FM ……...…...…….....….....….41

Figure 3.2. Topography (top) and indentation modulus image (bottom) of lyocell/PP composites without treatment ……...…….……...44

Figure 3.3. Topography (top) and indentation modulus image (bottom) of lyocell/PP composites with MAPP treatment ……...…….…...45

Figure 3.4. (a) Analysis of the modulus (top), and line profile image (bottom) showing the size of interphase based on the gradient in modulus…….....47

Figure 3.5. Average modulus across interphase region (between the vertical dotted lines) between the fiber and matrix for (a) lyocell/PP composites without any treatment and (b) with MAPP treatment …….....….... .. 48

.

Figure 3.6. Images of (a) topography and (b) box plot analysis of indentation modulus image of various cell wall layers …… …….……....53

Figure 3.7. (a) Topographical change between S_1 and S_2 and (b) corresponding line profile …….…….…….…... 55

Figure 3.8. (a) Schematics for contact mechanics for Hertzian contact on flat surface (left) and on a steep slope (right)……..56

CHAPTER 4

Figure 4.1. Example of AFM topography image of cellulose fiber reinforced polypropylene composite sample …….…..……..... 72

Figure 4.2. CR-FM images of indentation modulus for cellulose/PP composites with (a) 0%, (b) 2.5%, (c) 5%, and (d) 10% MAPP treatment……..…73

Figure 4.3. Example of radial line profile across the fiber-matrix boundary obtained from a CR-FM modulus map. The modulus profiles showing the fiber (μ_f - $3\sigma_f$) and matrix (μ_m + $3\sigma_m$) regions between the dashed lines and the interphase region between the vertical lines (between the fiber and matrix regions) ……..... 75

Figure 4.4. Average modulus profiles obtained for cellulose/PP composites with (a) 0% with (a) 0% , (b) 2.5% , (c) 5% , and (d) 10% MAPP treatment……..…78

Figure 4.5. Phase images and average phase shift profiles for composite samples with 0% MAPP [(a) and (c)] and 10% MAPP [(b) and (d)] treatment …… .80

Figure 4.6. Interphase outlines as described in the text for cellulose/ PP composites with (a) 0%, (b) 2.5%, (c) 5%, and (d) 10% MAPP treatment …… 83

CHAPTER 5

Figure 5.1. CR-FM modulus maps for each of the composite samples (left) and corresponding line profile (right) with different treatments…….…98

Figure 5.2. First three PCs or factors which contribute for major variations of 0% MAPP composites ……...…105

Figure 5.3. First three PCs or factors which contribute for major variations of 2.5% MAPP composites ……..... 106

Figure 5.4. First three PCs or factors which contribute for major variations of 10% MAPP composites……...… ……..…..107

Figure 5.5. AFM image showing the spacing of the MAPP treated fibers……..……..108

Figure 5.6. Effect of MAPP concentration on the tensile modulus (top) and tensile strength (bottom)…….....….... 110

.

Figure 5.7. Correlation of interphase width with tensile strength …….…….....…. 112

Figure 5.8. SEM images of the fracture surfaces of (top) lyocell/PP composites without MAPP, (middle) 2.5% MAPP, (bottom) 10% MAPP treatment …….…..... 113

Figure 5.9. Effect of MAPP concentration on impact strength ..…….……..115

Figure 5.10. Dependence of storage modulus at different temperature for different MAPP concentration measured at 1 Hz……..……..….....…. 117

Figure 5.11. Temperature depends of damping (tan δ) and the glass transition temperature (T_g) for different MAPP concentration measured at 1 Hz…….. 118

Figure 5.12. CR-FM modulus maps for each of the composite samples (left) and corresponding line profile (right) with different treatments……...120

Figure 5.13. PC or factors which contribute major variations for samples containing 5% SEBS composites……..……..… 123

Figure 5.14. PC or factors which contribute major variations for samples containing 10% SEBS composites…….…….……... 124

Figure 5.15. Effect of different MA-SEBS concentrations on the tensile modulus (top) and tensile strength (bottom)……..……..... .126

Figure 5.16. SEM images of the fracture surfaces of (left) 5% SEBS, (right) 10% SEBS treatment …….. 127

Figure 5.17. SEM images of the matrix fracture surfaces of (left) 5% SEBS, (right) 10% SEBS treatment……..……...….. 128

Figure 5.18. Effect of different MA-SEBS concentrations on the impact strength….…..129

Figure 5.19. Dependence of storage modulus on different concentrations of MA-SEBS measured at 1 Hz…….…….…….…..... 130

Figure 5.20. Temperature depends of damping (tan δ) and the glass transition temperature (T_g) for different MA-SEBS concentration measured at 1 Hz..……..... 130

APPENDIX B

Figure B.1. Phase image of cell wall layers ……...…. 150

Figure B.2. Thermal conductivity image of cell wall layers ……...… 151

Figure B.3. Thermal conductivity image (left) and the line profile (right) of the selected region……..…..……..….152

APPENDIX C

Figure C.1. Score maps for PC1 (top), PC2 (middle), PC3 (bottom) for 0% MAPP

composites……..…….....155

Figure C.2. Score maps for PC1 (top), PC2 (middle), PC3 (bottom) for 2.5% MAPP composites……..……..….....156

Figure C.3. Score maps for PC1 (top), PC2 (middle), PC3 (bottom) for 10% MAPP composites……..…….....157

Figure C.4. Score maps for PC1 (top), PC2 (middle), PC3 (bottom) for 5% SEBS composites……..…….……....158

Figure C.5. Score maps for PC1 (top), PC2 (middle), PC3 (bottom) for 10% SEBS composites……..…….....159

LIST OF TABLES

CHAPTER 4

Table 4.1. Percentage of MAPP treatment and corresponding interphase thickness determined from CR-FM modulus maps for cellulose fiber polypropylene composites……..……...…..75

CHAPTER 5

Table 5.1. Average interphase thickness for each treatment …….…..….. 99

Table 5.2. Average values for the slope and R^2 for each treatment ……..…..….…. 102

Table 5.3. Mean and standard deviation of the mechanical properties of lyocell/PP composites with different MAPP concentration…….…….…... 109

Table 5.4. Temperature depends of damping (tan δ) and the glass transition temperature (T_g) for different MAPP concentration measured at 1 Hz.....…..119

Table 5.5. Average and uncertainty in interphase thickness for each treatment……..…..121

Table 5.6. The average values for the slope and R^2 for each treatment…….....121

Table 5.7. Mean and standard deviation of the mechanical properties of composites with different MA-SEBS concentrations ……..……...…125

Table 5.8. Temperature depends of damping (tan δ) and the glass transition temperature (T_g) for different MA-SEBS concentration measured at 1 Hz…….…….131

APPENDIX B

Table B.1 Average phase shift and thermal conductivity for different cell wall layers…….....…151

CHAPTER 1. INTRODUCTION

1.1 Brief Background

Natural fiber reinforced polymer composites (NFRPC) have attracted great interest, both in industry and academia. The market for NFRPC has the greatest growth potential in automotive and building industries, especially in areas where biocompatibility and environmentally responsible design and construction are required. Compared to other reinforcing fibers such as carbon or glass fibers, natural fibers have various advantages such as low cost, low density for an acceptable specific strength, low energy consumption, high toughness, high sound attenuation, nonabrasiveness, undergo little damage during processing, high degree of flexibility, renewable nature and biodegradability.

The performance of NFRPC as a structural material mainly depends on the quality of stress transfer in the interphase. The interphase formation depends on the property of components in use such as the natural fiber and the polymer matrix and modifications made on the components. Extending over lengths from nanometers to micrometers, a “well engineered” interphase is critical for desirable mechanical properties of fiber-reinforced polymer composites.

In the past two decades, researchers have focused on characterizing various interphases, and its effect on the bulk properties of composites. The interphase widths of less than 100 nm with quantitative mechanical measurements at each position have rarely been reported in literature. The main reason for this is a lack of techniques that can measure the properties with such nanoscale spatial resolution. Although various methods which posses the spatial resolution to characterize narrow interphases in NFRPCs have been developed, they lack the ability to provide quantitative measurements at each position of the interphase. In addition to characterization of the composite interphase, a better understanding of the mechanical properties

of different fiber layers is necessary for the utilization of natural fibers as reinforcements in composites.

1.2. Research Objectives

There were three objectives of the dissertation study: 1) Nanoscale characterization of interphase in NFRPCs and different cell wall layers of natural fiber; 2) Define the effect of various treatments on the interphase of NFRPC; 3) Estimate the correlation between the interfacial properties and the macroscale performance of the whole composite. The dissertation is organized as follows.

In addition to the Introduction Chapter, three key chapters summarize the study results. Chapter 6 is the final chapter of conclusions and recommendations.

Chapter 3 described the use of contact resonance force microscopy (CR-FM) technique for evaluating the interphase of natural fiber-reinforced polymer composites and for characterizing the elastic properties of cell wall layers of natural fibers. This technique, which has previously been used to characterize various micro and nano structures, is used in this dissertation for the first time in the field of natural fibers. Chapter 4 describes property variation within the interphase region as well as the variation in interphase thickness with maleic anhydride grafted polypropylene (MAPP) concentration by quantitative imaging using CR-FM and qualitative images obtained by noncontact AFM phase imaging. Chapter 5 describes the effect of various coupling agents such as MAPP and maleic anhydride grafted styrene-ethylene/butylene-styrene (MA-SEBS) on the NFRPCs and finally correlated the interfacial effects created by these coupling agents on the macroscale performance of the composites.

1.3. Rational and Significance

Extending over lengths from nanometers to micrometers, a well-constructed interphase can significantly improve the composite strength, toughness, and environmental resistance. The performance of fiber reinforced polymer composites as a structural material mainly depends on the quality of stress transfer in the interphase between fiber and polymer in the composite. Therefore, a better understanding of the interphase mechanical properties and other essential characteristics is necessary for the optimum design of fiber reinforced polymer composites. Until now, the limitations in characterizing the mechanical properties within the interphase have been a major drawback, primarily due to the lack of appropriate techniques and the experimental difficulties for the accurate property measurement with nanoscale spatial resolution.

Also, growing environmental awareness, stringent legistalative measures for greener technologies for promoting the preservation and protection of the quality of environment, depleting resources have always stressed the need for bio-based composites. NFRPCs have a great potential for dramatic growth in coming years especially in automotive and building industries. The knowledge of interphase and mechanical properties within the interphase is very essential for the optimum use of NFRPC in various structural applications. Prior to this dissertation, researchers have not been able to measure the exact thickness and the mechanical properties of interphase in NFRPC which is a major drawback. The purpose of this dissertation was to characterize the interphase thickness and measure the mechanical properties of the interphase for first time using different advanced atomic force microscopic techniques in cellulose fiber-reinforced polypropylene composites also determining the mechanical properties of different cell wall layers of natural fibers. The influence of different treatments on interphase were analyzed and correlated to the bulk properties of composites. The results from this

research will enable scientists to get much more information about the nanoscale properties of the interphase and fibers. This work provides an interesting direction for future research, which is very important for optimum design of final NFRPC products.

CHAPTER 2. LITERATURE REVIEW

2.1. Abstract

Natural fiber-reinforce polymer composites (NFRPCs) represent one of the fastest growing industries. While manmade fibers can be produced with a definite range of properties, the efficiency of natural fibers as reinforcements in composites depends on inherent factors such as structure, degree of crystallinity, polymerization, and orientation of cellulose chains. The structural integrity of a composite mainly depends on the quality of stress transfer in the interphase region between the reinforcing fiber and the bulk polymer. The major disadvantage of NFRPCs is the incompatibility between the hydrophilic natural fiber and the hydrophobic polymer, which can be improved only by either physical or chemical modification of the fiber or polymer. This chapter reviews natural fibers, their composition and structure, various researches done to characterize natural fibers, modifications of fiber/matrix interphase, and the various efforts to characterize these interphases in NFRPCs. The interphase and its impact on the macroscale performance of the composites were also discussed here.

Keywords: Natural fiber, microfibrils, interphase, atomic force microscopy, mechanical property

2.2. Introduction

Natural fibers have various advantages like low cost, sustainable, high toughness, low density for an acceptable specific strength, reduced machine wear, reduced dermal and respiratory irritation, high degree of flexibility, acoustic insulation, and biodegradability, compared to conventional reinforcing fibers like glass, aramid and carbon fibers (Bledzki et al., 2005; Franco and Gonzalez, 2003; Lee and Wang, 2006; Mathew and Joseph, 2003). Natural fiber reinforced polymer composites are more recyclable compared with glass or carbon fiber-

reinforced ones (Karnani et al., 1997; Mohanty et al., 2000; Terenzi et al., 2007). Growing environmental awareness has also increased the use of natural fibers as reinforcing agents which are more compatible with the environment with respect to disposability (George et al., 2001; Mohanty et al., 2001). Combination of all these results has prompted a number of industrial sectors, especially the automotive industry, to consider natural fibers as substitute to conventional fibers in various products. While conventional fibers can be produced with a definite range of properties, the efficiency of natural fibers as reinforcements in composites depends on inherent factors such as structure, degree of crystallinity, polymerization, and orientation of cellulose chains. However, the major disadvantage of NFRPCs is the incompatibility between the hydrophilic natural fiber and the hydrophobic polymer leading to formation of narrow and weak interphase. This could also lead to the non-uniform dispersion of fibers within the matrix (Pickering et al., 2003; Tingaut et al., 2008; Valadez-Gonzalez et al., 1999). Also the processing temperatures of NFRPC are restricted to low temperatures due to the degradability of natural fibers at higher temperatures. The hydrophilic nature of natural fibers leads to high moisture uptake which can lead to low mechanical properties of the composites (Cantero et al., 2003; Paunikallio et al., 2004).

The interphase region between the reinforcing fiber and the bulk polymer matrix plays an important role in the performance of fiber-reinforced polymer composites. The structural integrity of a composite mainly depends on the quality of stress transfer in the interphase. Interphase by definition, starts from some point on the fiber where the local properties as a result of various surface treatments or reaction with the matrix, begins to change from the bulk fiber properties and extends till the local properties again equal to the bulk matrix properties (Terenzi et al., 2007). The response of this region to various forces acting on the composites affects the

mode of failure between the fiber and the matrix. Therefore it is very important to determine the size and properties of interphase of various natural fiber reinforced composites and its effect on the bulk mechanical properties of the composites. Interphases formed in NFRPC are relatively weak compared to conventional composites made of glass, carbon or aramid due to the inherent polar and non polar nature of fiber and polymer respectively. This can be improved only by either physical or chemical modification of the fiber or polymer. Various surface modifications have been developed in order to improve the compatibility of wood-polymer composites i.e., the natural fibers made less hydrophilic and more miscible with the oleophilic matrices. Esterifications and the silanations are the most common modifications used in NFRPC. Treatment with maleic-anhydride modified polyolefin (Borja et al., 2006; Ganster et al., 2006; Paunikallio et al., 2003; Paunikallio et al., 2004), silane based chemicals (Franco and Gonzalez, 2005; Kokta et al., 1990; Maldas et al., 1989; Valadez-Gonzalez et al.,1999), Isocyanate compounds (Lee and Wang, 2006; Maldas et al., 1989), alkaline solution (Franco and Valadez-Gonzalez , 2005; Valadez-Gonzalez et al.,1999) are most frequently used for modification.

This chapter reviews natural fibers, their composition and structure, various researches done to characterize natural fibers, modifications of fiber/matrix interphase, and the various efforts to characterize these interphases in NFRPCs. The interphase and its impact on the macroscale performance of the composites were also discussed here.

2.3. Natural Fibers

2.3.1. Composition and structure

The natural fibers can be broadly classified into those of plant, and animal origin. Natural fibers from plant origin mainly contain cellulose, which includes bast fibers, leaf fibers, seed, fruit, straw, grass and wood fibers. Natural fibers from animal origin contain protein. Examples of animal based natural fiber include wool and silk fibers (Mohanty et al., 2005). Figure 2.1 shows broad classification of natural fibers

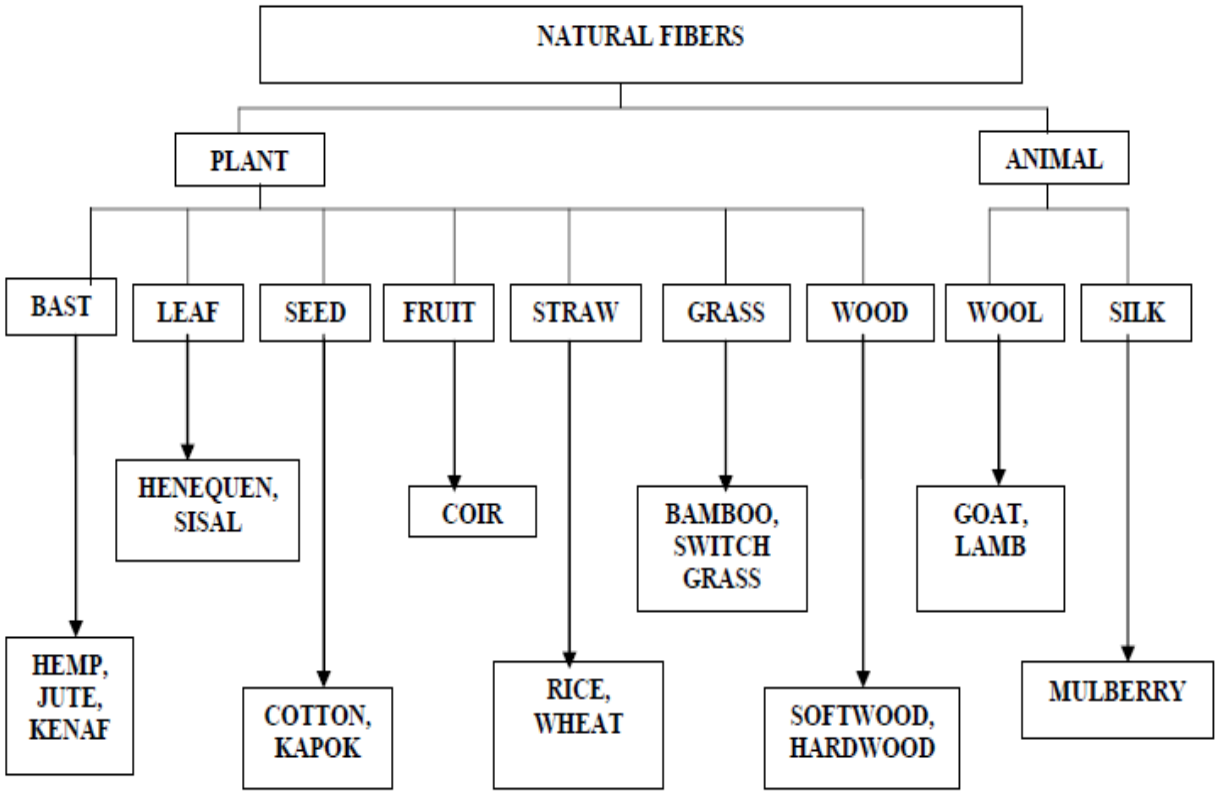

Figure 2.1. Classification of natural fibers

Plant fiber consists of different layers (Figure 2.2). Outermost layer is the primary wall, which is bound to the middle lamellae. Primary cell walls of adjoining fibers, together with the middle lamellae in between, form the compound middle lamellae (CML). The secondary wall has three layers such as *S1*, *S2* and *S3*. The cell walls are formed from oriented semicrystalline cellulose microfibrils embedded in hemicelluloses/lignin matrix. The orientation of the cellulose microfibrils is nearly perpendicular or a flat helix with respect to the fiber axis in the *S1* and *S3* layers, while it is almost parallel or a steep helix to the fiber axis in the *S2* layer (Brandstrom, 2001; Donaldson and Xu, 2005).

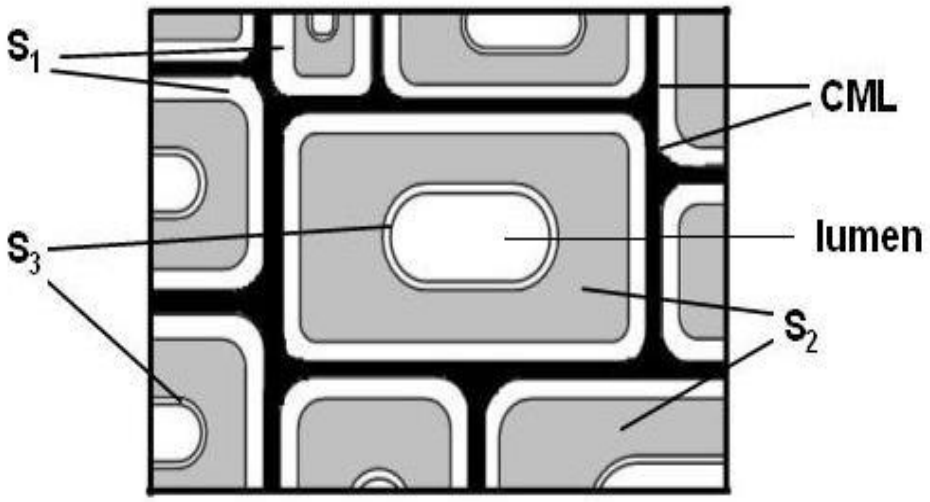

Figure 2.2. Schematic representation of cell wall layers

The primary components, which establish the chemical and physical nature of the cell wall and constitute the bulk of material of the wood cell wall, include cellulose (40-50%), hemicellulose (20-35%) and lignin (15-35%). Cellulose is a linear organic macromolecule consisting of several hundred to over ten thousand β(1-4) linked D-anhydroglucose units. Figure 2.3 shows the structure of cellulose. Each repeating units have hydroxyl groups which has the ability to form hydrogen bonding between cellulose molecules. The hydrogen bonding plays a major role in forming the crystalline structure of cellulose in plant cell wall (Fengel and Wegener, 1984).

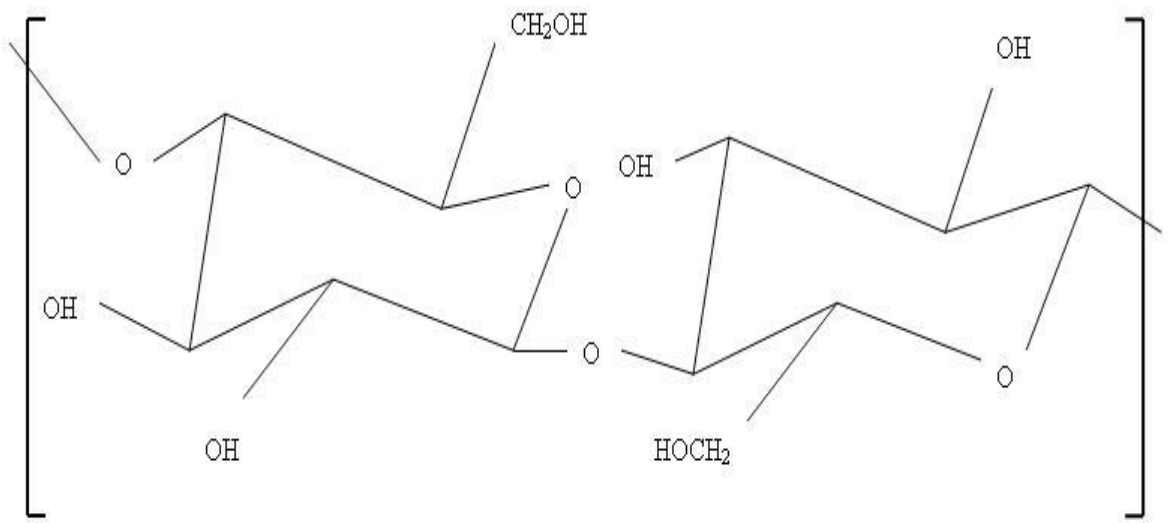

Figure 2.3. Structure of cellulose

According to “fringe micellar model”, the crystalline regions in cellulose molecules, which, without any distinctive boundary, change into disordered or amorphous regions (Astbury, 1933). Hemicellulose forms the supportive matrix for cellulose microfibrils. Hemicelluloses are composed of shorter chains, contain pendants groups, branched and are therefore noncrystalline in nature. Lignin gives rigidity to plants. They are polymers based on phenyl propane units. Exact chemical nature of lignin still remains unclear, but most of the functional groups and building units have been identified through isolated lignin preparations (Mohanty et al., 2005).

2.3.2. Characterization of natural fibers

It is critical to understand the mechanical properties of natural fiber to use it as reinforcement in composite materials. The knowledge of different cell wall layers of natural fibers is very critical to isolate single cellulose fibrils without degradation and use it in composites (Zhang et al., 2010). A better understanding of the mechanical properties such as hardness, yield stress and strength of different fiber layers is necessary to improve the use of natural fibers as reinforcements in composites. The arrangement of polymers such as cellulose, hemicelluloses and lignin influence the stiffness of the cell wall layers. Properties of cell wall were investigated using theoretically analyzed cell wall models (Bergander and Salmen, 2002; Watanabe and Norimoto, 2000; Yamamoto and Kojima, 2002). Cellulose was found to dominate the properties in the longitudinal direction of cell wall layers, while the properties of hemicelluloses was more pronounced in the transverse direction. Orientation of the cellulose microfibrils within each cell wall layer have great influence on the mechanical properties of natural fibers particularly in the longitudinal direction (Bergander and Salmen, 2002). Several researchers have shown (Tze et al., 2007; Watanabe and Norimoto, 2000) that the longitudinal

modulus of the *S2* layer decreased as the microfibril angle with respect to the fiber axis increased. Nanoindentation has been used to investigate the mechanical properties of *S2* layer in annual rings (Tze et al., 2007), lignifications (Gindl et al., 2002), melamine modified wood (Gindl and Gupta, 2002), and early or late wood (Wimmer et al., 1997). The elastic modulus values and hardness for the *S2* layer varied between 12-22 GPa and 0.2-0.55 GPa respectively from these experiments. Nanoindentation was found to less effective in characterizing mechanical properties of other layers due to the limits of its spatial resolution. Wimmer and Lucas (1997) conducted nano-indentation on the *S2* layer and CML and obtained an average value of 16 GPa for the longitudinal modulus of the S2 layer, double the value for the CML. Their indentation test on the CML was confined to the cell corner middle lamellae due to the narrowness of the CML layer. Clair et al. (2003) used advanced AFM method to obtain qualitative images of elastic contrast and quantitative values for middle lamellae, *S1* and *S3* layers for holm oak and boco wood specimens. Zhang et al. (2010) investigated the strength and fracture behavior of wood cell wall S2 layer through a uniaxial micro-compression test and obtained the value of 125 MPa for the compression strength of loblolly pine. Attempts to characterize fiber layers such as S1 and S3 with various microscopic methods such as scanning electron microscopy (SEM) (Abe and Funada, 2005), AFM have yielded only qualitative results (Fahlen and Salmen, 2002; Fahlen and Salmen, 2003). Most recently Nair et al., (2010) used CR-FM for the first time to evaluate the mechanical properties of the cell wall layers of natural fibers. Using this technique, the average values of indentation modulus obtained for different cell wall layers within a fiber were 22.5–28.0 GPa, 17.9–20.2 GPa, and 15.0–15.5 GPa for the *S2* and *S1* layers and the compound middle lamellae, respectively. This technique provided an image of the spatial distribution of quantitative modulus values within each layers in contrast to many

other AFM methods (Clair et al., 2002) which gives quantitative values only at certain points in each layer.

2.4. Interphase

By definition, Interphase starts from some point on the fiber were the physical, chemical, and mechanical properties begin to change from the bulk fiber as a result of various surface treatments or reaction with the matrix and extend until the properties equal to the bulk matrix properties. Therefore, interphase depends on the physical and chemical properties of constituents such as fiber and matrix as well as various treatments done on them. Figure 2.4 shows the schematic diagram of the fiber/matrix interphase. Extending over lengths from nanometers to micrometers, a ‘‘well engineered” interphase is essential for desirable mechanical properties of fiber-reinforced polymer composites (Mohanty et al., 2001). The structural integrity of a composite mainly depends on the quality of stress transfer in the interphase.

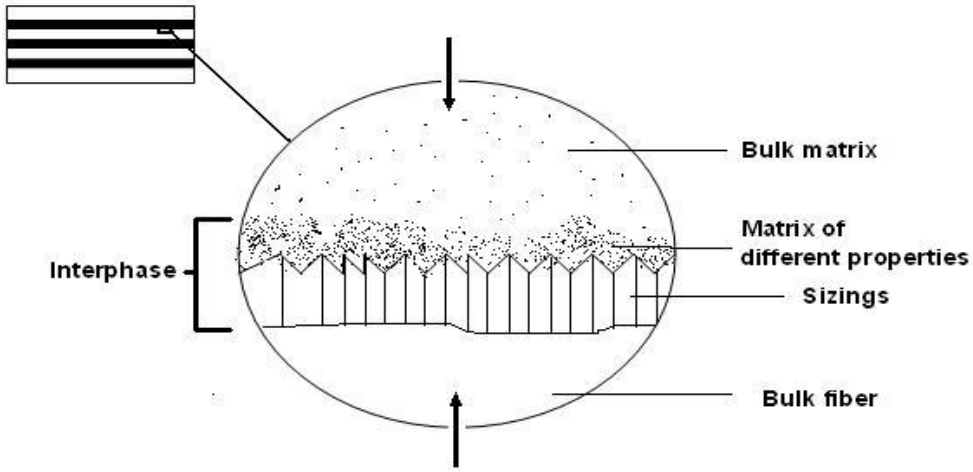

Figure 2.4. Schematic representation of interphase between fiber and matrix (Drzal et al., 1983)

2.4.1. Mechanisms at the interphase

The nature of adhesion between the fiber and matrix is not only dependent on the atomic and molecular arrangement of the fiber and matrix, but also on the morphological properties of fiber and diffusivity of elements in each constituent. Therefore, the interphase is unique to each fiber-matrix system (Kim and Mai, 1991). Cellulose, the most abundant component in the natural fibers has large number of hydroxyl group which gives natural fiber hydrophilic properties when used to reinforce hydrophobic polymer matrices. Hemicellulose has an open structure containing many hydroxyl and acetyl groups. This makes it partly soluble in water and hygroscopic in nature. Lignin which is the polymers of phenylpropane units has the least water sorption in natural fiber components. Cellulose (40-50%), hemicellulose (20-35%) contributes the bulk properties of natural fibers. So this contributes to the very weak and least resistant interphase in natural fiber reinforced polymer composites. This weak interphase reduces the potential of natural fibers as reinforcing agents (Li et al., 2007). These reinforcing fibers can be modified by physical and chemical methods for a better interphase or better adhesion between fiber and matrix.

Physical methods like surface fibrillation, and electric discharge (Belgacem et al., 1994; Wakida and Tokino, 1996) can change the structural and surface properties of fiber and thereby helps in the mechanical bonding with the matrix. Various processes such as low temperature plasma improves the surface characteristics of fibers using electrons, ions, radical and excited molecules produced bye electric discharge causing chemical implantation, polymerization, free radical formation, crystallization while process like sputter etching brings physical changes on the fibers like surface roughness which leads better interaction with the matrix (Wakida and Tokino, 1996). Corona treatment can cause surface oxidation activation which changes the

surface energy of the cellulosic fibers affecting the melt viscosity of the composites (Belgacem et al., 1994).

Chemical modifications of natural fibers or polymer matrix aimed at improving the adhesion between the fiber and matrix were investigated by a number of researchers. Coupling agents are substances that are used in small quantities to treat the fiber and matrix, so that bonding occurs between them. They act as bridges that link fibers and matrix by one or more of the following processes such as covalent bonding, polymer chain entanglement, and strong secondary interactions such as hydrogen bonding (Lu et al., 2000). The most important coupling agents are maleated coupling agents, silane coupling agents, and isocynate compounds.

MAPP coupling agent creates a better adhesion between the matrix and the fiber and improves the interfacial bond, which facilitates a much higher stress transfer from the matrix to the fiber and improves final mechanical properties in the resultant composites. The anhydride group of MAPP forms covalent bonding through esterification process and hydrogen bonding with cellulose fibers while the PP in MAPP due to the similarity to the bulk PP permits the segmental crystallization and, thus the cohesive coupling between them through entanglement of their macromolecular chains (Borja et al., 2006; Ganster et al., 2006; Paunikallio et al., 2003; Paunikallio et al., 2004). The bifunctional silane molecules act as a link between the resin and the cellulose by forming a chemical bond through a siloxane bridge while its organofunctional group bonds to the polymer resin. So this reactivity on both fiber and matrix forms covalent bonds which help promote adhesion and therefore mechanical properties (Franco and Gonzalez, 2005; Kokta et al., 1990; Maldas et al., 1989; Valadez-Gonzalez et al., 1999). Isocynates, especially poly(methylene) poly(phenyl) isocynate (PMPPIC) is chemically linked to the cellulose molecules by strong covalent bonds. The urethane group results from the reaction

between isocynate and hydroxyl compound (Lee and Wang, 2006; Maldas et al., 1989). Other major chemical treatments include alkaline treatment (Franco and Gonzalez, 2005; Valadez-Gonzalez et al., 1999), acetylation (Mwaikambo and Ansell, 1999), benzoylation (Nair et al., 2001), and peroxide treatment (Paul et al., 1997).

2.4.2. Characterization of interphase

Although various researchers have focused on the effect of interphase on the bulk properties of composites, very little research has been done to characterize and provide quantitative measurements in the interphase. Interphase widths of less than 100 nm with quantitative mechanical measurements at each position have rarely been reported in literature. The main reason for this is the lack of techniques that can measure the properties with such nanoscale spatial resolution (Nair et al., 2010).

Previous NFRPC research on interphase characterization has consisted mostly of examining the fracture surfaces of broken composite samples with scanning electron microscopy (SEM). Because these studies examined the interaction between the fibers and the matrix based on the nature of fracture surface, the results only gave an indirect inference of interphase (Felix and Gatenholm, 1991; Oksman and Clemons, 1997). Several other techniques such as single fiber pull out tests (Stamboulis et al., 1999), single fiber fragmentation test (Joffe et al., 2003; Torres and Cubillas, 2005) were also used to determine the average interfacial shear strength at the interface.

With the advent of scanning probe microscopy (AFM), nanoindentation, and nanoscratching which has the ability to probe materials in the nanoscale, more research has been focused on interphase. Lee et al. (2007) investigated the interphase properties of a natural fiber-

reinforced polypropylene composite by nanoindentation and finite element analysis and showed that the interphase width was less than 1 μm. Lee et al. (2009) investigated the interfacial zone of a lyocell/polypropylene composite modified by maleated polypropylene (MAPP) using atomic force microscopy phase imaging (AFM-PI) and the results indicated that the interphase transition zone ranged from approximately 113 nm to 128 nm. Since measurements involving SPM involves complex geometric considerations, it has been proved very difficult to obtain quantitative data on areas of different mechanical properties (Munz et al., 1998). Spectroscopic techniques such as XPS, NMR (Pickering et al., 2003) for characterization of various elements on the fiber or polymer surface, or FTIR (Harper and Wolcott, 2006; Tingaut et al., 2008; Valadez-Gonzalez et al., 1999) for looking on to various bonds have also been shown to be successful in interphase characterization.

Nanoindentation and AFM have been widely used to determine the property gradient such as the reduced elastic modulus within the interphase. It has been used in the epoxy/fiber glass system (Kumar et al., 2004), epoxy/aluminum joints (Li et al., 2002) to determine the fiber bias effect on the interphase, both nanoindentation and AFM-PI has been used (Downing et al., 2000; Griswold et al., 2005) to determine the interphase in epoxy/glass system. Interphase thickness was found to increase with the increasing silane concentration (Griswold et al., 2005). AFM phase imaging on the samples indicted a softer interphase than the bulk polymer matrix (Downing et al., 2000). Williams et al. (2005) showed that polishing the sample surface often resulted in formation of ridges and troughs near the interphase which resulted in artifacts which can be misinterpreted as softer interphase. Hodzic et al. (2000) conducted nanoindentation and nanoscratching on polymer/glass composite systems and determined the interphase thickness. Recently Nair et al (Nair et al., 2010) used contact resonance force microscopy (CR-FM), an

extended form of AFM for evaluating the interphase of natural fiber-reinforced polymer composites. The nanoscale spatial resolution of CR-FM, combined with its ability to provide quantitative modulus images, made it possible to investigate the mechanical properties of interphases as narrow as 50 nm.

2.4.3. Interphase impact on the macroscale performance of the composites

Fiber modification and usage of various coupling agents creates a better adhesion between the matrix and the fiber and improves the interfacial bond, which facilitates a much higher stress transfer from the matrix to the fiber and improves final mechanical properties in the resultant composites. With no coupling agent or modification, the bond between the fiber and matrix will be poor which will lead inferior mechanical properties. Use of maleated polypropylene as a modifier in NFRPC (Felix and Gatenholm, 1991; Ganster et al., 2008; Oksman and Clemons, 1997; Sanchez et al., 2008) has proved to have a substantial effect on the final composite mechanical properties. Tensile strength (Felix and Gatenholm, 1991; Oksman and Clemons, 1997) and elongation (Karnani et al., 1997; Paunikallio et al., 2004) had a positive impact by these modifications, in some researches the elongation showed negative impact too (Oksman and Clemons, 1997). Silane coupling agents (Franco and Gonzalez, 2005; Kokta et al., 1990; Maldas et al., 1989; Valadez-Gonzalez et al., 1999) have been widely used in NFRPC to improve the adhesion between the fiber and polymer. The most favored mechanical property was the strength (Franco and Gonzalez, 2005; Kokta et al., 1990; Maldas et al., 1989; Valadez-Gonzalez et al., 1999), while some works have shown positive impacts on elongation (Karnani et al., 1997), modulus and impact strength (Coutinha et al., 1997; Karnani et al., 1997) too. Some researchers have shown the use of impact modifiers such as ethylene/propylene/diene terpolymer

and styrene-ethylene/butylenes-styrene triblock copolymer (Oksman and Clemons, 1997; Wu et al., 1999) to improve adhesion between the fiber and matrix and their results have shown that these modifiers create a ductile interphase which helps in improving the impact strength property of the final composite. Several researches have been done on the interphase effect on the creep behavior of polymer composites. The increased adhesion between the fiber and matrix by the use of compatibilizer substantially reduced the creep formation (Acha et al., 2007; Romero-Balderrama et al., 2008). However, the presence of softer interphase was found to reduce the creep strength (Li and Weng, 1995).

Dynamic mechanical analysis (DMA) is an important tool which helps in the determination of viscoelastic behavior of the polymers and the influence of the interfacial agent on the final composite properties. Several researchers have used DMA to determine the influence of MAPP (Azizi and Ghasemi, 2009; Harper et al., 2004; Harper et al., 2009; Hristov et al., 2003; Nunez et al., 2002) and silane coupling agents (Jacob et al., 2006) on the composite properties. Better adhesion between the fiber and matrix was shown by an increase in complex viscosity (Azizi and Ghasemi, 2009), increase in storage modulus at low temperatures (Azizi and Ghasemi, 2009; Hristov et al., 2003; Jacob et al., 2006; Nunez et al., 2002), increase in loss modulus (Azizi and Ghasemi, 2009; Jacob et al., 2006), decrease in damping factor (Hristov et al., 2003; Jacob et al., 2006), and decrease in glass transition temperature (Jacob et al., 2006).

Researchers have shown that, a “well engineered” interphase is very important for desirable mechanical properties of fiber-reinforced polymer composites (Mohanty et al., 2001). An interphase which has lower modulus than the surrounding polymer results in low composite stiffness and strength, but greater resistance to fracture (Drzal, 1986; Williams et al., 1990). On the other hand, an interphase with higher modulus than the surrounding polymer results in lower

fracture resistance but greater strength (Drzal, 1983). Ciprari et al. (2006) investigated the interphase of alumina and magnetite nanoparticles embedded in polymethyl methacrylate and polystyrene samples with the help of thermal gravimetric analysis (TGA), and transmission electron microscopy (TEM) and showed the formation of a low density interphase which resulted in compliant composites.

2.5. Conclusions

The major disadvantage of NFRPCs is the incompatibility between the hydrophilic natural fiber and the hydrophobic polymer leading to formation of narrow and weak interphase. Although various researchers have focused on the effect of interphase on the bulk properties of composites, very little research has been done to characterize and provide quantitative measurements in the interphase. The main reason for this is the lack of techniques that can measure the properties with such nanoscale spatial resolution. Interphase widths of less than 100 nm with quantitative mechanical measurements at each position have rarely been reported in literature. In addition to characterization of interphase, a better understanding of the mechanical properties such as hardness, yield stress and strength of different fiber layers is necessary to improve the use of natural fibers as reinforcements in composites. Due to the limits of its spatial resolution, most of the studies have been confined to the S_2 layer.

2.6. References

Abe H, Funada R. Review–The orientation of cellulose microfibrils in the cell walls of tracheids in conifers. A model based on observations by field emission-scanning electron microscopy. IAWA journal 2005;26(2):161-174.

Acha BA, Reboredo MM, Marcovich NE. Creep and dynamic mechanical behavior of PP-jute composites: Effect of the interfacial adhesion. Composites Part A; applied science and manufacturing 2007;38:1507-1516.

Astbury WT. Some problems in the X-ray analysis of the structure of animal hairs and other protein fibers. Trans Faraday Soc 1933;29:193.

Azizi H, Ghasemi I. Investigation on the dynamic melt rheological properties of polypropylene/wood flour composites. Polymer Composites 2009;30:429-435

Belgacem MN, Bataille P, Sapieha S. Effect of corona modification on the mechanical properties of polypropylene cellulose composites. J Appl Polym Sci 1994;53:379-385.

Bergander A, Salmen L. Cell wall properties and their effects on the mechanical properties of fibers. Journal of Materials Science 2002;37:151-156.

Bledzki AK, Letman M, Viksne A, Rence L. A comparison of compounding processes and wood type for wood fibre-PP composites. Compos Part A: Appl Sci Manfact 2005;36(6):789-797.

Borja Y, Rie G, Lederer K. Synthesis and characterizations of polypropylene reinforced with cellulose 1 and 11 Fibers. J Appl Polym Sci 2006;101:364-369.

Brandstrom J. Micro- and ultrastructural aspects of Norway spruce tracheids: A review. IAWA 2001;22(4):333-353

Cantero G, Arbelaiz A, Liano-ponte R, Mondragon I. Effects of fibre treatment on wettability and mechanical behavior of flax/polypropylene composites. Composites Science and Technology 2003;63:1247-54.

Ciprari D, Jacob K, Tannenbaum R. Characterization of polymer nanocomposite interphase and its impact on mechanical properties. Macromolecules 2006;39:6565-6573

Clair B, Arinero R, Lévesque G, Ramonda M, Thibaut. Imaging the mechanical properties of wood cell wall layers by atomic force modulation microscopy. IAWA 2003;24(3):223–30.

Coutinha FMB, Costa THS, Carvalho DL. Polypropylene-wood fiber composites: effect of treatment and mixing conditions on mechanical properties. J Appl Polym Sci 1997;65:1227-1235.

Donaldson L, Xu P. Microfibril orientation across the secondary cell wall of radiate pine tracheids. Trees 2005;19:644-653.

Downing TD, Kumar R, Cross WM, Kjerengtroen L, Kellar JJ. Determining the interphase thickness and properties in polymer matrix composites using phase imaging atomic force microscopy and nanoindentation. J Adhesion Sci Technol 2000;14(14):1801-1812.

Drzal LT. The interphase in epoxy composites. Adv Polym Sci 1986;75:1-32.

Drzal LT, Rich MJ, Koenig MF, Lloyd PF. Adhesion of graphite fibers to epoxy matrices. Part 1. The role of fiber surface treatment. J Adhes 1983;16:1–30.

Drzal LT, Rich MJ, Koenig MF, Lloyd PF. Adhesion of graphite fibers to epoxy matrices. 2. The effect of fiber finish. J Adhesion 1983;16(2):133-152.

Fahlen J, Salmen L. On the lamellar structure of the tracheid wall. Plant Biol 2002;4:339–45.

Fahlen J, Salmen L. Cross-sectional structure of the secondary wall of wood fibers as affected by processing. J Mater Sci 2003;38:119–26.

Felix JM, Gatenholm P. The nature of adhesion in composites of modified cellulose fibers and polypropylene. J Appl Polym Sci 1991;42:609-620.

Fengel D, and Wegener G. 1984. Wood Chemistry, Ultrastructure, Reaction. Walter de Gruyter, Berlin, New York. ISBN 3-11-008481-3. P.234-238.

Franco PJH, Valadez - Gonzalez A. Mechanical properties of continuous natural fibre-reinforced polymer composites. Compos Part A: Appl Sci Manfact 2003;35:339-345.

Franco PJH, Gonzalez AV. A study of the mechanical properties of short natural fiber reinforced composites. Compos Part B: Eng 2005;36:597-608.

Ganster J, Fink HP. Novel cellulose fiber reinforced thermoplastic materials. Cellulose 2006;13:271-280.

Ganster J, Fink HP, Uihlein K, Zimmerer B. Cellulose man-made fibre reinforced polypropylene-correlations between fibre and composite properties. Cellulose 2008;15:561-569.

George J, Sreekala MS, Thomas S. A review on interface modifications and characterization of natural fiber reinforced plastic composites. Polymer Engineering and Science 2001; 41: 1471-1485.

Gindl W, Gupta HS, Grunwals C. Lignification of spruce tracheid secondary cell walls related to longitudinal hardness and modulus of elasticity using nano-indentation. Can J Bot 2002;80:1029-1033.

Gindl W, Gupta HS. Cell- wall hardness and young's modulus of melamine-modified spruce wood by nano-indentation. Compos Part A: Appl Sci Manfact 2002;33:1141-1145.

Griswold C, Cross WM, Kjerengtroen L, Kellar JJ. Interphase variation in silane- treated glass-fiber reinforced epoxy composites. J Adhesion Sci Technol 2005;19(3-5):279-290.

Harper DP, Laborie MP, Wolcott MP. Molecular relaxations in wood-polypropylene Composites. 32nd Annual Conference on Thermal Analysis and Applications, Williamsburg, VA, 2004.

Harper DP, Wolcott MP. Chemical imaging of wood-poly propylene composites. Applied

Spectroscopy 2006;60(8):898-905.

Harper DP, Pierre M, Laborie G, Wolcott MP. The impact of polypropylene –graft- maleic anhydride on the crystallization and dynamic mechanical properties of isotactic polypropylene. J Appl Polym Sci 2009;111:753-58.

Hodzic A, Stachurski ZH, Kim JK. Nano-indentation of polymer-glass interfaces. Part I. Experimental and mechanical analysis. Polymer 2000;41:6895-6905.

Hristov V, Vasileva S. Dynamic mechanical and thermal properties of modified poly(propylene) wood fiber composites. Macromolecular Materials and engineering 2003;288:798-806.

Jacob M, Francis B, Varughese KT, Thomas S. The effect of silane coupling agents on the viscoelastic properties of rubber biocomposites. Macromolecular Materials and engineering 2006;291:1119-1126.

Joffe R, Andersons J, Wallstrom L. Strength and adhesion characteristics of elementary flax fibers with different surface treatments. Compos Part A: Appl Sci Manfact 2003;34:603-612.

Karnani R, Krishnan M, Narayan R. Biofiber-reinforced polypropylene composites. Polymer Engineering and Science 1997;37(2): 476–483.

Kokta BV, Maldas D, Daneault C, Beland P. Composites of polyvinyl chloride-wood fibers. Part 111: Effect of silane as coupling agent. Journal of Vinyl Technology 1990;12:146-153.

Kim JK, Mai YW. High strength high fracture toughness fiber composites with interface control-a review. Composites Science and Technology 1991;41:333-378.

Kumar R, Cross WM, kjerengtroen L, Kellar JJ. Fiber bias in nanoindentation of polymer matrix composites. Composite Interfaces 2004;11(5-6):431-440.

Lee SH, Wang S. Biodegradable polymers/bamboo fiber biocomposite with bio-based coupling

agent. Compos Part A: Appl Sci Manfact 2006; 37(1): 80-91.

Lee SH, Wang S, Pharr GM, Xu H. Evaluation of interphase in a cellulose fiber-reinforced polypropylene composite by nanoindentation and finite element analysis. Compos Part A: Appl Sci Manfact 2007;38:1517-1524.

Lee SH, Wang S, Takashi E, Kim NH. Visualization of interfacial zones in lyocell fiber-reinforced polypropylene composite by AFM contrast imaging based on phase and thermal conductivity measurements. Holzforschung 2009;63:240-247.

Li J, Weng GJ. Effect of a viscoelastic interphase on the creep and stress/strain behaviour of fiber- reinforced polymer matrix composites. Composites Part B 1996;27B:589-598.

Li F, Williams JG, Altan BS, Miskioglu I, Whipple RL. Studies of interphase in epoxy aluminum joints using nano-indentation and atomic force microscopy. J Adhesion Sci Techol 2002;16(7):935-949.

Li X, Tabil LG, Panigrahi S. Chemical treatments of natural fiber for use in natural fiber-reinforced composites: A review. J Polym Environ 2007;15:25-33.

Liao B, Huang Y, Cong G. Influence of modified wood fibers on the mechanical properties of wood fiber-reinforced polyethylene. J Appl Polym Sci 1997;66:1561-1568.

Lu JZ, Wu Q, McNabb HS. Chemical coupling in wood fiber and polymer composites. Wood Fiber and Science 2000;32:88-104.

Maldas D, Kokta BV, Daneault C. Influence of coupling agents and treatments on the mechanical properties of cellulose fiber-polystyrene composites. J Appl Polym Sci 1989;37:751-775.

Mathew L, Joseph R. Mechanical properties of short-isora-fiber-reinforced natural rubber composites: effects of fiber length, orientation, and loading, alkali treatment, and bonding

agent. J Appl Polym Sci 2007;1640-1650.

Mohanty AK, Misra M, Hinrichsen G. Biofibers, biodegradable polymers and biocomposites: an overview. Macromol. Mater. Eng 2000;276/277:1-24.

Mohanty AK, Misra M, Drza, LT. Surface modification of natural fibers and performance of the resulting biocomposites: An overview. Composites Interfaces 2001;8: 313-343.

Mohanty AK, Misra M, Drzal LT. 2005. Natural fibers, biopolymers, and biocomposites. CRC Press, Boca Raton, F.L.

Munz M, Sturm H, Schulz E, Hinrichsen G. The scanning force microscope as a tool for the detection of local mechanical properties within the interphase of fiber reinforced polymers. Compos Part A1998;29:1251-1259.

Mwaikambo LY, Ansell MP. The effect of chemical treatment on the properties of hemp, sisal, jute and kapok for composite reinforcement. Angew Makromol. Chem 1999;272:108-116.

Nair KCM, Thomas S, Groeninckx G. Thermal and dynamic mechanical analysis of polystyrene composites reinforced with short sisial fibers. Composites Science and Technology 2001;61:2519-2529.

Nair SS, Wang S, Hurley DC. Nanoscale characterization of natural fibers and their composites using contact-resonance force microscopy. Compos Part A:Appl Sci Manfact 2010; 41: 624-631.

Nunez AJ, Kenny JM, Reboredo MM, Aranguren MI, Marcovich NE. Thermal and dynamic mechanical characterization of polypropylene-wood flour composites. Polymer Engineering and Science 2002;42(4):733-742.

Oksman K, Clemons C. Mechanical properties and morphology of impact modified

polypropylene-wood flour composites. J Appl Polym Sci 1997;67:1503-1513.

Paul A, Joseph K, Thomas S. Effect of surface treatments on the electrical properties of low density polyethylene composites reinforced with short sisal fibers. Composites science and Technology 1997;57:67-69.

Paunikallio T, Kasanen, Suvanto M, Pakkanen TT. Influence of maleated polypropylene on mechanical properties of composite made of viscose fiber and polypropylene. J Appl Polym Sci 2003;87:1895-1900.

Paunikallio T, Suvanto M, Pakkanen TT. Composition, tensile properties, and dispersion of polypropylene composites reinforced with viscose fibers. J Appl Polym Sci 2004;91:2676-2684.

Pickering KL, Abdalla A, Ji C, McDonald AG, Franich RA. The effect of silane coupling agents on radiate pine fibre for use in thermoplastic matrix composites. Compos Part A: Appl Sci Manfact 2003; 34: 915-926.

Romero-Balderrama L, Mendoza-Duarte ME, Gasper-Rosas A, Flores-Gallardo SG, Ibarra-Gomez R. Composites of polystyrene/wood fiber, processing effect to creep resisitance. AIP Conference Proceedings 2008;1027(1):135-137.

Sanchez CG, Quesada MG, Orden DL, Urreaga JM. Comparison of the effects of polyethylenimine and maleated polypropylene coupling agents on the properties of cellulose-reinforced polypropylene composites. J Appl Polym Sci 2008;110:2555-2562.

Stamboulis A, Baillie C, Schulz E. Interfacial characterization of flax fibre-thermoplastic polymer composites by the pull out test. Die Angewandte Makromolekulare Chemie 1999;272:117-120.

Terenzi, A., Kenny, M.J., Barbosa, S.E. 2007. Natural Fiber suspensions in thermoplastic

polymers. 1. Analysis of fiber damage during processing. Journal of Applied Polymer Science 103: 2501-2506.

Tingaut P, Henry N, Rials T, Harper D, Dadmun M. Compatibilization of natural fibers with synthetic polymers using triblock copolymers as coupling agents. Macromolecular Chemistry and Physics 2008;209:832-845.

Torres FG, Cubillas ML. Study of the interfacial properties of natural fibre reinforced polyethylene. Polymer testing 2005;24:694-698.

Tze WTY, Wang S, Rials TG, Pharr GM, Kelley SS. Nanoindentation of wood cell walls: Continuous stiffness and hardness measurements. Compos Part A: Appl Sci Manfact 2007;38:945-953.

Valadez-Gonzalez A, Cervantes-UC JM, Olayo R, Herrera-Franco PJ. Chemical modification of henequen fibers with an organosilane coupling agent. Compos Part B: Eng 1999a;30:321-331.

Valadez-Gonzalez A, Cervantes-UC JM, Olayo R, Herrera-Franco PJ. Effect of fiber surface treatment on the fiber-matrix strength of natural fiber reinforced composites. Compos Part B: Eng 1999b;30:309-320.

Wakida T, Tokino S. Surface modification of fiber and polymeric materials by discharge treatment and its application to textile processing. Indian Journal of Fibre & Textile Research 1996;21:69-78.

Watanabe U, Norimoto M. Three dimensional analysis of elastic constants of the wood cell wall. Wood Research 2000;87:1-7.

Wimmer R, Lucas BN, Tsui TY, Oliver WC. Longitudinal hardness and Young's modulus of spruce tracheid secondary walls using nanoindentation. Wood Science and Technology

1997;31:131-141.

Williams JG, Donnellan ME, James MR, Morris WL. Properties of the Interphase in organic matrix composites. Mater Sci Eng A 1990;126:305-312.

Williams JG, Li F, Miskioglu I. Characterization of the interphase in epoxy/aluminum bonds using atomic force microscopy and a nano-indenter. J Adhesion Sci Technol 2005;19(3-5):257-277.

Wimmer R, Lucas BN. Comparing mechanical properties of secondary wall and cell corner middle lamellae in spruce wood. IAWA 1997;18(1):77–88.

Wu J, Yu D, Chan C M, Kim J, Mai Y W. Effect of fiber pretreatment condition on the interfacial strength and mechanical properties of wood fiber/pp composites. J of Appl Poly Sci. 1999;76:1000-1010.

Yamamoto H, Kojima Y. Properties of cell wall constituents in relation to longitudinal elasticity of wood. Wood Science and Technology 2002;36:55-74.

Zhang X, Zhao Q, Wang S, Trejo R, Lara-Curzio E, Du G. Characterizing strength and fracture of wood cell wall through uniaxial micro-compression test. Compos Part A: Appl Sci Manuf 2010;41:632-638.

CHAPTER 3. CHARATERIZATION OF NATURAL FIBERS AND THEIR COMPOSITES USING ADVANCED AFM BASED TECHNIQUE

This chapter is a revised version of a journal article by Sandeep Sudhakaran Nair and Siqun Wang et al:

Nair SS, Wang S, Hurley DC. Nanoscale characterization of natural fibers and their composites using contact-resonance force microscopy. Compos Part A: Appl Sci Manfact 2010; 41: 624-631.

My primary contributions to this paper includes (i) development of the problem into a work, (ii) identification of the study areas and objectives, (iii) design and conducting of the experiments, (iv) gathering and reviewing literature, (v) processing, analyzing and interpretation of experimental data, (vi) pulling various contributions to single paper, (vii) most of the writing.

3.1. Abstract

Contact resonance force microscopy (CR-FM) has been used for the first time to evaluate the mechanical properties of the interphase in natural fiber-reinforced composites and of cell wall layers of natural fibers. With CR-FM, quantitative images of the elastic properties with nanoscale spatial resolution were acquired. The images were calibrated with nanoindentation values. From the modulus images, the average interphase width was found to be (49 ± 5) nm for composite without any treatment, and (139 ± 21) nm for one with a maleic anhydride polypropylene treatment. There was a gradient of modulus across the interphase that ranged between the values of fiber and the polymer. The average values of indentation modulus obtained for different cell wall layers within a fiber were 22.5 GPa to 28.0 GPa, 17.9 GPa to 20.2 GPa, and 15.0 GPa to 15.5 GPa for the S_2 and S_1 layers and the compound middle lamellae, respectively.

Keywords: Polymer-matrix composites, fibres, interphase, mechanical properties

3.2. Introduction

Natural fiber-reinforced polymer composites (NFRPCs) represent one of today's fastest growing industries. Possessing mechanical properties comparable to those of manmade fibers such as carbon, glass or aramid, natural fibers are a potential alternative in reinforced composites because of growing environmental awareness and legislated requirements. Natural fibers also have various advantages compared to conventional reinforcing fibers like glass and carbon fibers such as low cost, low density for an acceptable specific strength, low energy consumption, high toughness, high sound attenuation, nonabrasiveness, undergo little damage during processing, high degree of flexibility, less dermal and respiratory irritation, relatively reactive surface, ease of separation, renewable nature and biodegradability (Coutinha et al., 1997; Lee and Wang, 2006; Mathew et al., 2007; Mohanty et al., 2000). The combination of all these factors has prompted a number of industrial sectors, especially the automotive industry, to consider natural fibers as a substitute for conventional fibers in various products (Mohanty et al., 2001).

The interphase region between the reinforcing fiber and the bulk polymer matrix plays an important role in the performance of fiber-reinforced polymer composites. The structural integrity of a composite mainly depends on the quality of stress transfer in the interphase. The interphase formation depends on the properties of components in use and modifications made on the components (Drzal, 1986). Extending over lengths from nanometers to micrometers, a "well engineered" interphase is critical for desirable mechanical properties of fiber-reinforced polymer composites (Mohanty et al., 2001). An interphase which has lower modulus than the surrounding polymer results in low composite stiffness and strength, but greater resistance to fracture

(Drzal, 1986; Williams et al., 1990). On the other hand, an interphase with higher modulus than the surrounding polymer results in lower fracture resistance but greater strength (Drzal et al., 1983).While conventional fibers can be produced with a definite range of properties, the efficiency of natural fibers as reinforcements in composites depends on inherent factors such as structure, degree of crystallinity, polymerization, and orientation of cellulose chains. The major disadvantage of NFRPCs is the incompatibility between the hydrophilic natural fiber and the hydrophobic polymer, which can be improved only by either physical or chemical modification of the fiber or polymer (Gassan and Bledzki, 1997; Lee and Wang, 2006). Although various researchers have studied the effect of interphase on the bulk properties of composites (Coutinha et al., 1997; Gassan and Bledzki, 1997; Lee and Wang, 2006), very little research has been done to characterize and provide quantitative measurements in the interphase. Previous NFRPC research on interphase characterization has consisted mostly of examining the fracture surfaces of broken composite samples with scanning electron microscopy (SEM). Because these studies examined the interaction between the fibers and the matrix based on the nature of fracture surface, the results only gave an indirect inference of interphase (Felix and Gateholm, 1991; Oksman and Clemons, 1997). Nanoindentation and nanoscratching have also been used to quantify interphase mechanical properties on micrometer or submicrometer length scales. Lee et al. (2007) evaluated the interphase properties of a natural fiber-reinforced polypropylene composite by nanoindentation and finite element analysis. Although they could not measure the interphase directly, their results indicated that the interphase width was less than 1 μm. More recently, researchers have used scanning probe microscopy (SPM) methods to get qualitative images and evaluate the extent of the interphase in various composites. Lee et al. (2009) investigated the interfacial zone of a lyocell/polypropylene composite modified by maleated

polypropylene (MAPP) using atomic force microscopy phase imaging (AFM-PI). Phase imaging records the phase lag when the AFM tip interacts with areas of different mechanical properties. They showed that the interphase transition zone ranged from approximately 113 nm to 128 nm. Since the measurements involving SPM involves complex geometric considerations, it has proved very difficult to obtain quantitative data on areas of different mechanical properties (Munz et al., 1998).

In NFRPCs, the plastic material which serves as the matrix is tough but relatively weak. These plastics are reinforced by stronger stiffer natural fibers. It is critical to understand the mechanical properties of natural fiber to use it as reinforcement in composite materials. The knowledge of different cell wall layers of natural fibers is very critical to isolate single cellulose fibrils without degradation and use it composites (Zhang et al., 2010). Therefore, in addition to characterization of the composite interphase, a better understanding of the mechanical properties (modulus, hardness, yield stress and strength) of different fiber layers is necessary to improve the utilization of natural fibers as reinforcements in composites. The mechanical properties of the wall depend on the amount of constitutive polymers, their spatial organization, and also on the way they are bound to each other (Watanabe and Norimoto, 2000). Each wood fiber consists of different layers, as shown in Figure 2.2. The primary wall of the fiber is the outermost layer, which is bound to the middle lamellae, which acts as a cementing agent between fibers. The primary cell walls of adjoining fibers, together with the middle lamellae in between, form the compound middle lamellae (CML). The secondary wall is divided into the S_1, S_2 and S_3 layers. The orientation of the cellulose microfibrils within each cell wall layer strongly influences the mechanical properties of natural fibers in their longitudinal direction (Bergander and Salmen, 2002). The orientation of the cellulose microfibrils is nearly perpendicular (flat helix) to the fiber

axis in the S_1 and S_3 layers, while it is almost parallel (steep helix) to the fiber axis in the S_2 layer (Brandstrom, 2001; Donaldson and Xu, 2005). Using theoretical cell wall unit models, Watanabe et al. (2000) showed that the longitudinal modulus of the S_2 layer decreased as the microfibril angle with respect to the fiber axis increased. Several researchers have studied the mechanical properties of single wood fibers, mainly with nanoindentation, atomic force microscopy or a combination of both. However, most of these studies were conducted on refined natural fibers (Xing et al., 2009) or isolated single cellulose fibrils (Cheng and Wang, 2008), both of which are prone to mechanical or chemical modification. Nanoindentation is currently one of the most-used methods to quantify the mechanical properties of cell wall layers of natural fibers. Due to the limits of its spatial resolution, most nanoindentation studies have been confined to the S_2 layer. These studies have considered annual rings (Tze et al., 2007), lignifications (Gindl et al., 2002), comparisons with middle lamellae, melamine modified wood (Gindl and Gupta, 2002), and early or late wood (Wimmer et al., 1997). Wimmer et al. (1997) conducted nanoindentation on the S_2 layer and CML and obtained an average value of 16 GPa for the longitudinal modulus of the S_2 layer, double the value for the CML. Their indentation test on the CML was confined to the cell corner middle lamellae due to the narrowness of the CML layer. Since the average thickness of the S_1 layer is approximately 0.4 µm and that of the CML layer is around 0.1 µm, the mechanical properties of these layers have rarely been studied. Zhang et al. (2010) investigated the strength and fracture behavior of wood cell wall S_2 layer through an uniaxial micro-compression test and obtained the 125 MPa compression strength for loblolly pine. Attempts to characterize fiber layers such as S_1 and S_3 with various microscopic methods have yielded only qualitative results (Fahlen and Salmen, 2002).

The above discussion highlights the need for a measurement method capable of providing

quantitative information about mechanical properties with nanoscale spatial resolution, while at the same time providing images of the spatial distribution in properties. Such a method would prove invaluable for studies of the interphase region in NFRPCs as well as of cell wall layers. Here we show how contact resonance force microscopy (CR-FM) methods (Hurley, 2009) can be used to meet this need. CR-FM has the imaging capability of AFM, combined with the ability to determine quantitative modulus values. In this way, it is possible to image or visualize the nanoscale spatial distribution of properties, rather than relying on a single average value or a point by point estimation of quantitative values.

3.3. Experimental

3.3.1. Materials and sample preparation

For the NFRPC experiments, isotactic polypropylene (PP) (Exxon Mobil Corporation, Irving, TX) with a melt flow index of 35 and maleated polypropylene (MAPP) (Epolene G-3003, Eastman Chemicals, Kingsport, TN) were used. Dry solid states of PP and MAPP were mixed with a HAAKA MiniLab extruder (Thermo Fischer Scientific, Karlsruhe, Germany). The temperature, rotation speed, and processing period were 180^0C, 100 rpm, and 10 min, respectively. One mixture contained 10 wt % of MAPP, while the other contained 0 % MAPP. The dry mixtures were compression molded into films approximately 0.25 mm thick. Lyocell fibers (Lenzing AG, Lenzing, Austria) approximately 10 µm in diameter and 30 mm long were unidirectionally placed on top of the PP-MAPP films. The films were then stacked and compression molded at 200^0C for 10 min and then cold water was used to cool down the mold temperature to 32^0C under pressure in order to obtain unidirectional lyocell fiber-reinforced composites (Nair et al., 2008). The cell wall layer experiments involved samples collected

from a 45-year-old red oak. A latewood portion of the 45th annual ring was cut with dimensions of 2 mm X 5 mm X 5 mm in the radial, tangential and longitudinal directions, respectively.

The NFRPC and cell wall samples were embedded in an epoxy medium under vacuum and cured by heating and drying for 8 h at 70^0C (Spur, 1969). A cross section of the sample was prepared by use of an ultramicrotome with a diamond knife. The microtome process yielded sufficiently smooth surfaces for the CR-FM experiments.

3.3.2. Nanoindentation techniques

Modulus values for the lyocell fiber and PP matrix for the composites and the S_2 layer of the wood sample were obtained by displacement-controlled nanoindentation (Triboindenter, Hysitron, Eden Prairie, MN). The Berkovich indenter tip was loaded to a maximum displacement of 250 nm. The indentation modulus of the sample is inferred from the initial unloading contact stiffness *S*, *i.e.*, the slope *dP/dh* of the tangent to the initial unloading curve in the load-displacement curve, where *P* is the indentation force and *h* is the displacement. The sample reduced indentation modulus (E_r) is then calculated from (Oliver and Pharr, 1997).

$$E_r = \frac{\sqrt{\pi}}{2\beta}\frac{S}{\sqrt{A}} \qquad (3.1)$$

where β is a constant that depends on the geometry of the indenter (β = 1.034 for a Berkovich indenter) and A is the contact area. The indentation modulus M_s of the sample is then obtained from

$$\frac{1}{E_r} = \frac{1}{M_s} + \frac{1}{M_{tip}} \qquad (3.2)$$

where M_{tip} is the indentation modulus of the diamond indenter tip. The value M_{tip} = 1146 GPa was used (Kopycinska-Muller et al., 2005). The average value of M for the S_2 layer obtained by nanoindentation was 24.6 GPa. The average indentation modulus reference values for the composites obtained by nanoindentation on the fiber and matrix were M_{fiber} = 12.4 ± 0.3 GPa and M_{matrix} = 3.2 ± 0.3 GPa, respectively.

3.3.3. CR-FM techniques

Contact-resonance force microscopy (CR-FM) (Hurley, 2009) was used for quantitative imaging of the nanoscale elastic properties of the samples. CR-FM is based on the atomic force acoustic microscopy (AFAM) method (Hurley et al., 2003; Rabe et al., 2000), which determines elastic properties at a fixed sample position. The basic measurement procedure involves measuring the resonant frequencies of the vibrating AFM cantilever in free space and contact resonance frequencies when the tip is in contact with the sample. CR-FM consists of acquiring contact resonance frequencies for two samples in alteration: the test (unknown) sample and a reference sample whose elastic properties are known. The elastic properties of the reference samples were obtained using nanoindentation. In our composite samples, we used lyocell fiber and PP matrix as the reference samples to determine the elastic properties of interphase and for the cell wall experiments; we used S_2 layer as the reference sample to determine the properties of different cell wall layers. Data analysis consisted of two different steps, each a separate model. First, the measured frequencies were related to the tip-sample interaction force by means of a model for the dynamic motion of the cantilever. Next the interaction force which is the contact stiffness (k^*) was used to determine the elastic properties of the sample using a model for the contact mechanics between the tip and the sample (Hurley, 2009; Hurley et al., 2003; Rabe et al.,

2000). An extension of AFAM for quantitative imaging, CR-FM techniques have been described in detail elsewhere (Hurley, 2009; Hurley, 2010; Hurley et al., 2007). The imaging experiments were performed with custom electronics that interface with a commercial AFM instrument (Kos and Hurley, 2008). A conceptual schematic of the experimental apparatus is shown in Figure 3.1. The sample under investigation is bonded to a piezoelectric actuator (ultrasonic transducer) affixed to the positioning stage of the AFM instrument. The transducer is driven by a swept sine wave voltage, and the resulting vibrations excite the resonant modes of the cantilever. The signal from the AFM position-sensitive photodiode is used as input to the custom electronics in order to determine the contact resonance frequency at a given image position. Through the use of an auxiliary AFM input channel, an image of these frequencies is acquired in parallel with the topographic image.

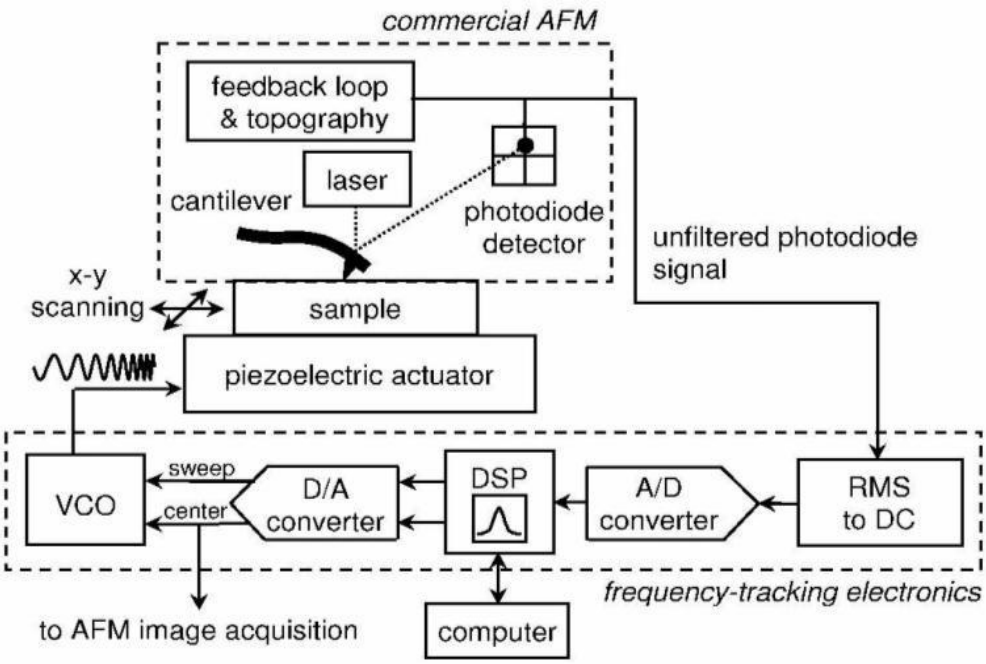

Figure 3.1. Schematic representation of CR-FM

The AFM cantilevers used in these experiments had nominal dimensions of length L = 225 ± 10 µm, width w = 30 ± 8 µm, and thickness t = 3 ± 1 µm, and nominal spring constant k_c = 2.8 N/m. The applied static force $F_N = k_c d$, where d is the deflection, was approximately 50 nN to 80 nN. To avoid registration difficulties and artifacts due to scanner drift and hysteresis in scanning the same area twice, frequency images were acquired for only one resonant mode, namely the second flexural mode (Hurley, 2010). The second mode is the most sensitive mode for the experimental conditions used here, that is, it exhibits the greatest change in resonant frequency for a given change in contact stiffness (Hurley, 2009). Images of the normalized contact stiffness k^*/k_c for a sample ("test") region were calculated from the frequency images assuming a fixed value for the relative tip position L_1/L = 0.97, where L_1 is the position of tip relative to the total length L of the cantilever. This approach was feasible due to the relatively small variation in contact stiffness with L_1/L for the second flexural mode (Hurley, 2009). The contact stiffness images were transformed into images of the reduced modulus E^*_{test} by use of the nanoindentation measurements on a reference specimen. It is necessary to convert the reduced modulus value E_r obtained by nanoindentation with a diamond tip into a reduced modulus E^*_{ref} corresponding to contact with the AFM tip. A relation identical to Eq. (3.2) is used, except that M_{tip} = 165 GPa for the <001> silicon tip. Values of the reduced modulus E^*_{test} for the sample region were then calculated with (Hurley, 2009; Hurley et al., 2003; Rabe et al., 2000).

$$E^*_{test} = E_{ref}^* \left(\frac{k^*_{test}}{k^*_{ref}} \right)^n \qquad (3.3)$$

where k^*_{test} and k^*_{ref} are the contact stiffness values for the test sample and reference sample, respectively. The value n = 3/2 was used, corresponding to Hertzian contact. Finally, the reduced modulus images were converted to images of the indentation modulus M_{test} using Eq. (3.2).

This approach was used to calculate indentation modulus values for the images of the cell wall layers. E_r and hence M_{ref} and E^*_{ref} were obtained by nanoindentation for the S_2 layer. For each experimental image, the mean value of the contact stiffness was determined for a region containing the S_2 layer and was used as k^*_{ref} in Eq. (3). For images of the composite interphase, a dual reference approach was used. Nanoindentation values for both the fiber (M_{fiber}) and the matrix (M_{matrix}) were obtained and used in (Stan and Price, 2006).

$$M_{test} = \frac{\left(\frac{k_{fiber}}{k_{matrix}}\right)^n - 1}{\left(\frac{k_{fiber}}{k_{test}}\right)^n \left(\frac{1}{M_{matrix}} - \frac{1}{M_{fiber}}\right) + \left(\frac{k_{fiber}}{k_{matrix}}\right)^n \left(\frac{1}{M_{fiber}} - \frac{1}{M_{matrix}}\right)} \quad (3.4)$$

In this case, two reference values of the contact stiffness were determined for each image. One value was the average value k^*_{fiber} for an image region that contained only the fiber, and one was the average value k^*_{matrix} for a region that contained only the matrix.

3.4. Results and Discussion

3.4.1. Evaluation of interphase in fiber reinforced composites

Contact resonance frequency images were obtained at the boundary region between the fiber and the matrix. In order to avoid signal artifacts due to topographical effects, regions as flat as possible were selected (height ~20 nm or less) for imaging. Figures 3.2 and 3.3 show topography and indentation modulus images for two composite samples with different treatments. Differences in modulus values for the fiber, fiber-matrix boundary zone, and matrix regions are clearly visible in the images.

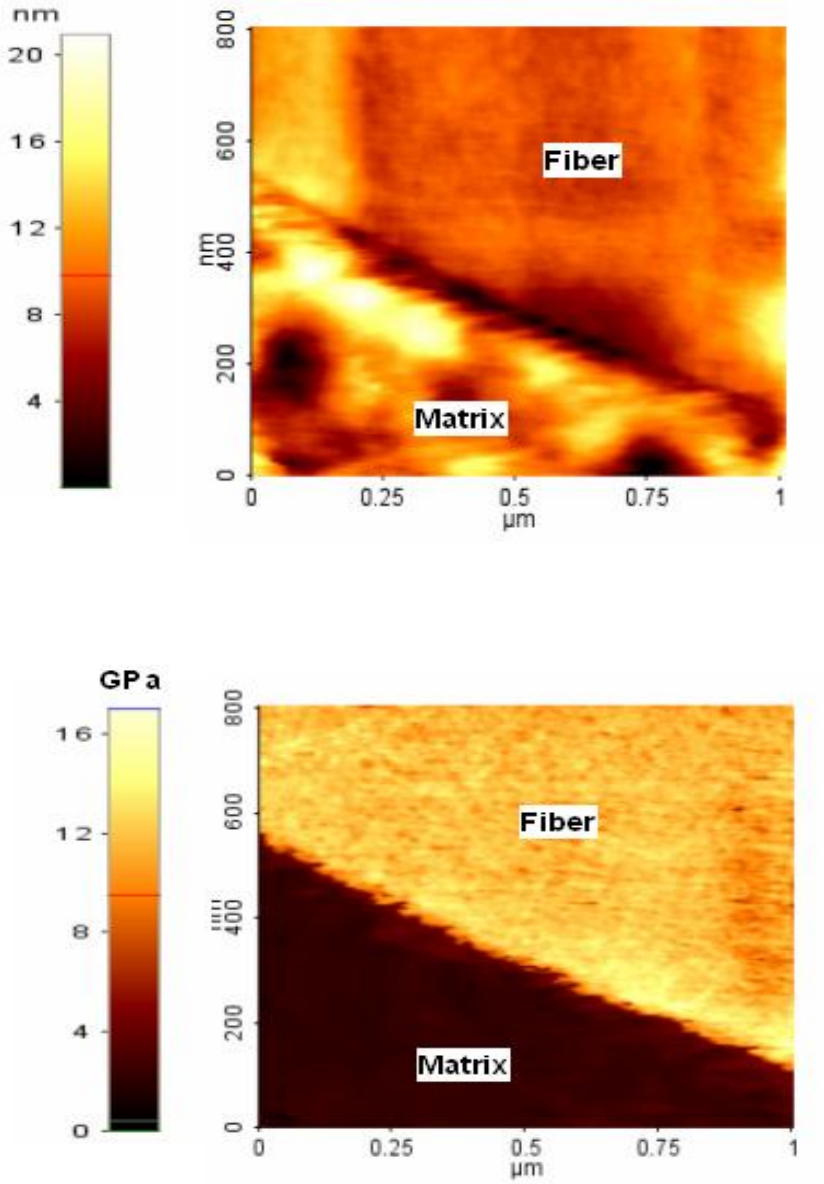

Figure 3.2. Topography (top) and indentation modulus image (bottom) of lyocell/PP composites without treatment

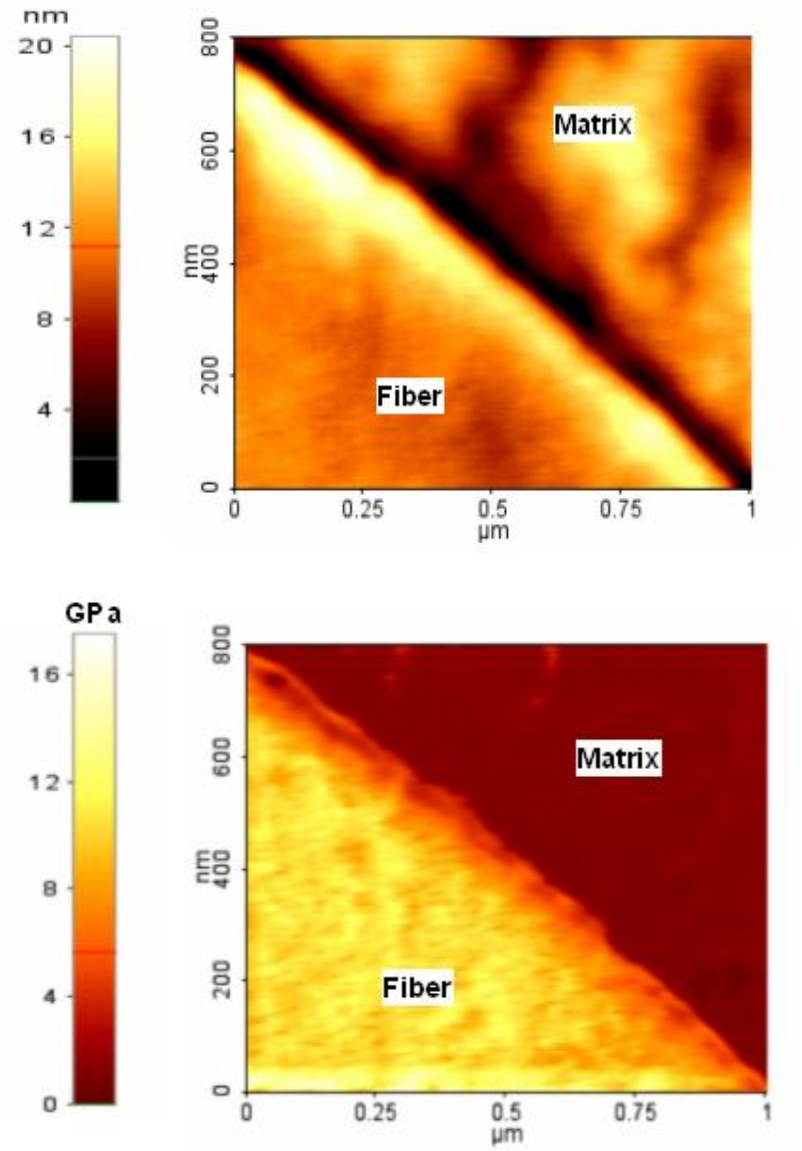

Figure 3.3. Topography (top) and indentation modulus image (bottom) of lyocell/PP composites with MAPP treatment

The interphase zone properties were analyzed with commercial image processing software. Mean indentation modulus values for regions consisting entirely of fiber and matrix were obtained from the area enclosed within the box plots shown in Figure 3.3(a). Figure 3.3(b) shows the line profile corresponding to the radial line segment in Figure 3.3(a) across the fiber-matrix boundary region. The left pointer in Figure 3.3(b) corresponds to the mean indentation value for the fiber (12.4 GPa), while the right pointer indicates that of the matrix (3.2 GPa). In Figure 3.3(b), the distance between the two pointers, where the properties differ from those of the bulk fiber and matrix corresponds to the interphase thickness (in this case was about 135 nm). By definition, the interphase starts from some point on the fiber where the local properties as a result of various surface treatments or reaction with the matrix, begin to change from those of the bulk fiber and extends until the local properties equal the bulk matrix properties (Drzal 1986). In order to minimize any morphological variations near the fiber or the matrix surface, this approach was applied to 15 radial lines across the fiber-matrix boundary. The width of interphase obtained by averaging these line scans was found to be (49 ± 5) nm for the composite without MAPP treatment, and (139 ± 21) nm for the one with 10 % MAPP treatment. Figure 3.4 shows the line profiles obtained by averaging 15 radial line scans across the fiber-matrix boundary region for both composites. The average line profile for each composite exhibited a gradient of modulus across the interphase region that ranged between the modulus values of fiber and the polymer.

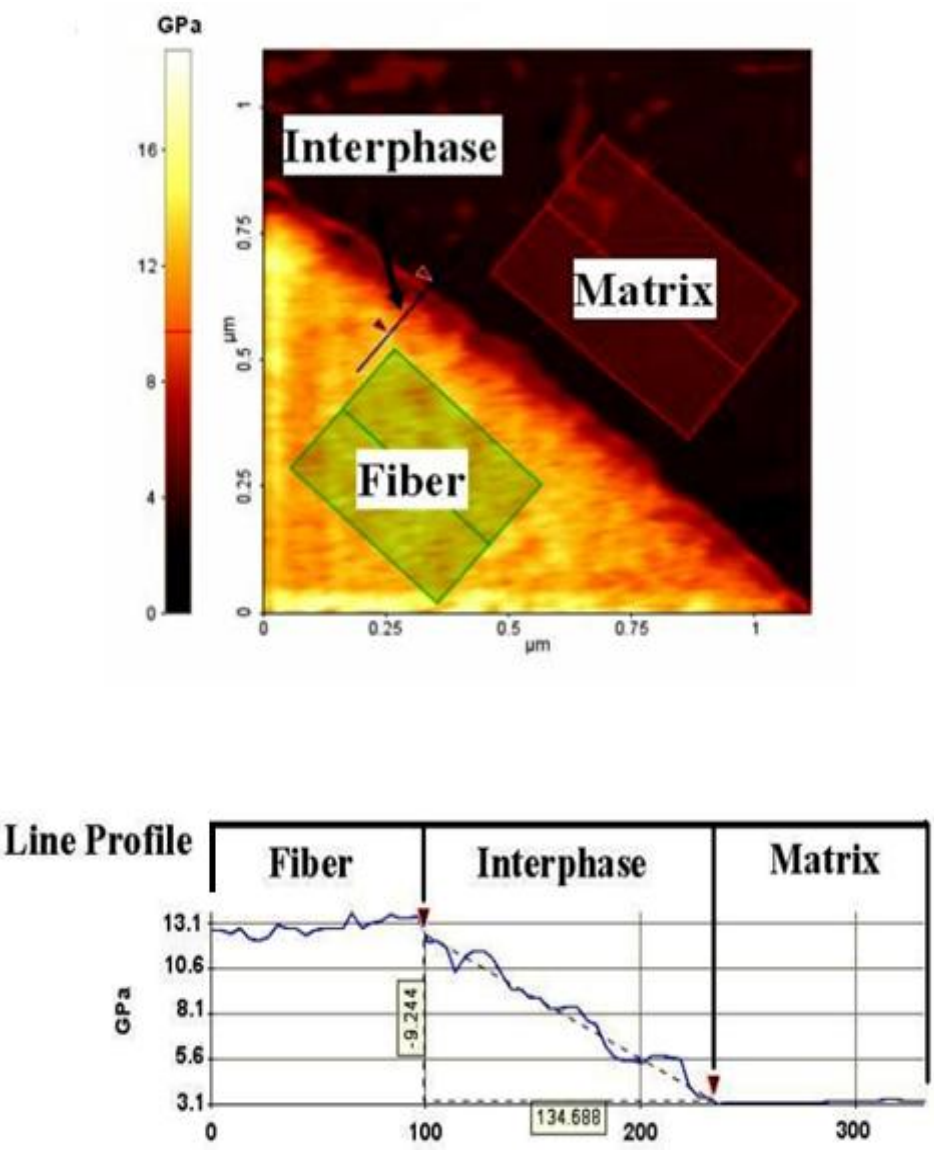

Figure 3.4. Analysis of the modulus (top), and line profile image (bottom) showing the size of interphase based on the gradient in modulus

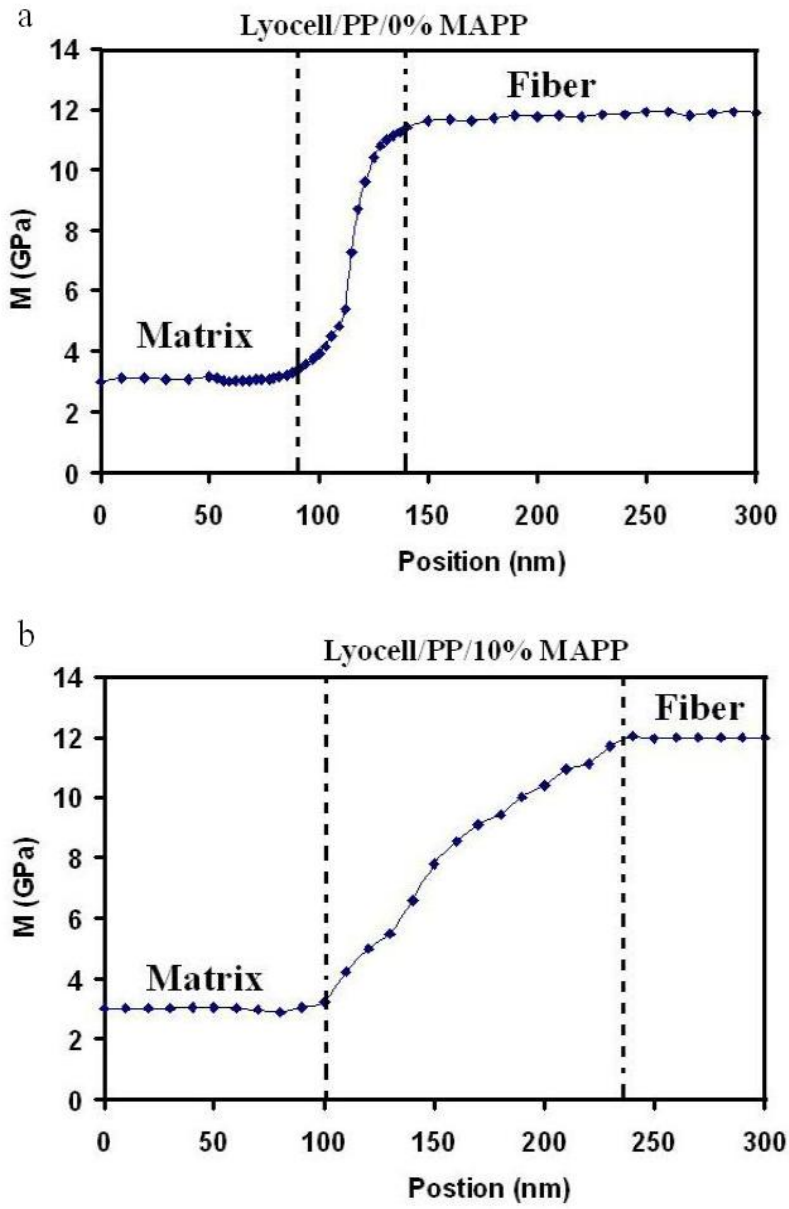

Figure 3.5. Average modulus across interphase region (between the vertical dotted lines) between the fiber and matrix for (a) lyocell/PP composites without any treatment and (b) with MAPP treatment

As mentioned above, chemical modification of the hydrophilic fiber and/or the hydrophobic matrix is necessary for a strong fiber-matrix bond. These results indicate that the MAPP treatment has substantially increased the interphase transition zone. This is consistent with previous results in the literature. For instance, Lee et al. (2009) showed that the use of MAPP as a compatibilizer in lyocell/polypropylene composite increased the interphase transition zone. Also, they have shown that the combined use of MAPP and γ-amino propyltrimethoxy silane (γ-APS) have further increased the interphase transition zone.

Interphase widths of less than 100 nm with quantitative mechanical measurements at each position have rarely been reported in literature. The main reason for this is the lack of techniques that can measure the properties with such nanoscale spatial resolution. Griswold et al. (2005) examined the interphase region of an epoxy/glass composite with atomic force microscopy phase imaging (AFM-PI) and nanoindentation and showed that interphase thickness varied between 110 nm and 888 nm for different silane concentrations. Although they used SPM methods such as AFM-PI which possess the spatial resolution needed to characterize such narrow interphases, the lack of ability to provide quantitative measurements at each position in the interphase was a major drawback. In AFM-PI techniques, the tips are either at large distance from the surface as in non contact mode (Lee et al., 2009) or very low force is applied to the tip as in light tapping mode (Griswold et al., 2005). Therefore, in addition to surface elastic properties, adhesion, viscoelasticity, and hydrophilicity/hydrophobicity also contribute to the phase lag (Gao and Mader, 2002). Whereas in CR-FM, sufficient force is applied on the tip which ensures that the scanning is in contact with the surface and proper contact area is obtained, which means that the tip sample interactions are more influenced by the surface elastic properties. But care has to be taken to protect the test sample and reference sample from the formation of any oxides or

adsorbed water on the surface. These can prevent the tip from pure elastic contact with sample (Hurley, 2009). Hodzic et al. (2000) conducted nanoindentation and nanoscratching on polymer/glass composite systems and reported that the interphase varied between 2 µm and 6 µm. Kim et al. (2001) found that the interphase width measured by nanoscratching for a polymer/glass system varied from 0.8 µm to 1.5 µm, and that the width increased with silane concentration.

All of these values are much larger than the values obtained in this study. One explanation is that the limited spatial resolution of nanoindentation prevents accurate measurements of narrow interphases. In addition to the limit imposed by the size of the indenter tip, the lateral resolution is reduced by other effects. The spacing of indents made by nanoindentation should be sufficiently wide enough to avoid the overlapping of the zone associated by plastic deformation. For instance, finite element analysis has shown that the interphase thickness measured by nanoindentation can appear larger than the true value due to the effect of neighboring materials (Lee et al., 2007). In this study involving the CR-FM technique, we have demonstrated the ability to measure interphase zones as narrow as 50 nm in lyocell/polypropylene composites. The extremely small tip radius (25 nm to 35 nm) and low forces (50 nN to 80 nN) involved in these CR-FM experiments mean that the deformation of the sample surface is very small and is elastic. This feature is quite valuable for characterizing the narrow interphase widths in NFRPCs. One of the major limitations of CR-FM is that the elastic properties of the reference samples were obtained using nanoindentation. These reference values were used to obtain the modulus values of unknown sample in Eq. (3.3) and Eq. (3.4). The AFM tips used in CR-FM experiments uses low forces, so that the tip-sample contact is predominantly elastic. In nanoindentation, the Berkovich indenter tip was loaded to a maximum displacement of

250 nm which means that the tip sample contact creates plastic deformation. So the indentation modulus obtained by these methods can be different. One way to avoid this is to obtain the reference values using nanoindentation techniques using AFM tips having similar tip radius and using low forces similar to those used in CR-FM technique. However, experimental uncertainties such as depth of penetration, tip wear and tear, piezo creep, and hysteresis effects limit the utility of AFM based nanoindentation measurements (Li et al., 2009).

3.4.2. Evaluation of mechanical properties of cell wall layers

Contact resonance frequency images were obtained at the boundary region between two fibers within the growth ring. Modulus maps were calculated from the frequency images using the procedure described above. Figure 3.5 shows images for the topography and indentation modulus. Contrasts in modulus between the CML and S_1 and S_2 layers are clearly visible. Mean values of the indentation modulus for the CML and S_1 and S_2 layers were obtained from the area enclosed within the box plots, as shown in Figure 3.5. To avoid signal artifacts due to topographical effects, regions as flat as possible were selected for the box plot analysis. The values of indentation modulus were 22.5 GPa to 28.0 GPa, 17.9 GPa to 20.2 GPa, and 15.0 GPa to 15.5 GPa for the S_2, S_1, and CML layers, respectively. The higher values of the S_2 layer compared to other layers are consistent with previous results in the literature (Clair et al., 2003; Wimmer and Lucas, 1997). Although the S_2 layer has a steeper helix and the S_1 layer has a flatter helix of microfibril orientation with respect to the fiber axis, various studies have shown that there is a shift of microfibril orientation from the outer S_1 layer to the inner S_2 layer and from the outer S_2 layer to the inner S_3 layer. Abe et al. (1991) reported that the cellulose microfibril orientation in the secondary cell wall layers of Sakhalin fir, as seen from the lumen side,

gradually changed in a clockwise direction from the outermost S_1 to the middle of the S_2 and then to counterclockwise to the innermost S_3. Xing et al. (2008) examined the cell wall layers of refined fibers of loblolly pine by use of nanoindentation and showed that there exists a clear interphase between S_2 and S_1 and between S_2 and S_3. The wider range of indentation modulus values obtained in this study for each of the secondary layers can be explained partly by differences in the cellulose microfibril angle within each layer (Bergander and Salmen, 2002; Watanabe and Norimoto, 2000).

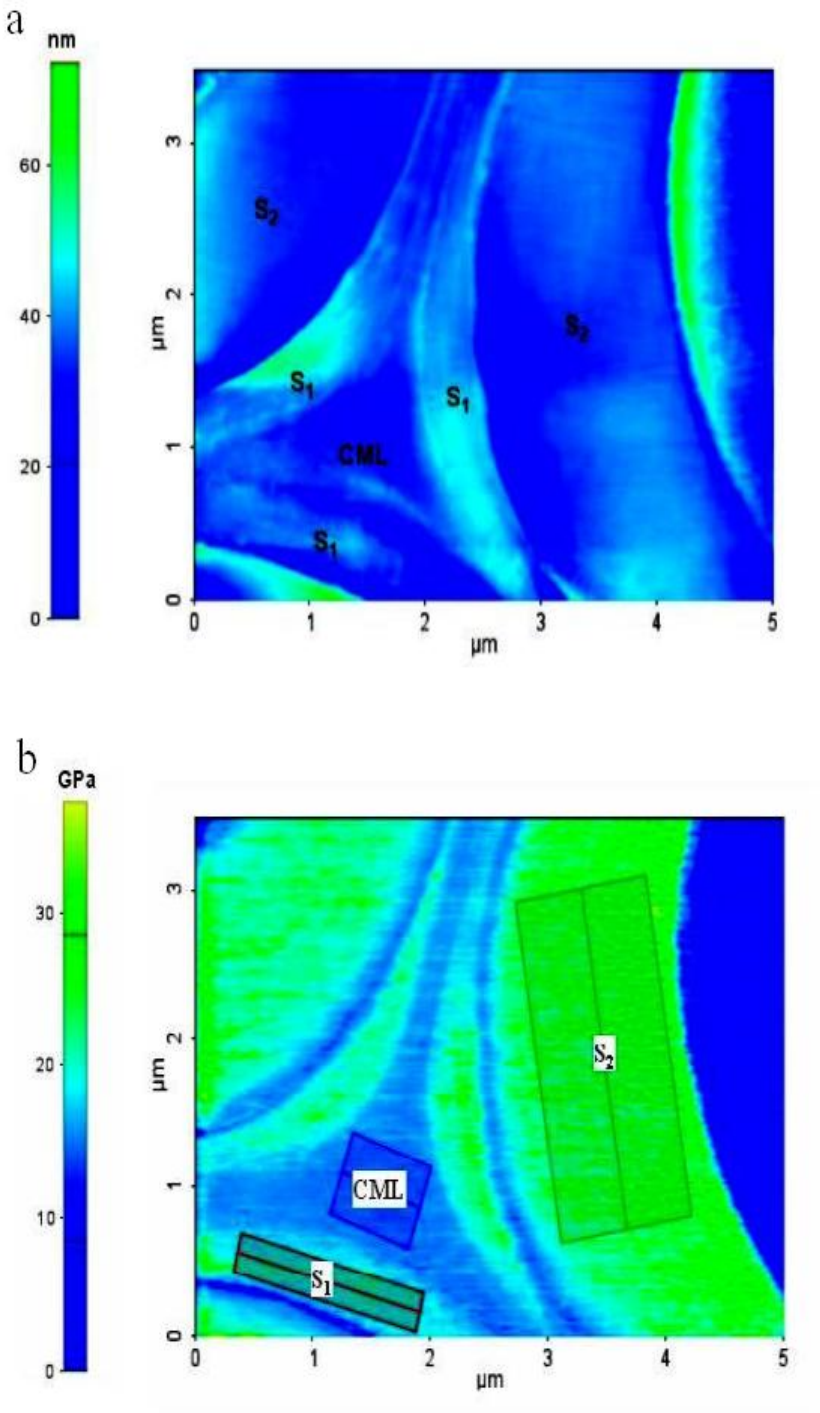

Figure 3.6. Images of (a) topography and (b) box plot analysis of indentation modulus image of various cell wall layers

The images in Figure 3.5 also show a thin region between the S_1 and S_2 layers with apparently lower modulus than that of other secondary layers. Line profile analysis of these regions, as shown in Figure 3.6 indicates that signal artifacts due to topography are the most likely cause of the effect. In CR-FM experiments, the measured resonant frequency depends not only on the local contact stiffness, but also on the contact area between the tip and sample. For a perfectly flat sample, the contact area remains the same during scanning, and frequency changes correspond only to contact stiffness variations. However, as indicated in Figure 3.7 sharp or significant changes in topography will affect the contact area. The resulting change in frequency leads to false changes in modulus. Finally, the innermost layer of the fiber, the S_3 layer, could not be reliably identified in the CR-FM modulus maps. Because it is adjacent to the lumen and is the thinnest layer, the distinction of this layer might have been lost- when the lumen region was replaced with epoxy during sample preparation. Improved sample preparation methods are required in order to better characterize this layer with CR-FM techniques.

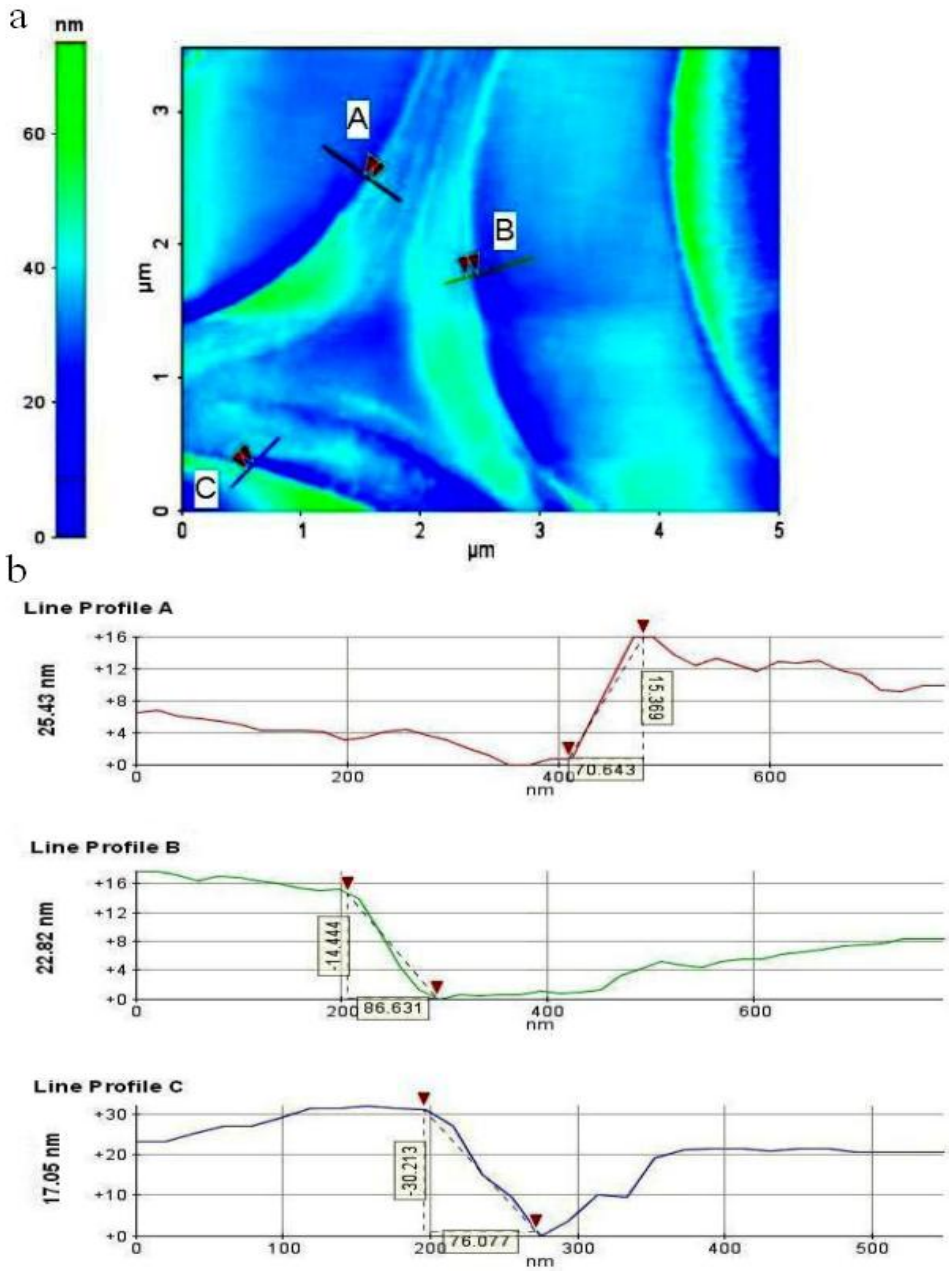

Figure 3.7. (a) Topographical change between S_1 and S_2 and (b) corresponding line profile

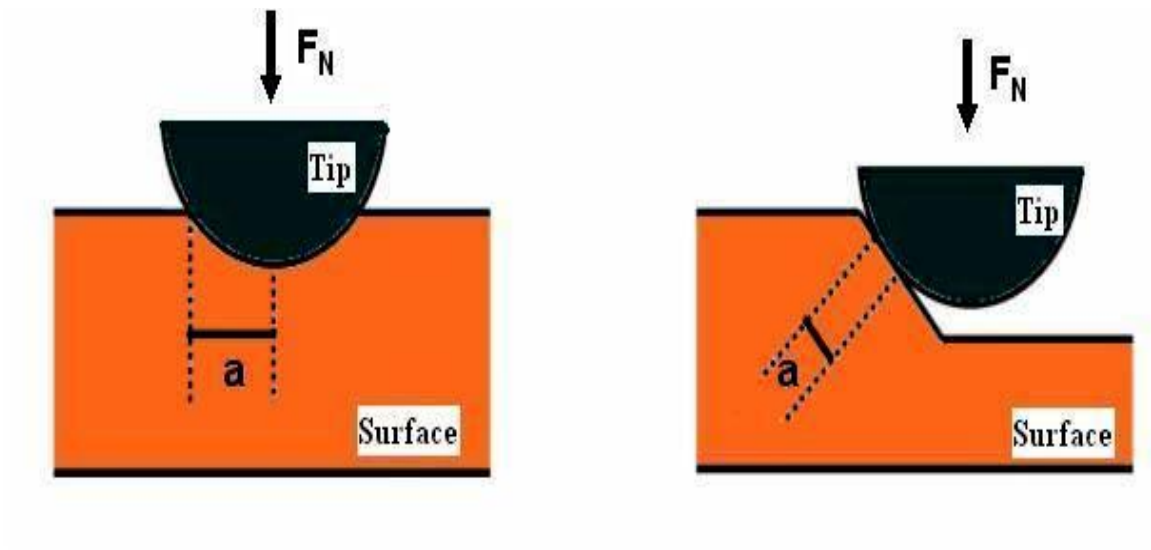

Figure 3.8. (a) Schematics for contact mechanics for Hertzian contact on flat surface (left) and on a steep slope (right)

CR-FM methods present a number of advantages over other methods for studying the elastic properties of cell walls. Because it is the thickest cell wall layer, the S_2 layer has been the subject of earlier studies. The presence of various adjacent layers in fibers can alter the deformation fields surrounding indents made by nanoindentation, potentially leading to incorrect estimates of the indentation modulus. Jakes et al. (2008) showed that the structural compliance observed in nanoindentation experiments on the S_2 layer was mainly due to the effect of the nearby free edge of the lumen. In CR-FM technique, the fact that the deformation is much smaller and elastic largely solves this problem. The improvement in lateral spatial resolution afforded by CR-FM methods using a smaller tip and lower applied forces opens the door to

detailed studies of cell wall structure. CR-FM also provides an image of quantitative modulus values, in contrast to many other AFM methods. For instance, the AFM methods used by Clair et al. (2003) to investigate holm oak and boco wood specimens provide only qualitative images of elastic contrast and quantitative values at only a handful of sample positions. The ability of contact- resonance methods to provide quantitative images of nanoscale mechanical properties has not been demonstrated in any of the previously conducted cell wall studies.

3.5. Conclusion

Study results in this chapter demonstrate that contact resonance force microscopy is a valuable technique for evaluating the interphase of natural fiber-reinforced polymer composites and for characterizing the elastic properties of cell wall layers of natural fibers. The nanoscale spatial resolution of CR-FM, combined with its ability to provide quantitative modulus images, makes it possible to investigate the mechanical properties of interphases as narrow as 50 nm in NFRPCs and thin cell wall layers in natural fibers. This technique, which has previously been used to characterize various micro-nano structures, is used here for the first time in the field of natural fibers. The extremely low loads and small tip radius characteristic of CR-FM enable *in-situ* elastic property information with significantly higher spatial resolution than other, destructive methods like nanoindentation. The use of a reference material with similar modulus values removes much of the uncertainty arising in the final modulus values from tip wear and tear, which is very common with other AFM methods. One of the major limitations of CR-FM technique used here is that the elastic properties of the reference samples were obtained using nanoindentation. The indentation modulus obtained by these methods can be different. One way to avoid this is to obtain the reference values using nanoindentation techniques using AFM tips

having similar tip radius and using low forces similar to those used in CR-FM technique. However, experimental uncertainties such as depth of penetration, tip wear and tear, piezo creep, and hysteresis effects limit the utility of AFM based nanoindentation measurements. Also, proper care has to be taken to protect the test sample and reference sample from the formation of any oxides or adsorbed water on the surface. These can prevent the tip from pure elastic contact with sample. These results suggest that this method will enable researchers to get much more information about the nanoscale properties of interphase and fibers, and correlate these information to macroscale performance provides an interesting direction for future work, which is very important for optimum design of final NFRPC products.

3.6. References

Abe H, Ohtani J, Fukazawa K. FE-SEM observations on the microfibrillar orientation in the secondary wall of tracheids. IAWA 1991;12:431-438.

Bergander A, Salmen L. Cell wall properties and their effects on the mechanical properties of fibers. Journal of Materials Science 2002;37:151-156.

Brandstrom J. Micro- and ultrastructural aspects of Norway spruce tracheids: A review. IAWA 2001;22(4):333-353.

Cheng Q, Wang S. A method for testing the elastic modulus of single cellulose fibrils via atomic force microscopy. Compos Part A: Appl Sci Manfact 2008;39:1838-1843.

Clair B, Arinero R, Lévesque G, Ramonda M, Thibaut. Imaging the mechanical properties of wood cell wall layers by atomic force modulation microscopy. IAWA 2003;24(3):223-230.

Coutinha FMB, Costa THS, Carvalho DL. Polypropylene-wood fiber composites: effect of treatment and mixing conditions on mechanical properties. J Appl Polym Sci 1997;65:1227-1235.

Donaldson L, Xu P. Microfibril orientation across the secondary cell wall of radiate pine tracheids. Trees 2005;19:644-653.

Drzal LT, Rich MJ, Koenig MF, Lloyd PF. Adhesion of graphite fibers to epoxy matrices. 2. The effect of fiber finish. J Adhesion 1983;16(2):133-152.

Drzal LT. The interphase in epoxy composites. Adv Polym Sci 1986;75:1-32.

Fahlen J, Salmen L. On the lamellar structure of the tracheid wall. Plant boil 2002;4:339-345.

Fahlen J, Salmen L. Cross-sectional structure of the secondary wall of wood fibers as affected by processing. Journal of Materials Science 2003;38:119-126.

Felix JM, Gatenholm P. The nature of adhesion in composites of modified cellulose fibers and polypropylene. J Appl Polym Sci 1991;42:609-620.

Gassan J, Bledzki A. The influence of fiber-surface treatment on the mechanical properties of jute-polypropylene composites. Compos Part A: Appl Sci Manfact 1997;28A:1001-1005.

Gao S-L, Mader E. Characterization of interphase nanoscale property variations in glass fibre reinforced polypropylene and epoxy resin composites. Compos Part A: Appl Sci Manfact 2002;33:559-576.

Gindl W, Gupta HS, Grunwals C. Lignification of spruce tracheid secondary cell walls related to longitudinal hardness and modulus of elasticity using nano-indentation. Can J Bot 2002;80:1029-1033.

Gindl W, Gupta HS. Cell- wall hardness and young’s modulus of melamine-modified spruce wood by nano-indentation. Compos Part A: Appl Sci Manufact 2002;33:1141-1145.

Griswold C, Cross WM, Kjerengtroen L, Kellar JJ. Interphase variation in silane-treated glass-fiber-reinforced epoxy composites. J Adhesion Sci Technol 2005;19(3-5):279-290.

Hodzic A, Stachurski ZH, Kim JK. Nano-indentation of polymer-glass interfaces. Part I. Experimental and mechanical analysis. Polymer 2000;41:6895-6905.

Hurley DC. Contact resonance force microscopy techniques for nanomechanical measurements. Applied Scanning Probe Methods Vol. XI, eds. Bhushan B, Fuchs H. Springer-Verlag, Berlin, 2009; 5: 97-138.

Hurley DC. Measuring mechanical properties on the nanoscale with contact resonance force microscopy methods: Scanning probe microscopy of functional materials. Nanoscale imaging and spectroscopy, eds. Kalinin S, Gruverman A. Springer-Verlag, Berlin 2010. P. 95-124.Hurley DC, Shen K, Jennett NM, Turner JA. Atomic force microscopy methods to determine thin film elastic properties. J App Phy 2003;94(4):2347-2354.

Hurley DC, Kopycinska-Müller M, Kos AB. Mapping mechanical properties on the nanoscale with atomic force acoustic microscopy. JOM 2007;59**:** 23-29.

Jakes JE, Frihart CR, Beecher JF, Moon RJ, Stone DS. Experimental method to account for structural compliance in nanoindentation measurements. J Mater Res 2008;23:1113-1127.

Kim JK, Sham ML, Wu J. Nanoscale characterization of interphase in silane treated glass fibre composites. Compos Part A: Appl Sci Manfact 2001;32:607-618.

Kopycinska-Muller M, Geiss RH, M¨uller J, Hurley DC. Elastic property measurements of ultra thin films using atomic force acoustic microscopy. Nanotechnology 2005;16:703-709.

Kos AB, Hurley DC. Nanomechanical mapping with resonance tracking scanned probe microscope. Meas Sci Technol 2008;19:015504.

Lee SH, Wang S. Biodegradable polymers/bamboo fiber biocomposite with bio-based coupling

agent. Compos Part A: Appl Sci Manfact 2006; 37(1): 80-91.

Lee SH, Wang S, Pharr GM, Xu H. Evaluation of interphase in a cellulose fiber-reinforced polypropylene composite by nanoindentation and finite element analysis. Compos Part A: Appl Sci Manfact 2007;38:1517-1524.

Lee SH, Wang S, Takashi E, Kim NH. Visualization of interfacial zones in lyocell fiber-reinforced polypropylene composite by AFM contrast imaging based on phase and thermal conductivity measurements. Holzforschung 2009;63:240-247.

Li AG, Burggraf LW, Phillips DM. Nanometer-scale elastic modulus of surfaces and thin films determined using an atomic force microscope. In: Proceedings of Nanotechnology Materials and Devices Conference (Traverse City, US, 2-5 June 2009).

Mathew L, Joseph R. Mechanical properties of short-isora-fiber-reinforced natural rubber composites: effects of fiber length, orientation, and loading, alkali treatment, and bonding agent. J Appl Polym Sci 2007;1640-1650.

Mohanty AK, Misra M, Hinrichsen G. Biofibers, biodegradable polymers and biocomposites: an overview. Macromol. Mater. Eng 2000;276/277:1-24.

Mohanty AK, Misra M, Drzal LT. Surface modifications of natural fibers and performance of the resulting biocomposites: an overview. Composite Interfaces 2001;8(5):313-343.

Munz M, Sturm H, Schulz E, Hinrichsen G. The scanning force microscope as a tool for the detection of local mechanical properties within the interphase of fiber reinforced polymers. Compos Part A 1998;29:1251-1259.

Nair SS, Wang S, Hurley DC. Evaluation of interphase properties in fiber reinforced polymer composite using contact resonance force microscopy. In: Proceedings of the 51st annual meeting of the society of wood science and technology (Concepción, Chile, 10-12

November 2008).

Oksman K, Clemons C. Mechanical properties and morphology of impact modified polypropylene-wood flour composites. J Appl Polym Sci 1997;67:1503-1513.

Oliver WC, Pharr GM. An improved technique for determining hardness and elastic modulus using load and displacement sensing indentation experiments. J Mater Res 1997;7(6):1564-1583.

Rabe U, Amelio S, Kester E, Scherer V, Hirsekorn S, Arnold W. Quantitative determination of contact stiffness using atomic force acoustic microscopy. Ultrasonics 2000;38:430-437.

Spur AR. A low-viscosity epoxy resin embedding medium for electron microscope. J Ultrastruct Res 1969;26:31-43.

Stan G, Price W. Quantitative measurements of indentation moduli by atomic force acoustic microscopy using a dual reference method. Rev Sci Instr 2006;77:103707.

Tze WTY, Wang S, Rials TG, Pharr GM, Kelley SS. Nanoindentation of wood cell walls: Continuous stiffness and hardness measurements. Compos Part A: Appl Sci Manfact 2007;38:945-953.

Watanabe U, Norimoto M. Three dimensional analysis of elastic constants of the wood cell wall. Wood Research 2000;87:1-7.

Williams JG, Donnellan ME, James MR, Morris WL. Properties of the Interphase in organic matrix composites. Mater Sci Eng A 1990;126:305-312.

Wimmer R, Lucas BN, Tsui TY, Oliver WC. Longitudinal hardness and Young's modulus of spruce tracheid secondary walls using nanoindentation. Wood Science and Technology 1997;31:131-141.

Wimmer R, Lucas BN. Comparing mechanical properties of secondary wall and cell corner

middle lamellae in spruce wood. IAWA 1997;18(1):77-88.

Xing C, Wang S, Pharr GM, Groom LH. Effect of thermo-mechanical refining pressure on the properties of wood fiber cell walls: measured by nanoindentation and atomic force microscopy. Holzforschung 2008;62(2): 230-236.

Xing C, Wang S, Pharr GM. Comparison of the effects of thermomechanical refining pressure on the properties of refined fibers of juvenile and mature wood. Wood Science and Technology 2009;43:615-625.

Zhang X, Zhao Q, Wang S, Trejo R, Lara-Curzio E, Du G. Characterizing strength and fracture of wood cell wall through uniaxial micro-compression test. Compos Part A: Appl Sci Manfact 2010;41(5):632-638.

CHAPTER 4. CHARATERIZATION OF INTERPHASE NANOSCALE PROPERTY VARIATIONS IN MALEATED POLYPROPYLENE TREATED NATURAL FIBER REINFORCED POLYMER COMPOSITES

This chapter is a revised version of a paper by Sandeep Sudhakaran Nair and Donna C Hurley et al submitted to a journal article and is in review now:

Nair SS, Hurley DC, Wang S, Young TM. Nanoscale characterization of interphase properties in maleated polypropylene-treated natural–fiber reinforced polymer composites. Polym. Eng. Sci (In revision).

My primary contributions to this paper includes (i) development of the problem into a work, (ii) identification of the study areas and objectives, (iii) design and conducting of the experiments, (iv) gathering and reviewing literature, (v) processing, analyzing and interpretation of experimental data, (vi) pulling various contributions to single paper, (vii) most of the writing.

4.1. Abstract

Contact resonance force microscopy (CR-FM) has been used to evaluate the effect of MAPP (maleated polypropylene) concentration on interphase thickness as well as the spatial distribution of mechanical properties within the interphase of cellulose fiber reinforced PP (polypropylene) composites. The average interphase thickness thus obtained was (25 ± 10) nm, (44 ± 11) nm, (54 ± 23) nm, and (104 ± 22) nm for composite specimens prepared with 0 %, 2.5 %, 5 %, and 10 % MAPP, respectively. The interphase region showed a gradient in elastic modulus, with a gradual decrease in modulus from fiber to matrix. The interphase region in the specimen containing 0 % MAPP showed a narrow interphase with steep gradient in modulus from fiber to matrix, while use of MAPP significantly increased the interphase thickness, resulting in a more gradual change in modulus from fiber to matrix.

Keywords: Interphase, coupling agent, modulus, modulus image, phase image

4.2. Introduction

The structural integrity of a composite mainly depends on the quality of stress transfer across the interphase. Extending over lengths from nanometers to micrometers, a well-engineered interphase is essential to obtain fiber-reinforced polymer composites with the desired mechanical properties (Mohanty et al., 2001). Although many researchers have studied the effect of interphase on the bulk properties of composites, very little research has been done on the nanoscale properties of the interphase. Previous research on interphase characterization has consisted mostly of fiber pull-out tests (Stambolis et al., 1999), fragmentation tests (Joffe et al., 2003; Torres and Cubillas, 2005), nanoindentation (NI) (Lee et al., 2007), and nanoscratching (Hodzic et al., 2000), but all of these were either single-fiber microcomposite tests or on micrometer length scales. The advent of scanning probe microscopy (SPM), which has the ability to probe materials with nanoscale spatial resolution, has allowed more research focused directly on the interphase. Because SPM measurements can involve complex geometric considerations, it has proven difficult to obtain quantitative data (Munz et al., 1998). Few reports exist in the literature concerning interphases with sub-100 nm widths, especially with quantitative mechanical information. This lack of quantitative data for interphase mechanical properties is a major barrier to success for natural fiber reinforced polymer composites (NFRPCs), where the incompatibility between the hydrophilic natural fiber and the hydrophobic polymer results in a narrow interphase (Nair et al., 2010). Growing environmental awareness has increased the use of natural fibers as reinforcing agents to produce polymer composites that are more environmentally friendly with respect to recyclability (George et al., 2001). Natural

fibers have various other advantages compared to conventional reinforcing fibers like glass, aramid, and carbon, including: low cost, ready availability, low density, high toughness, acceptable specific strength, reduced machine wear, reduced dermal and respiratory irritation, high degree of flexibility, improved acoustic insulation, and biodegradability (Karnani et al., 1997; Lee et al., 2006; Terenzi et al., 2007). In combination, all these factors have prompted a number of industrial sectors, especially the automotive industry, to consider natural fibers as a substitute for synthetic fibers in various products. Natural fiber-reinforced polymer composites (NFRPCs) therefore represent one of today's fastest-growing industries.

An interphase with lower modulus than the surrounding polymer results in low composite strength but greater resistance to fracture (Drzal, 1986; Williams et al., 1990). On the other hand, an interphase with higher modulus than the surrounding polymer results in lower fracture resistance but greater strength (Drzal et al., 1983). A stiffer interphase is more effective for strain development within the fiber and improves reinforcement. At the same time, a brittle interphase can fail catastrophically, because there is no barrier for crack propagation and hence no means of stress relief. A ductile interphase can yield and protect the fiber from crack propagation in the matrix, thereby saving the composite from premature fracture. Therefore a proper balance between interphase stiffness and ductility is critical for optimizing the design of composites with the desired mechanical properties (Lane et al., 1999). Furthermore, the interphase thickness plays a major role in the rate of stress transfer from the matrix to the fiber (Haynes et al., 2001). All these factors emphasize the importance of quantifying the interphase properties in order to optimize the final design of composites.

A variety of coupling agents have been used in NFRPCs to enhance the adhesion between the natural fiber and the matrix. Maleated polypropylene (MAPP) and silane coupling agents

have been widely used in NFRPC to enhance the tensile properties (Karnani et al., 1997). The use of coupling agents such as maleic anhydride grafted styrene-ethylene-butylene-styrene (MA-SEBS) and ethylene propylene diene terpolymer (EPDM) has very little effect on composite tensile properties but substantially improves impact toughness (Wu et al., 1999). However, earlier research did not quantify the spatial distribution of mechanical properties within the interphase, which ultimately affects the macroscale properties. Many studies have used nanoindentation (Gao and Mader, 2002) and nanoscratching (Hodzic et al., 2000) techniques to characterize the interphase and to measure interphase mechanical properties in various synthetic fiber reinforced thermoset matrix composites. These methods were found to be ineffective in NFRPCs due to the narrow width of the interphase (Lee et al., 2007).

In this chapter, we investigate the effect of MAPP concentration on the spatial distribution of mechanical properties within the interphase of natural fiber reinforced composites. We also study the effect of MAPP concentration on interphase thickness. Measurements are performed with contact resonance force microscopy (CR-FM) (Hurley, 2009; Hurley et al., 2007), a dynamic atomic force microscopy (AFM) approach. CR-FM enables quantitative imaging or mapping of the spatial distribution in mechanical properties with nanoscale spatial resolution. AFM phase imaging (AFM-PI) was also used to qualitatively evaluate the variation of properties within the interphase region.

4.3. Experimental

4.3.1. Materials and sample preparation

Isotactic polypropylene (PP) (Exxon Mobil Corporation, Irving, TX) with a melt flow index of 35 and maleated polypropylene (MAPP) (Epolene G-3003, Eastman Chemicals, Kingsport, TN) were used. Quantities of PP and MAPP were mixed in the dry solid state with an extruder (HAAKA MiniLab, Thermo Fischer Scientific, Karlsruhe, Germany). The temperature, rotation speed, and processing period were 180^0C, 100 rpm, and 10 min, respectively. Mixtures containing 0 %, 2.5 %, 5 %, and 10 % MAPP by weight were obtained. The dry mixtures were compression molded into films approximately 0.25 mm thick. Commercial regenerated cellulose fibers (Lyocell, Lenzing AG, Lenzing, Austria) approximately 10 µm in diameter and 30 mm long were placed unidirectionally on top of the PP-MAPP films. The fibers were placed in between the polymer films one on top and one on bottom and were then stacked and compression molded at 200^0C for 10 min and then cold water was used to cool down the mold temperature to 32^0C under pressure in order to obtain unidirectional lyocell fiber-reinforced composites (Nair et al., 2008). The samples were embedded in an epoxy medium under vacuum and cured by heating and drying for 8 h at 70^0C (Spur, 1969). A cross section of each sample was prepared with an ultramicrotome with a diamond knife. The ultramicrotome process yielded sufficiently smooth surfaces for AFM and CR-FM experiments (Kim et al., 2001).

4.3.2. Nanoindentation techniques

Displacement-controlled nanoindentation (Triboindenter, Hysitron, Eden Prairie, MN) was used to determine values for the indentation modulus of the lyocell fibers and the PP matrix. The indenter tip was loaded to a maximum displacement h_{max} = 250 nm. The indentation modulus

of the sample was then inferred from the initial unloading contact stiffness *S* (*i.e.*, the slope *dP/dh* of the tangent to the initial unloading curve in the load-displacement curve, where *P* is the indentation force and *h* is the displacement). The sample reduced indentation modulus E_r was then calculated from Eq (3.1) (Oliver and Pharr, 1997).

Finally, the plane strain or indentation modulus M_s of the sample was obtained from Eq (3.2). The average indentation modulus reference values for the composites obtained across all samples by nanoindentation on the fiber and matrix were M_{fiber} = (13.1 ± 0.8) GPa and M_{matrix} = (3.2 ± 0.2) GPa, respectively.

4.3.3. CR-FM techniques

Contact resonance force microscopy (CR-FM) is based on the atomic force acoustic microscopy (AFAM) method (Hurley et al., 2003; Rabe et al., 2000) and is used for quantitative imaging of nanoscale elastic properties (Hurley, 2009; Hurley et al., 2007). A schematic of the experimental apparatus is shown in Figure 3.1. CR-FM experiments involve measuring the resonance frequency of the vibrating AFM cantilever in free space and when the tip is contact with the sample. The contact stiffness k* that describes the elastic interaction between the tip and the sample is then determined from the resonance frequencies. Finally, the indentation modulus M_s of the sample is determined from the contact stiffness with use of a model for the tip-sample contact mechanics (Hurley, 2009; Hurley et al., 2003). Detailed descriptions of the theoretical and experimental methods for determining the elastic properties are available elsewhere (Hurley, 2009; Hurley et al., 2007).

The AFM cantilevers used in these CR-FM experiments had nominal dimensions of

length L = 225 µm, width w = 30 µm, and thickness t = 3 µm, and a nominal spring constant k_c = 2.8 N/m. The applied static force F_N was approximately 50 nN to 80 nN. Frequency images were acquired for the second flexural eigenmode of the cantilever, because it is the most sensitive mode for these experimental conditions (*i.e.*, showing the greatest change in contact resonance frequency for a given change in contact stiffness) (Hurley, 2009). Images of the normalized contact stiffness $k = k^*/k_c$ for the sample were calculated from the contact resonance frequency images, and mean values were determined for the normalized contact stiffness k_{fiber} of the fiber and k_{matrix} of the matrix in each image. Finally, the contact stiffness images were used to calculate images of the indentation modulus M_{test} with use of a dual reference approach (Stan and Price, 2006) using Eq (3.4).

4.3.4. AFM-PI techniques

Phase images were obtained with True Noncontact AFM mode (XE-100, Park Systems, Suwon Korea). Noncontact AFM (NC-AFM) is one of several AFM methods in which the cantilever is oscillated near the surface of a sample. In NC-AFM, the spacing between the tip and the sample is on the order of one to ten nanometers. NC-AFM monitors the phase shift data obtained from the images. Phase shift is defined as the phase lag between the sinusoidal excitation signal and the resulting cantilever oscillation signal. Changes in phase angle reveal differences in the surface properties of the material (Lee et al., 2009). The AFM cantilevers used in these experiments had nominal dimensions L = 225 µm and w = 40 µm, tip radius of curvature 10 nm or less, and k_c = 48 N/m. The resonant frequency of the cantilever was approximately 190 kHz.

4.4. Results and Discussion

Figure 4.1 shows the AFM topography image of a lyocell fiber reinforced polypropylene composite sample. Contact resonance frequency images were obtained at the interfacial region between the fiber and matrix. In order to minimize topography effects, regions between the fiber and matrix approximately 1 mm x 1 mm that were as flat as possible (height differences of ~20 nm or less) were selected for imaging.

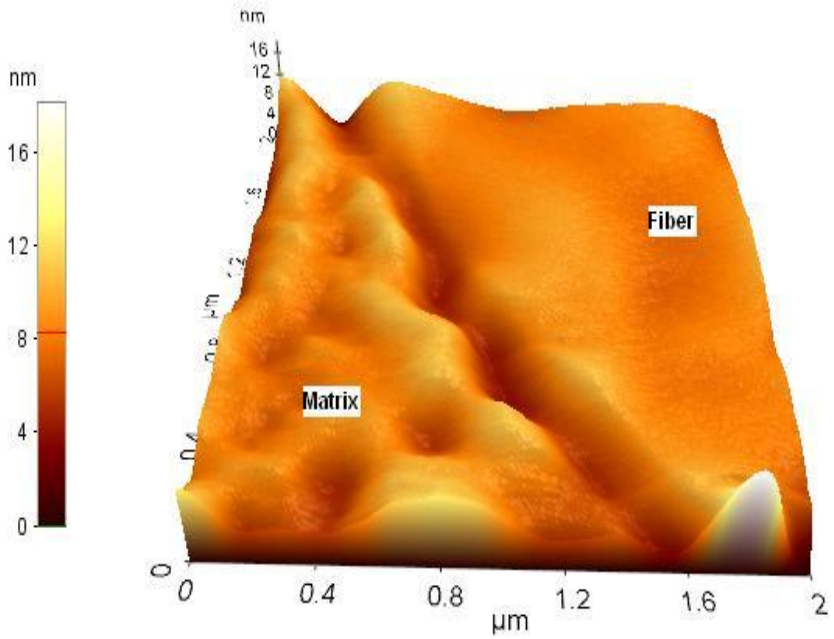

Figure 4.1. Example of AFM topography image of cellulose fiber reinforced polypropylene composite sample

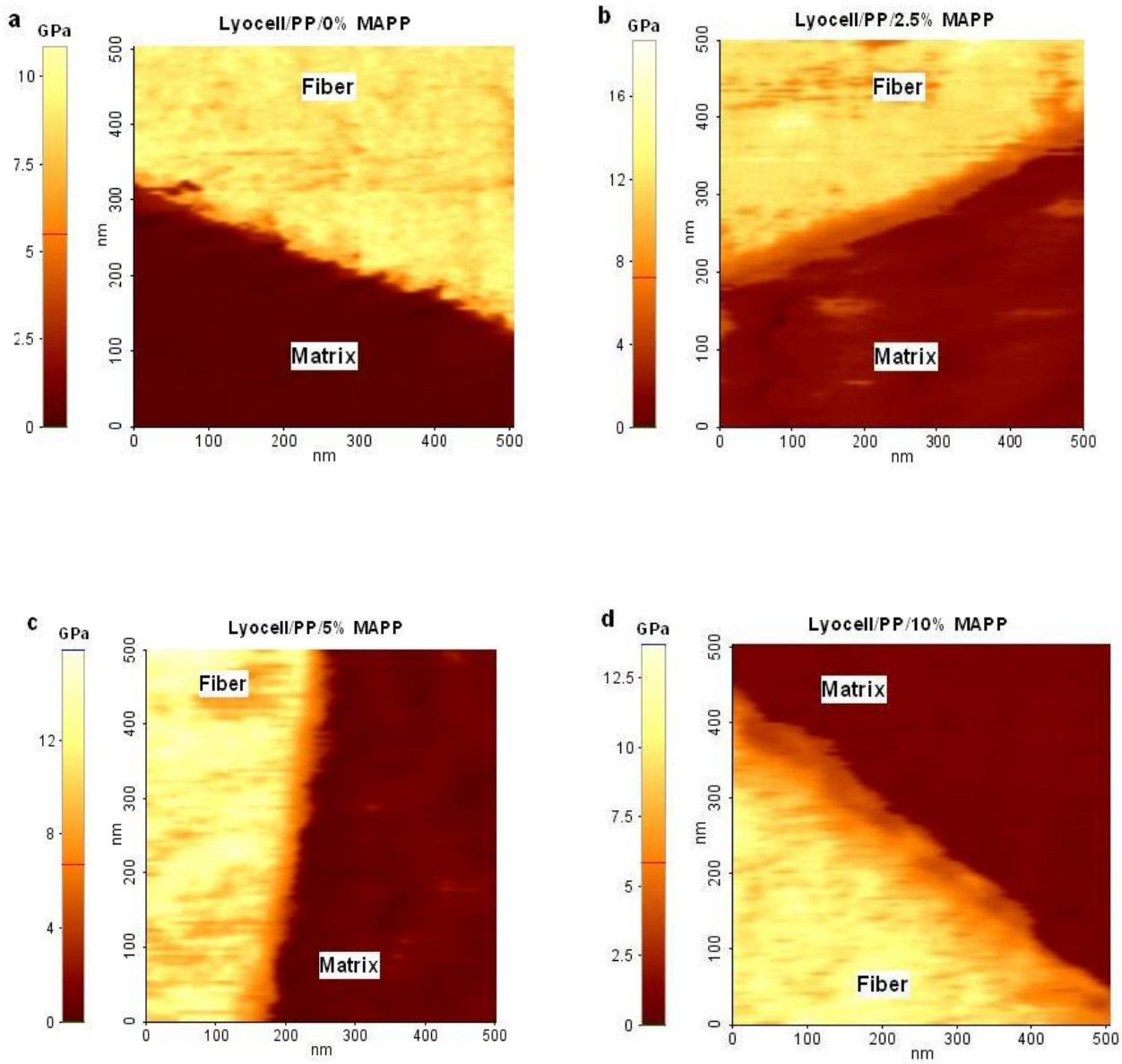

Figure 4.2. CR-FM images of indentation modulus for cellulose/PP composites with (a) 0 %, (b) 2.5 %, (c) 5 %, and (d) 10 % MAPP treatment

Figure 4.2 shows CR-FM modulus maps for each of the four composite samples with different treatments. The images clearly show that a region with intermediate modulus exists between the matrix and the fiber. This region between the matrix and the fiber, where the local properties are different from those of the bulk fiber and the matrix, is defined as the interphase (Drzal 1986). The average interphase thickness around the fiber was determined by a statistical analysis of the CR-FM modulus maps with use of image processing XEP software (Park Systems, Suwon, South Korea). Radial lines were drawn across the fiber-matrix boundary for each image. Each line showed a gradient of modulus across the interphase region that ranged between the modulus values of the fiber and the matrix. Figure 4.3 shows an example profile for a radial line across the fiber-matrix boundary. The mean μ, standard deviation σ, and the control limits $\pm 3\sigma$ for the fiber and matrix were obtained for each line profile. The control limits were extended until they intersected the data in order to define an interphase region where the indentation modulus value ranged from $\mu_m + 3\sigma_m$ to $\mu_f - 3\sigma_f$. The subscripts "m" and "f" refer to the polymer matrix and the fiber, respectively. This approach was applied to 15 radial lines across the fiber-matrix boundary for each image to determine the average interphase thickness.

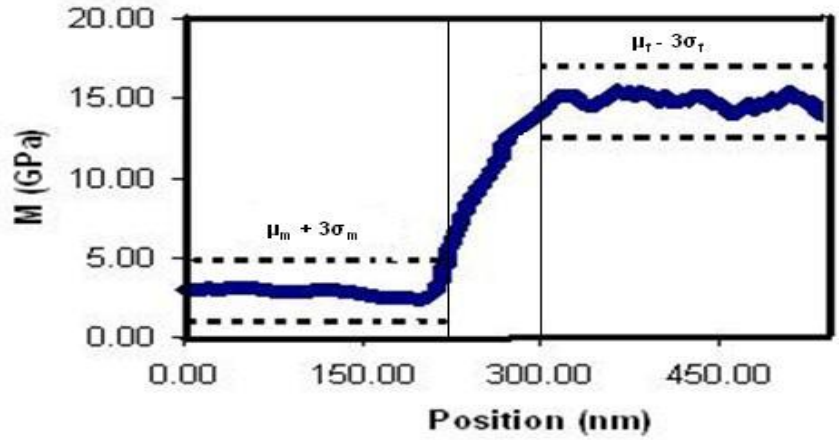

Figure 4.3. Example of radial line profile across the fiber-matrix boundary obtained from a CR-FM modulus map. The modulus profiles showing the fiber (μ_f - $3\sigma_f$) and matrix (μ_m + $3\sigma_m$) regions between the dashed lines and the interphase region between the vertical lines (between the fiber and matrix regions)

Table 4.1. Percentage of MAPP treatment and corresponding interphase thickness determined from CR-FM modulus maps for cellulose fiber polypropylene composites

wt. % MAPP	**Average interphase thickness (nm)**
0	25 ± 10
2.5	44 ± 11
5	54 ± 23
10	104 ± 22

Table 4.1 shows values for the average and uncertainty in interphase thickness for each treatment. The uncertainty represents one standard deviation in the individual measurements. The values ranged from 25 nm to 104 nm or different concentrations of MAPP. The average interphase thickness was found to increase with increasing MAPP concentration. This is not entirely surprising; a number of previous studies have observed interphase thickness to vary with the concentration of coupling agents such as MAPP. Lee et al. (2009) used AFM-PI to show qualitatively that MAPP as a compatibilizer in a lyocell/polypropylene composite increased the interphase thickness. Combined use of MAPP and γ-amino propyltrimethoxy silane (γ-APS) further increased the thickness. With AFM nanoindentation, Gao et al. (2002) showed that an epoxy polymer matrix did not form a measurable interphase around unsized glass fibers, while use of γ-APS/polyurethane as a coupling agent yielded an interphase with measurable thickness. Kim et al. (2001) used AFM-PI and Griswold et al. (2005) used nanoscratching in other studies on glass fiber composites. Both found that the interphase thickness increased with increasing concentration of silane as a coupling agent.

In order to further characterize the interphase, representative modulus profiles were obtained by averaging the 15 individual line scans. Figure 4.4 shows these profiles for each sample. The line profiles within the vertical dotted lines correspond to the average modulus profiles of the interphase region for each treatment. The vertical dotted lines indicate the location of the control limits $\mu_m + 3\sigma_m$ and $\mu_f - 3\sigma_f$. Values for the slope and coefficient of determination R^2 for a linear fit across the interphase region are also indicated. In the profile in Fig. 4.4 (a) for the 0 % MAPP sample, the interphase thickness is quite small. As a consequence, there is a sharp spatial gradient in modulus (steeper slope) between the fiber and the matrix that can easily cause the fiber to debond from the matrix under stress, resulting in poor overall mechanical properties.

Use of MAPP was found to significantly increase the interphase thickness, resulting in a more gradual gradient in modulus from fiber to matrix. This behavior was most prominent in the sample containing 10 % MAPP, which had the widest interphase. From the average profiles, it is quite evident that the interphase region accounts for the entire modulus gradient from fiber to matrix. The interphase region showed a gradient in modulus that could be described to first order by a linear fit, with a gradual decrease in modulus from fiber to matrix. Also, it is quite evident that the interphase thickness accounts for the majority of property variations within the interphase for different treatments.

Use of small AFM tips (estimated tip radius of curvature 25 nm to 35 nm after use) and low forces (50 nN to 80 nN) in the CR-FM experiments ensured that the deformation of the sample surface was very small and elastic, which prevented or at least minimized the so-called boundary effect. Indentation on a material creates a corresponding stress field, *i.e.*, a zone associated with plastic deformation. The presence of a fiber or a successive indent in close

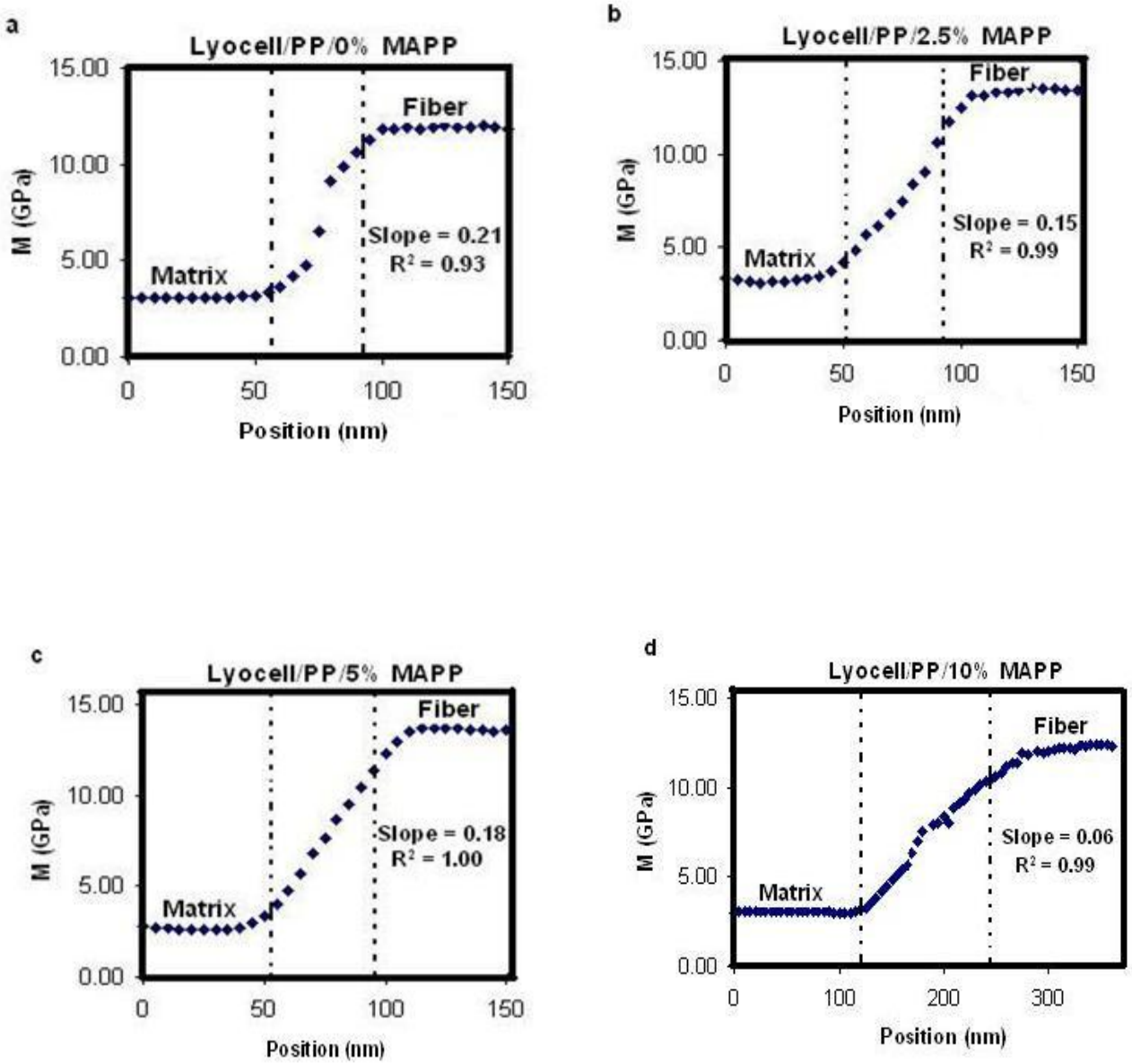

Figure 4.4. Average modulus profiles obtained for cellulose/PP composites with (a) 0 %, (b) 2.5 % , (c) 5 % , and (d) 10 % MAPP treatment

proximity to the first indent without proper spacing to avoid overlapping of the plastic zone of neighboring indent results in increasing the resistance to indentation. This is known as boundary effect. Methods such as nanoindentation (Lee et al., 2007) and nanoscratching (Hodzic et al., 2000) to characterize the interphase often exhibit such boundary effects and can lead not only to false modulus values within the interphase but also to overestimates of the interphase width. By using CR-FM methods that operate in the elastic regime, we were able to characterize interphases as narrow as 25 nm.

The distribution of modulus within the interphase obtained by CR-FM was qualitatively confirmed by AFM-PI. Figure 4.5 shows phase images and representative line profiles for the composite samples without MAPP treatment and with 10 % MAPP. The phase shift images clearly differentiate the fiber, interphase, and matrix regions. Phase shifts are obtained due to changes in the tip-sample force caused by differing mechanical properties of the sample surface and are a particularly sensitive way to detect qualitative local stiffness variations in the surface (Lee et al., 2009). In addition to surface elastic properties, adhesion, viscoelasticity, and hydrophilicity/hydrophobicity also contribute to the phase lag. In Figure 4.5 matrix regions showed the greatest phase shifts relative to fiber and interphase and appeared brighter in the images, while fiber regions showed the least relative phase shift and appeared darker in the images. The region between the cursors corresponds to the interphase. Interphase regions showed relative phase shifts between those of matrix and fiber, suggesting that the interphase showed surface properties different from that of fiber and matrix. The variation of properties across the interphase region was qualitatively similar to that of the modulus variations observed in the CR-FM images.

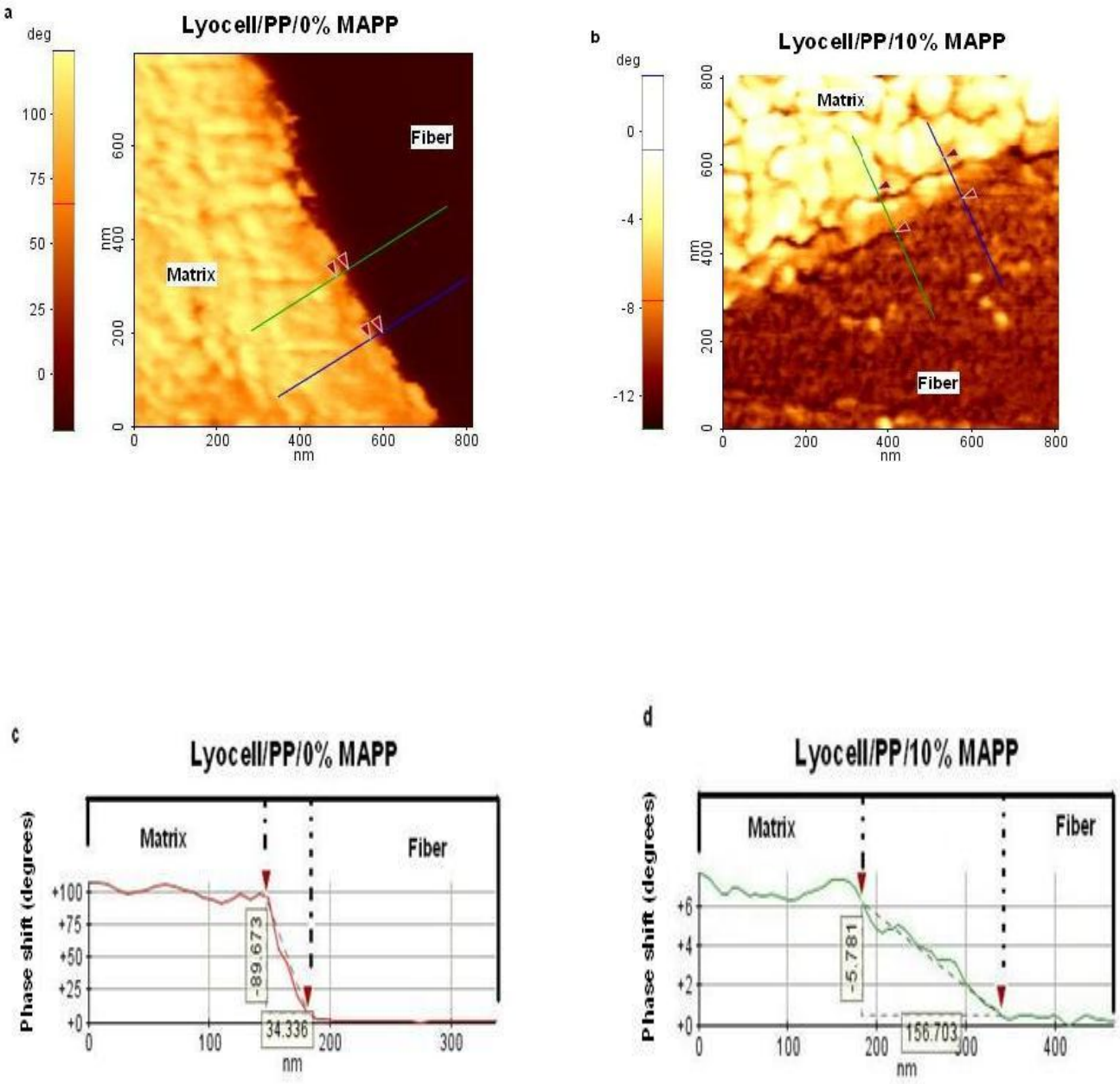

Figure 4.5. Phase images and average phase shift profiles for composite samples with 0 % MAPP [(a) and (c)] and 10 % MAPP [(b) and (d)] treatment

The interphase thickness was analyzed with XEP software. The statistical method used to calculate the interphase thickness for the CR-FM image was found to be ineffective for phase images due to increased scatter in the phase shift images. This is thought to be due primarily to the increased sensitivity of noncontact phase imaging to surface roughness compared to contact methods such as CR-FM (Lee et al., 2009). Mean phase shifts for the fiber and matrix regions were obtained from areas consisting entirely of fiber and matrix away from the fiber–matrix interface area. Fifteen radial lines were drawn across the fiber- matrix boundary for each image. Each line showed a gradient of phase shifts across the interphase region that ranged between the mean values for pure fiber and pure matrix. For each line, the interphase starts from some point next to the fiber, where the phase shift value changes from that of the bulk fiber value, and extends until the phase shift value equal the bulk matrix value. The average interphase thickness was obtained by averaging these line scans. The average thickness was (34 ± 15) nm and (157 ± 35) nm for the composites made with 0 % and 10 % MAPP, respectively. These thickness values are not as accurate as the values obtained from the CR-FM images, mainly due to differences in the statistical analysis approach. However, the trends of increasing interphase thickness with increasing MAPP concentration and property variations with the interphase region are clearly evident.

MAPP lowers the surface tension of natural fibers such as lyocell, making the surface tension closer to that of molten polymer. This results in better wetting and adhesion of the fiber to the matrix via mechanisms such as chemical bonding, interdiffusion, and mechanical interlocking (Arbelaiz, 2005). The anhydride group of MAPP forms covalent bonding through esterification and hydrogen bonding with cellulose fibers. Due to its similarity to bulk polymer matrix, the grafted PP in MAPP permits segmental crystallization and thus cohesive coupling

through entanglement of its macromolecular chains (Felix and Gateholm, 1993). Image J (Rasband, 1997) processing software was used to obtain the outline of the interphase. With the software, an outline was made that included all the pixels in the image with modulus values different from those of both the bulk fiber and the matrix. Figure 4.6 shows images with the outline of the interphase for samples with varying amounts of MAPP. It is quite clear that the interphase increased with the addition of MAPP. For the treated samples, the edge of the interphase that bordered the fiber was much more irregular than the edge next to the matrix. This could be due to differences in the reaction processes with MAPP that occur on the fibers and matrix. Chemical linkages on the fiber surface could contribute to a stiffer region of the interphase close to the fiber, and more physical entanglements or physisorbed regions close to the matrix could be the reason for a softer region there. Attempts to characterize the interphase in glass/polymer composites have also shown that the occurrence of chemically reacted sites close to the fiber forms stiffer regions, and that the stiffness decreases as the distance from the fiber increases due to physisorbed regions (Hodzic et al., 2001).

The mechanical properties of the interphase are very important for the final performance of composite. Figure 4.2 shows that the interphase region is stiffer than the matrix. Hayes et al., 2001 used finite element analysis to show that at low applied strains in the elastic limit, the strain transfer depended on the properties of both the matrix and the interphase. It was found that for stiff interphases, increasing the interphase width increased the strain rate. At higher applied strains, the yield was not restricted to the interphase but extended to the more compliant matrix in the presence of stiffer interphase, which further proceed the fragmentation process. This effect was found to increase with interphase thickness. Thus, an increase in MAPP concentration can enhance the strength by increasing the interphase thickness. However, use of MAPP has shown a

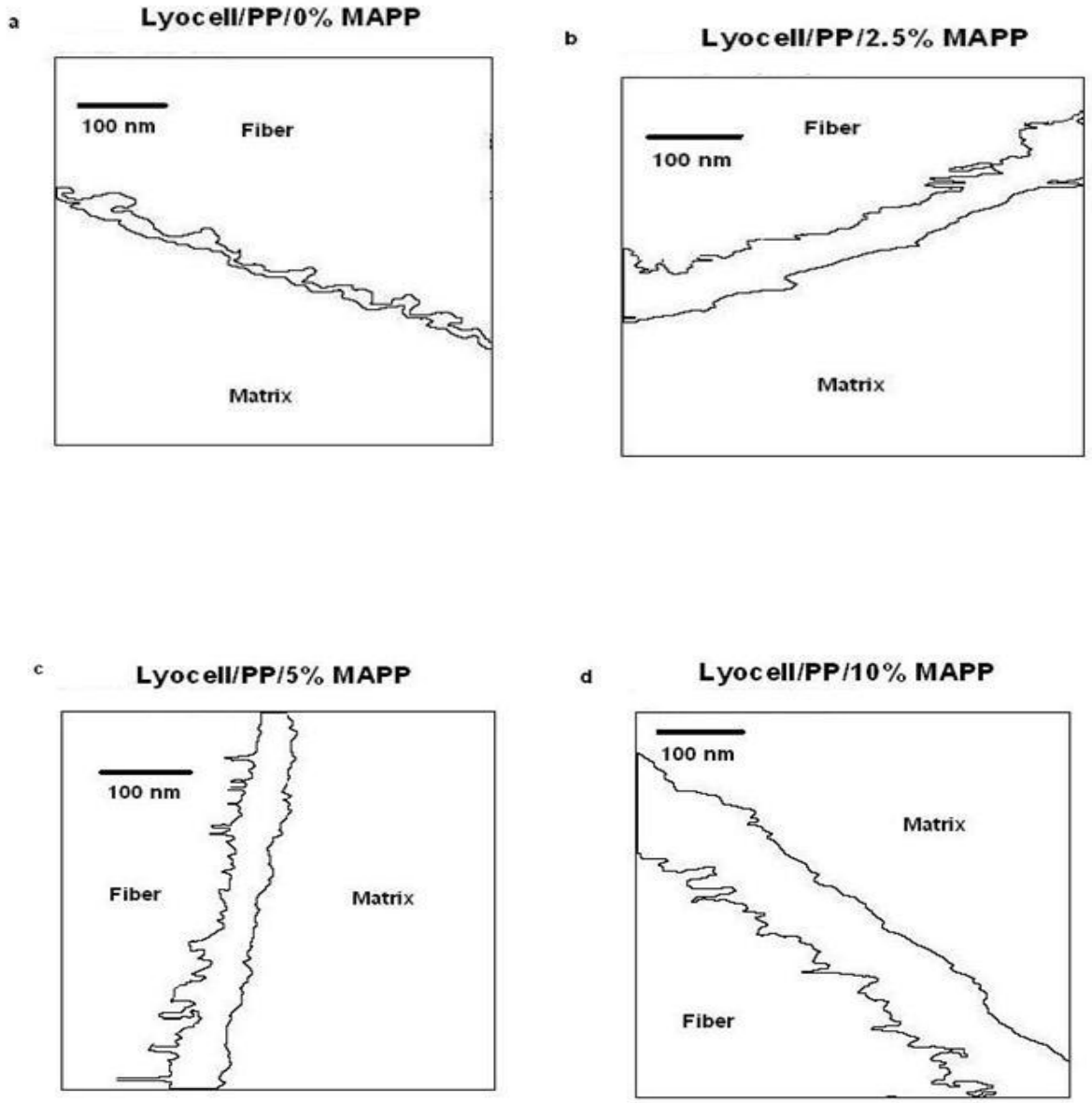

Figure 4.6. Interphase outlines as described in the text for cellulose/PP composites with (a) 0 %, (b) 2.5 %, (c) 5 %, and (d) 10 % MAPP treatment

negative effect on impact toughness in comparison to other elastomer coupling agents like MA-SEBS and EPDM. These elastomers form a more ductile interphase that improves toughness (Oksman and Clemons, 1997). Composites in which the interphase and matrix have sufficient ductility and modulus can yield during the deformation process due to increased stress concentration, resulting in a tougher composite (Goh et al., 2004; Wu et al., 1998).

4.5. Conclusions

Understanding the mechanical properties of the fiber-matrix interphase is critical for the manufacture of composites with desired properties. A significant issue with many AFM methods is their lack of ability to obtain quantitative information about mechanical properties within the nanoscale interphase. In this work, we used CR-FM, a dynamic mode of contact AFM, to obtain quantitative modulus maps of the composite interphase region with nanoscale spatial resolution. We investigated the effect of maleated polypropylene (MAPP) concentration on the interphase characteristics of cellulose fiber-PP fiber composites. From the CR-FM modulus maps, values for the average interphase thickness as well as the spatial distribution of elastic modulus values within interphase were determined. The average interphase thickness was found to increase from 25 nm to 104 nm as the MAPP concentration increased from 0 % to 10 %. The interphase region showed a gradient in modulus that could be described to first order by a linear fit, with a gradual decrease in modulus from fiber to matrix. The modulus distribution within the interphase region as well as the variation in interphase thickness with MAPP concentration was confirmed by qualitative images obtained by noncontact AFM phase imaging. The results of this study provide valuable information to improve the design of NFRPC products that use MAPP as coupling agent.

4.6. References

Arbelaiz A, Fernandez B, Ramos JA, Retegi A, Llano-Ponte R, Mondragon. Mechanical properties of short flax fibre bundle/polypropylene composites: Influence of matrix/fibre modification, fibre content, water uptake and recycling. Comp Sci Tech 2005;65:1582-1592.

Drzal LT, Rich MJ, Koenig MF, Lloyd PF. Adhesion of graphite fibers to epoxy matrices: 11. The effect of fiber finish. J Adhes 1983;16(2):133–152.

Drzal LT. The interphase in epoxy composites. Adv Polym Sci 1986;75:1–32.

Felix JM, Gateholm P. Formation of entanglements at brushlike interfaces in cellulose-polymer composite. J Appl Polym Sci 1993;50:699-708.

Gao S-L, Mader E. Characterization of interphase nanoscale property variations in glass fibre reinforced polypropylene and epoxy resin composites. Compos Part A: Appl Sci Manfact 2002;33:559-576.

George J, Sreekala MS, Thomas S. A review on interface modifications and characterization of natural fiber reinforced plastic composites. Polymer Engineering and Science 2001;41:1471-1485.

Goh KL, Aspden RM, Hukins DWL. Review: finite element analysis of stress transfer in short-fibre composite materials. Comp Sci Tech 2004;64:1091-1100.

Griswold C, Cross WM, Kjerengtroen L, Kellar JJ. Interphase variation in silane-treated glass-fiber-reinforced epoxy composites. J Adhesion Sci Technol 2005;19(3-5):279-290.

Hayes SA, Lane R, Jones FR. Fibre/matrix stress transfer through a discrete interphase. Part 1: single-fibre model composites. Compos Part A: Appl Sci Manfact 2001;32:379-389.

Hodzic A, Stachurski ZH, Kim JK. Nano-indentation of polymer-glass interfaces. Part 1: experimental and mechanical analysis. Polymer 2000;41:6895-6905.

Hodzic A, Kim JK, Stachurski ZH. Nano-indentation and nano-scratch of polymer/glass interfaces. 11: model of interphase in water aged composite materials. Polymer 2001;42:5701-5710.

Hurley DC, Shen K, Jennett NM, Turner JA. Atomic force microscopy methods to determine thin film elastic properties. J App Phy 2003;94(4):2347-2354.

Hurley DC, Kopycinska-Müller M, Kos AB. Mapping mechanical properties on the nanoscale with atomic force acoustic microscopy. JOM 2007;59**:** 23-29.

Hurley DC. Contact Resonance Force Microscopy Techniques for Nanomechanical Measurements. Applied Scanning Probe Methods Vol. XI, eds. Bhushan B, Fuchs H. Springer-Verlag, Berlin, 2009; 5: 97-138.

Joffe R, Andersons J, Wallstrom L. Strength and adhesion characteristics of elementary flax fibers with different surface treatments. Compos Part A: Appl Sci Manfact 2003;34:603-612.

Karnani R, Krishnan M, Narayan R. Biofiber-reinforced polypropylene composites. Polymer Engineering and Science 1997;37(2):476–483.

Kim JK, Sham ML, Wu J. Nanoscale characterization of interphase in silane treated glass fibre composites. Compos Part A: Appl Sci Manfact 2001;32:607-618.

Lane R, Hayes SA, Jones FR. Modelling the efficiency of strain transfer across an interphase region in fibre reinforced composites. Composite Interfaces 1999;6(5):425-440.

Lee SH, Wang S. Biodegradable polymers/bamboo fiber biocomposite with bio-based coupling agent. Compos Part A: Appl Sci Manfact 2006; 37(1): 80-91.

Lee SH, Wang S, Pharr GM, Xu H. Evaluation of interphase in a cellulose fiber reinforced polypropylene composite by nanoindentation and finite element analysis. Compos Part A: Appl Sci Manuf 2007;38:1517–24.

Lee SH, Wang S, Takashi E, Kim NH. Visualization of interfacial zones in lyocell fiber-reinforced polypropylene composite by AFM contrast imaging based on phase and thermal conductivity measurements. Holzforschung 2009;63:240-247.

Mohanty AK, Misra M, Drzal LT. Surface modifications of natural fibers and performance of the resulting biocomposites: an overview. Compos Interfaces 2001;8(5):313–43.

Munz M, Sturm H, Schulz E, Hinrichsen G. The scanning force microscope as a tool for the detection of local mechanical properties within the interphase of fiber reinforced polymers. Compos Part A: Appl Sci Manfact 1998;29:1251-1259.

Nair SS, Wang S, Hurley DC. Evaluation of interphase properties in fiber reinforced polymer composite using contact resonance force microscopy. In: Proceedings of the 51st annual meeting of the society of wood science and technology (Concepción, Chile, 10–12 November 2008).

Nair SS, Wang S, Hurley DC. Nanoscale characterization of natural fibers and their composites using contact-resonance force microscopy. Compos Part A: Appl Sci Manfact 2010; 41: 624-631.

Oksman K, Clemons C. Mechanical properties and morphology of impact modified polypropylene-wood flour composites. J Appl Polym Sci 1997;67:1503-1513.

Oliver WC, Pharr GM. An improved technique for determining hardness and elastic modulus using load and displacement sensing indentation experiments. J Mater Res 1997;7(6):1564-1583

Rabe U, Amelio S, Kester E, Scherer V, Hirsekorn S, Arnold W. Quantitative determination of contact stiffness using atomic force acoustic microscopy. Ultrasonics 2000;38:430-437.

Rasband WS. ImageJ, U. S. National Institutes of Health, Bethesda, Maryland, USA, http://imagej.nih.gov/ij/, 1997-2011.

Spur AR. A low-viscosity epoxy resin embedding medium for electron microscope. J Ultrastruct Res 1969;26:31-43.

Stamboulis A, Baillie C, Schulz E. Interfacial characterization of flax fibre-thermoplastic polymer composites by the pull-out test. Die Angewandte Makromolekulare Chemie 1999; 272: 117-120.

Stan G, Price W. Quantitative measurements of indentation moduli by atomic force acoustic microscopy using a dual reference method. Rev Sci Instr 2006;77:103707.

Terenzi A, Kenny MJ, Barbosa SE. Natural fiber suspensions in thermoplastic polymers. 1. Analysis of fiber damage during processing. Journal of Applied Polymer Science 2007;103: 2501-2506.

Torres FG, Cubillas ML. Study of the interfacial properties of natural fiber reinforced polyethylene. Polymer Testing 2005;24:694-698.

Williams JG, Donnellan ME, James MR, Morris WL. Properties of the interphase in organic matrix composites. Mater Sci Eng A 1990;126:305–312.

Wu W, Verpoest I, Varna J. An improved analysis of the stresses in a single-fibre fragmentation test-11. 3-Phase model. Comp Sci Tech 1998;58:41-50.

Wu J, Yu D, Chan C M, Kim J, Mai Y W. Effect of fiber pretreatment condition on the interfacial strength and mechanical properties of wood fiber/pp composites. Journal of Appl Poly Sci 1999;76:1000-1010.

CHAPTER 5. EFFECTS OF MAPP AND MA-SEBS MODIFICATIONS ON THE MACROSCALE PERFORMANCE OF NATURAL FIBER REINFORCED POLYMER COMPOSITES

5.1. Abstract

Contact-resonance force microscopy (CR-FM) modulus images were obtained at the interphase regions of natural fiber reinforced polymer composites made with different concentrations of maleic anhydride grafted polypropylene (MAPP) and maleic anhydride grafted styrene-ethylene/butylene-styrene (MA-SEBS) coupling agents. The images clearly showed the difference in modulus values for fiber, fiber-matrix boundary zone, and matrix regions. The interphase thickness was found to be 30.5 ± 2.6 nm, 100 ± 12.4 nm, and 70.3 ± 20.6 nm for the composites made with 0 %, 2.5 %, and 10 % MAPP, respectively and 79.1 ± 15.2 and 100.1 ± 34.7 for composites made with 5% and 10% MA-SEBS, respectively. The interphase thickness was found to increase with increasing the MAPP concentration from 0 % to 2.5 %, but further addition of MAPP did not have any effect on the average interphase thickness. The interphase thickness was found to increase with the increasing MA-SEBS concentration. The interphase region showed a gradient in modulus that could be described to first order by a linear fit, with a gradual decrease in modulus from fiber to matrix. Also, it is quite evident that the interphase thickness accounts for the majority of property variations within the interphase for different treatments. Composites made without any coupling agent showed a very thin interfacial zone with an abrupt change in modulus from fiber to matrix. These composites had the least interaction between the fiber and matrix. There was significant increase of tensile strength with the addition 2.5 wt% of MAPP. The average interphase thickness increased with the addition of 2.5 % MAPP and further addition to 10% MAPP decreased the average interphase thickness of the composites. There was a strong correlation between the tensile strength and interphase thickness for lyocell/PP/MAPP composites. Multivariate analysis using FTIR indicated the presence of ester bonds in the interphase use of MAPP and MA-SEBS. From the CR-FM and

FTIR results, it was quite clear that the excess amount of MAPP was on the PP matrix than on interphase for 10% MAPP composites. The average interphase thickness increased with the addition of 5 % MA-SEBS and further addition to 10% MAPP increased the average interphase thickness of the composites. However, the tensile strength was not a direct reflection of interphase thickness in MA-SEBS treated composites. The use of MA-SEBS leads to the formation of separate domains on the polypropylene matrix.

Keywords: Interphase, Contact-resonance force microscopy, Indentation modulus, Nano characterization, Tensile strength, Impact strength

5.2. Introduction

The structural integrity of a composite mainly depends on the quality of stress transfer in the interphase. Although various researchers have focused on the effect of interphase on the bulk properties of composites, very little research has been done to characterize and provide quantitative measurements in the interphase. Previous research on interphase characterization has consisted mostly of fiber pull out tests (Stamboulis et al., 1999), fragmentation test (Joffe et al., 2003; Torres and Cubillas, 2005), nanoindentation (NI), and nanoscratching (Hodzic et al., 2000), but all of them were either single fiber tests or on micrometer or submicrometer length scales. With the advent of scanning probe microscopy (SPM), which has the ability to probe materials in the nanoscale, more researches have been focused on interphase. Since measurements using SPM involve complex geometric considerations, it has proved very difficult to obtain quantitative data (Munz et al., 1998). Interphase of less than 100 nm width with quantitative mechanical measurements at each position has rarely been reported in literatures.

This is a major limiting factor for interphase research in the case of natural fiber reinforced polymer composites (NFRPC's), where the incompatibility between the hydrophilic natural fiber and the hydrophobic polymer forms a narrow interphase. Recently, we (Nair et al., 2010; Nair et al., 2011) have used contact resonance force microscopy (CR-FM) for evaluating the interphase of NFRPCs. The nanoscale resolution of CR-FM, combined with its ability to provide quantitative modulus images, made it possible to investigate the mechanical properties of interphases as narrow as 50 nm.

An interphase that has lower modulus than the surrounding polymer results in low composite strength, but greater resistance to fracture (Drzal, 1986, William et al., 1990). On the other hand, an interphase with higher modulus than the surrounding polymer results in lower fracture resistance but greater strength (Drzal, 1983). A stiffer interphase shows more effectiveness of strain development within the fiber and can have better reinforcement efficiency than a ductile interphase and better mechanical properties. But at the same time, a brittle interphase can fail catastrophically as there is no barrier for crack propagation and hence unable to release the stress. However a ductile interphase can yield and protect the fiber form crack propagation in the matrix and thereby save the composite from an early fracture (Lane et al. 1999). Doubts still exist on the exact nature of interphase for the desirable properties. Also there is a need for understanding the influence of various interphase widths on the final composite properties. Maleated polypropylenes (MAPP) and silane coupling agents have been widely used in NFRPC to enhance the tensile and impact strength (Karnani et al., 1997). Use of coupling agents like maleic anhydride grafted styrene-ethylene-butylene-styrene (MA-SEBS) has very little effect on tensile properties while it substantially improved the impact strength (Wu et al., 1999).

Many questions need to be addressed here. How does the interphase mechanical property change for different coupling agents such as MAPP, and MA-SEBS? Does the interphase property vary for stiffer coupling agent like MAPP compared to ductile MA-SEBS? How does the spatial distribution of properties within the interphase vary for different coupling agents? Does the interphase width change with different concentrations of coupling agents? What are the effects of the interphase property on the final composite properties? What are the interphase properties needed for the optimum mechanical properties?

The above questions highlights the need for a measurement technique capable of providing quantitative information about mechanical properties with nanoscale spatial resolution, while at the same time providing images of the spatial distribution in properties. Such a technique would prove invaluable for studies of the interphase region in NFRPCs. The nanoscale resolution of CR-FM, combined with its ability to provide quantitative modulus images, made it possible to investigate the mechanical properties of interphases as narrow as 31 nm. In this study, our goal was to characterize the interphase formed of different concentrations of coupling agent and to compare its effect on the bulk mechanical properties.

5.3. Experimental

5.3.1. Materials and sample preparation

Lyocell fibers (Lenzing AG, Lenzing, Austria) approximately 10 µm in diameter and 3 mm, Isotactic PP (PP) (HGX-030-01, Phillips Chemical Company, Woodlands, TX)) with melt flow of 3.5, MAPP (Honeywell A-C 950P, Honeywell, Morristown NJ) were used. The fiber loading was kept at constant weight of 30% for every experiment. Different quantities of MAPP

used in this experiment was 0, 2.5, 5, 7.5, 10 wt % based on the weight of PP. The quantities of MA-SEBS are 5 and 10 % based on the weight of PP. Manually mixed dry solid states of PP and MAPP/MA-SEBS were mixed with fibers in a co-rotating twin screw extruder (Leistriz Extruder Corp). The temperature profile ranged from 180-190^{0}C, and the screw speed set at 70 RPM. The compounded material was immediately cooled in a water bath and pelletized. The obtained pellets were used to make injection molded tensile test specimens and impact resistance specimens defined with ASTM 638 Type IV and ASTM D 256, respectively. The barrel and mold temperatures of the pneumatic injection molder were 200^{0}C and 140^{0}C, respectively.

The samples were embedded in an epoxy medium under vacuum and cured by heating and drying for 8 h at 70^{0}C (Nair et al., 2010; Nair et al., 2011). A cross section of the sample was prepared by using an ultramicrotome with a diamond knife. The microtome process yielded sufficiently smooth surfaces for the CR-FM experiments.

5.3.2 Nanoindentation techniques

Displacement-controlled nanoindentation (Triboindenter, Hysitron, Eden Prairie, MN) was used to determine the indentation modulus of lyocell fiber and PP. The indenter tip was loaded to a maximum displacement of 250 nm. The indentation modulus of the sample was then inferred from the initial unloading contact stiffness *S*, *i.e.*, the slope *dP/dh* of the tangent to the initial unloading curve in the load-displacement curve, where *P* is the indentation force and *h* is the displacement. The sample reduced indentation modulus (E_r) is then calculated from Eq (3.1) (Oliver and Pharr 1997), where β is a constant that depends on the geometry of the indenter (β = 1.034 for a Berkovich indenter) and A is the contact area. The indentation modulus M_s of the sample is then obtained from Eq (3.2), where M_{tip} is the indentation modulus of the diamond

indenter tip. The value M_{tip} = 1146 GPa was used (Kopycinska et al 2005). The average indentation modulus reference values for the composites obtained by nanoindentation on the fiber and matrix were M_{fiber} = 14.0 ± 0.9 GPa and M_{matrix} = 3.6 ± 0.2 GPa, respectively.

5.3.3 CR-FM techniques

Contact-resonance force microscopy (CR-FM) (Rabe et al., 2000, Hurley et al., 2003) is based on the atomic force acoustic microscopy (AFAM) method. This technique has been used for quantitative imaging of the nanoscale elastic properties of the samples (Hurley, 2009). Schematic of the experimental apparatus is shown in Figure 3.1. The measurement procedure involves measuring the free and contact resonant frequencies of the vibrating AFM cantilever. The contact stiffness k^* are then determined from these resonant frequencies, describing the elastic interaction between the tip and the sample. Finally, the indentation modulus is determined from the contact stiffness with a model for the tip-sample contact mechanics. Detailed description of the theoretical and experimental methods for determining the elastic properties have been explained in detail elsewhere (Hurley, 2007; Hurley, 2009).

The AFM cantilevers used in these experiments had nominal dimensions of length L = 225 ± 10 µm, width w = 30 ± 8 µm, and thickness t = 3 ± 1 µm, and nominal spring constant k_c = 2.8 N/m. The applied static force $F_N = k_c d$, where d is the deflection, was approximately 50 nN to 80 nN. Frequency images were acquired for only one resonant mode, namely the second mode. This was to avoid the registration difficulties and artifacts due to scanner drift and hysteresis in scanning the same area twice. The second mode is the most sensitive mode for the experimental condition here. It shows the greatest change in resonant frequency for a given change in contact stiffness (Hurley, 2009). Images of the normalized contact stiffness $k = k^*/k_c$ for the sample were

calculated from the frequency images. Mean values for the normalized contact stiffness of the fiber (k^*_{fiber}) and matrix (k^*_{matrix}) regions in each image were determined. The average indentation modulus reference values for both the fiber (M_{fiber}) and the matrix (M_{matrix}) were determined from the reduced indentation modulus (E_r) obtained from the nanoindentaion and used in Eq (3.4).

5.3.4 FTIR and multivariate analysis

Infrared absorption spectra of samples were recorded using a Perkin-Elmer Spectrum One Fourier transform infrared spectroscopy (FTIR) spectrometer. 40 µm thick samples were prepared using sliding microtome. The samples were carefully placed on a 2 mm thick KBr window. For each sample, the diamond crystal of an ATR accessory was brought into contact with the area to be analyzed. All spectra were recorded between 4000 and 650 cm^{-1}, at a wave number resolution of 4 cm^{-1}, with 16 scans per sample. Multivariate analysis was performed on the samples to analyze the uniqueness of the information in the infrared spectral dataset. Two samples per treatment were analyzed, with three measurements per sample. All data were imported into the Hyperview software (PerkinElmer version 1, Irvine, CA, USA). Principal component analysis (PCA) was then used to isolate spectral variables (wavelength) that can be associated with differences between the surface chemistry of the samples.

5.3.5 Tensile testing

The tensile testing and modulus were measured using a universal testing machine (model 5567, Instron, Inc., Canton, MA) in accordance with ASTM D 638. Ten replicates were used for

each type of treatment. The impact testing was done in accordance with ASTM D 256 using Impact Tester (Tinius Olsen ® Model 899, Horsham, PA, USA).

5.3.6 Dynamic mechanical analysis (DMA)

The injection molded tensile specimens were cut and machined to dimensions of 3.5 mm x 7.7 mm x 20 mm to fit a Diamond dynamic mechanical analyzer (PerkinElmer, Waltham, MA) operated in single cantilever bending mode. DMA conducted at a heating rate of 3^0C/ min from -50^0C to 100^0C with a wide range of frequencies (1, 2, 4, 10, and 20 Hz) under a nitrogen flow. Viscoelastic properties were measured as a function of temperature and frequency. Three replicates were taken for each treatment.

5.4. Results and Discussion

5.4.1. MAPP

5.4.1.1. Interphase characterization

5.4.1.1.1. CR-FM

Contact resonance frequency images were obtained at the interfacial region between the fiber and matrix for composites made with 0 %, 2.5 %, and 10 % MAPP. In order to minimize topography effects, regions between the fiber and matrix approximately that were as flat as possible (height differences of ~20 nm or less) were selected for imaging. Figure 5.1 shows CR-FM modulus maps for each of the composite samples and corresponding line profile with different treatments.

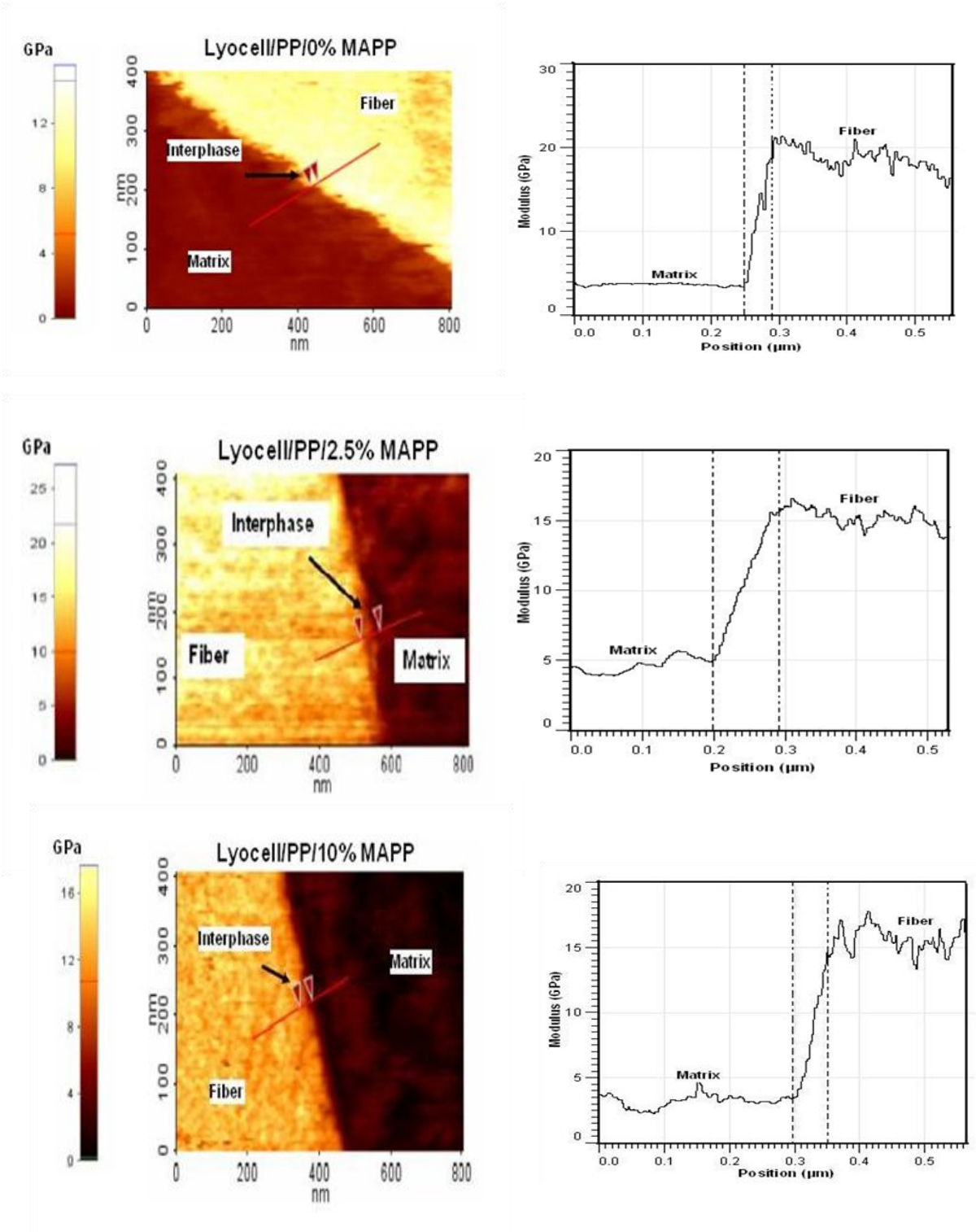

Figure 5.1. CR-FM modulus maps for each of the composite samples (left) and corresponding line profile (right) with different treatments

The images clearly show that a region with intermediate modulus exists between the matrix and the fiber. This region between the matrix and the fiber, where the local properties are different from those of the bulk fiber and the matrix, is defined as the interphase (Drzal, 1986). The average interphase thickness around the fiber was determined by a statistical analysis of the CR-FM modulus maps with use of image processing XEP software (Park Systems, Suwon, South Korea). Ten radial lines were drawn across the fiber-matrix boundary for each image. This method was applied to 3 different fibers within a sample to determine the average thickness. Each line showed a gradient of modulus across the interphase region that ranged between the modulus values of the fiber and the matrix. Figure 5.1 shows an example profile for a radial line across the fiber-matrix boundary. Table 5.1 shows values for the average and uncertainty in interphase thickness for each treatment.

Table 5.1. Average interphase thickness for each treatment

Composite type	**Estimated average interphase width (nm)**
Lyocell/PP/0% MAPP	**30.5 ± 2.6**
Lyocell/PP/2.5% MAPP	**100 ± 12.4**
Lyocell/PP/10% MAPP	**70.3 ± 20.6**

The uncertainty represents one standard deviation in the individual measurements. The values ranged from 30 nm to 100 nm for different concentrations of MAPP. The average interphase thickness was found to increase with use of MAPP. This is not entirely surprising; a number of previous studies have observed interphase thickness to vary with the concentration of coupling agents such as MAPP. MAPP coupling agent creates a better adhesion between the matrix and the fiber and improves the interfacial bond, which facilitates a much higher stress transfer from the matrix to the fiber and improves final mechanical properties in the resultant composites. Lee et al. (2009) with the help of atomic force microscopy phase imaging (AFM-PI) have showed that the use of MAPP as a compatibilizer in lyocell/polypropylene composite increased the interphase thickness and the combined use of MAPP and γ-amino propyltrimethoxy silane (γ-APS) have further increased the thickness. Kim et al. (2001) and Griswold et al. (2005) have found that the interphase thickness increased with the increasing silane coupling agent concentration for glass fiber composites.

Very little research has been done on direct characterization of interphase in NFRPCs. This is mainly due to the lack of technique that can measure the properties of interphase widths of less than 100 nm. The reason for formation of such small interphase widths in NFRPCs is due to the incompatibility between the hydrophilic natural fiber and the hydrophobic polymer. Use of extremely small tip radius (25 nm to 35 nm) and low forces (50 nN to 80 nN) used in CR-FM technique have been very valuable for the determination of interphase properties in NFRPCs with such nanoscale spatial resolution.

From the results, the interphase thickness was found to increase with increasing the MAPP concentration from 0 % to 2.5 %, but further addition of MAPP did not have any effect on the average interphase thickness. Instead of being concentrated on the interphase, MAPP can

act as nucleating agent and can accelerate the nucleation of PP and can affect nucleation rate and size of spherulites (Duvall et al., 1994; Seo et al., 1999). This can change the morphology of the matrix polymer and the whole composite. Also, the existence of too much coupling agent can enlarge the gap between the fiber and matrix and weaken the interphase (Lu et al., 2005). However, in our experiments using CR-FM, the addition of excessive MAPP, i.e., from 2.5 % to 10 %, did not widen the interphase between the fiber and matrix. However, the results obtained for the interphase widths for different treatments were totally different from the results obtained from Chapter 4. In Chapter 4, the interphase width increased with the increasing use of MAPP i.e., the average interphase thickness obtained were (25 ± 10) nm, (44 ± 11) nm, (54 ± 23) nm, and (104 ± 22) nm for composite specimens prepared with 0 %, 2.5 %, 5 %, and 10 % MAPP, respectively. The reason for this could be attributed the difference in processing of composites. In Chapter 4, the samples were compression molded at 200^0C for 10 min and then cold water was used to cool down the mold temperature to 32^0C under pressure in order to obtain unidirectional lyocell fiber-reinforced composites. Here, the samples were fed into a heated barrel at 200^0C and then forced into a mold cavity where it cools to 140^0C for 5 minutes. Different research have proved that process parameters like difference in cooling rates substantially affect the crystallization kinetics of polymer composites, affecting the morphology and the final mechanical properties (Grozdanov et al., 2007; Klien et al., 1995).

In order to further characterize the interphase, slope and coefficient of determination R^2 for each radial line scans were determined. Table 5.2 shows the average values for the slope and R^2 for the different radial lines drawn across the interphase for each treatment.

Table 5.2. Average values for the slope and R^2 for each treatment

Composite type	**Coefficient of determination (R^2)**	**Slope**
Lyocell/PP/0% MAPP	0.95 ± 0.05	0.40 ± 0.10
Lyocell/PP/2.5% MAPP	0.90 ± 0.06	0.09 ± 0.04
Lyocell/PP/10% MAPP	0.91 ± 0.06	0.17 ± 0.05

In the Figure 5.1 for the 0 % MAPP sample, the interphase thickness is quite small. As a consequence, there is a sharp spatial gradient in modulus (steeper slope) between the fiber and the matrix that can easily cause the fiber to debond from the matrix under stress, resulting in poor overall mechanical properties. Addition of MAPP was found to significantly increase the interphase thickness, resulting in a more gradual gradient in modulus from fiber to matrix. This behavior was most prominent in the sample containing 2.5 % MAPP, which had the widest interphase. The anhydride group of MAPP forms covalent bonding through esterification process and hydrogen bonding with cellulose fibers while the grafted PP in MAPP due to the similarity to the bulk PP permits the segmental crystallization and, thus the cohesive coupling between them through entanglement of their macromolecular chains (Felix and Gateholm 1993). It is quite clear that MAPP is not deposited on the interphase with further addition of MAPP from 2.5% to 10 %. The interphase region showed a gradient in modulus that could be described to first order by a linear fit, with a gradual decrease in modulus from fiber to matrix. Also, it is quite evident that the interphase thickness accounts for the majority of property variations within the interphase for different treatments.

5.4.1.1.2. FTIR

Figure 5.2 shows the first three PCs or factors which contribute for major variations of 0% MAPP composites. The bands in the 3500-3100 cm^{-1} region are due to various hydroxyl (OH) stretching vibrations. The bands in the region between 3100-2600 cm^{-1} are due to CH stretching of methlene and methyl (CH_2 and /or CH_3) stretching vibrations. The bands in the region of 1400-1300 cm^{-1} are due to CH deformation of CH_2 and CH_3 stretching vibrations. Also, the bands between 1300-1000 cm^{-1} are due to C-O, C-O-C stretching and OH deformation vibrations (Kazayawoko et al 1997).

Figure 5.3 shows the first three PC or factors which contribute major variations for samples containing 2.5% MAPP composites. The PC1 or factor one contributes to 94% of the total variation. The PC1 did not show any wavelength corresponding to maleic anhydride. The absence of vibrations corresponding to maleic anhydride may be explained due to the fact that composite contained only 2.5 % of MAPP. However, PC2 or factor two showed bands in the region 1870-1770 cm-1. These are associated with the anhydride carbonyl (C=O) symmetric and asymmetric stretching vibrations. PC3 or factor three (1% of total variation) showed bands in the region of 1740 cm-1, the confirmation of esterification between the lyocell fiber and MAPP. Figure 5.4 shows the first three PC or factors which contribute major variations for samples containing 10% MAPP composites. The PC1 or factor one contributes to 89% of the total variation. Compared to 0% and 2.5% MAPP, PC1 of 10% MAPP showed sharp and strong bands at 1775 cm-1 and 1707 cm^{-1}, which are due to anhydride carbonyl symmetric and asymmetric stretching vibrations and carbonyl stretching vibrations of carboxyl groups in maleated polypropylene (Kazayawoko et al., 1997), respectively. From the CR-FM results, it was evident that the interphase width formed from 2.5% MAPP was greater than that of 10% MAPP. So it is

quite clear that the strong bands at 1775 cm-1 and 1707 cm^{-1} were due to excess amount of MAPP on the PP matrix than on interphase for 10% MAPP composites. Also, PC3 (2% of total variation) of 10% MAPP showed very weak bands in the region of 1730-1740 cm^{-1} showing very little esterification occurred between the fiber and MAPP (Kazayawoko et al., 1997). The rest of PCs did not show any signs on maleic anhydride bands.

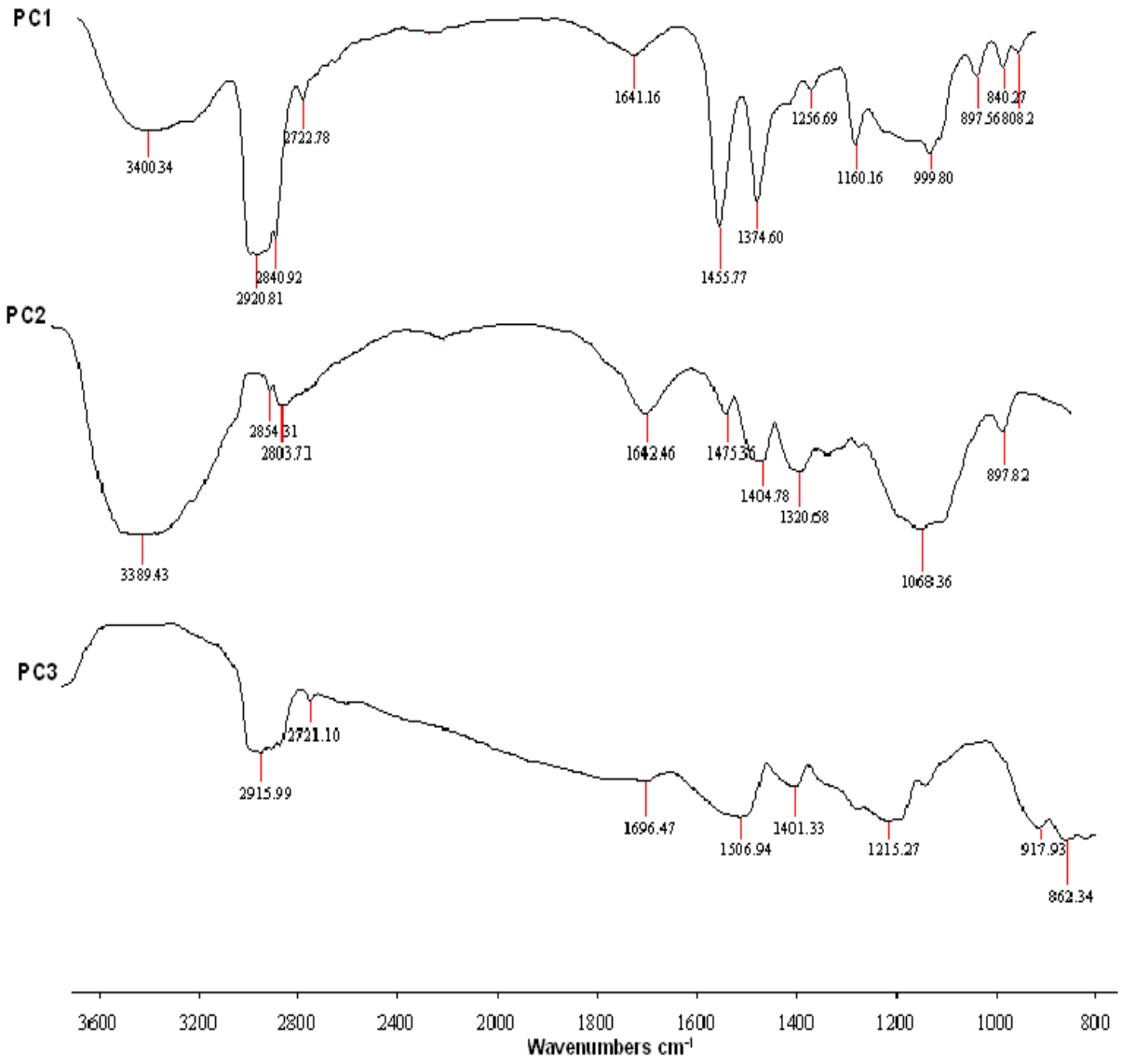

Figure 5.2. First three PCs or factors which contribute for major variations of 0% MAPP composites

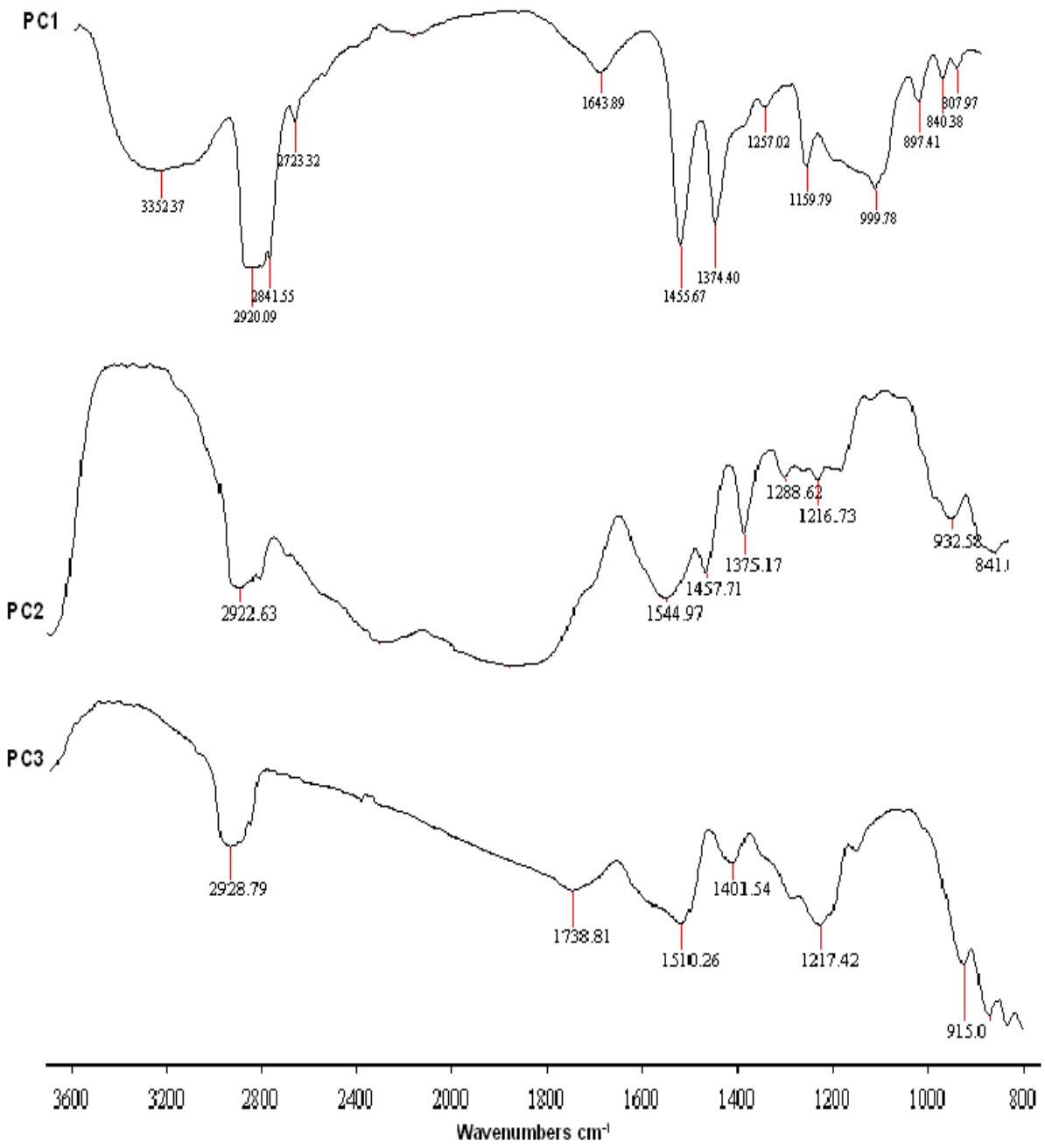

Figure 5.3. First three PCs or factors which contribute for major variations of 2.5% MAPP composites

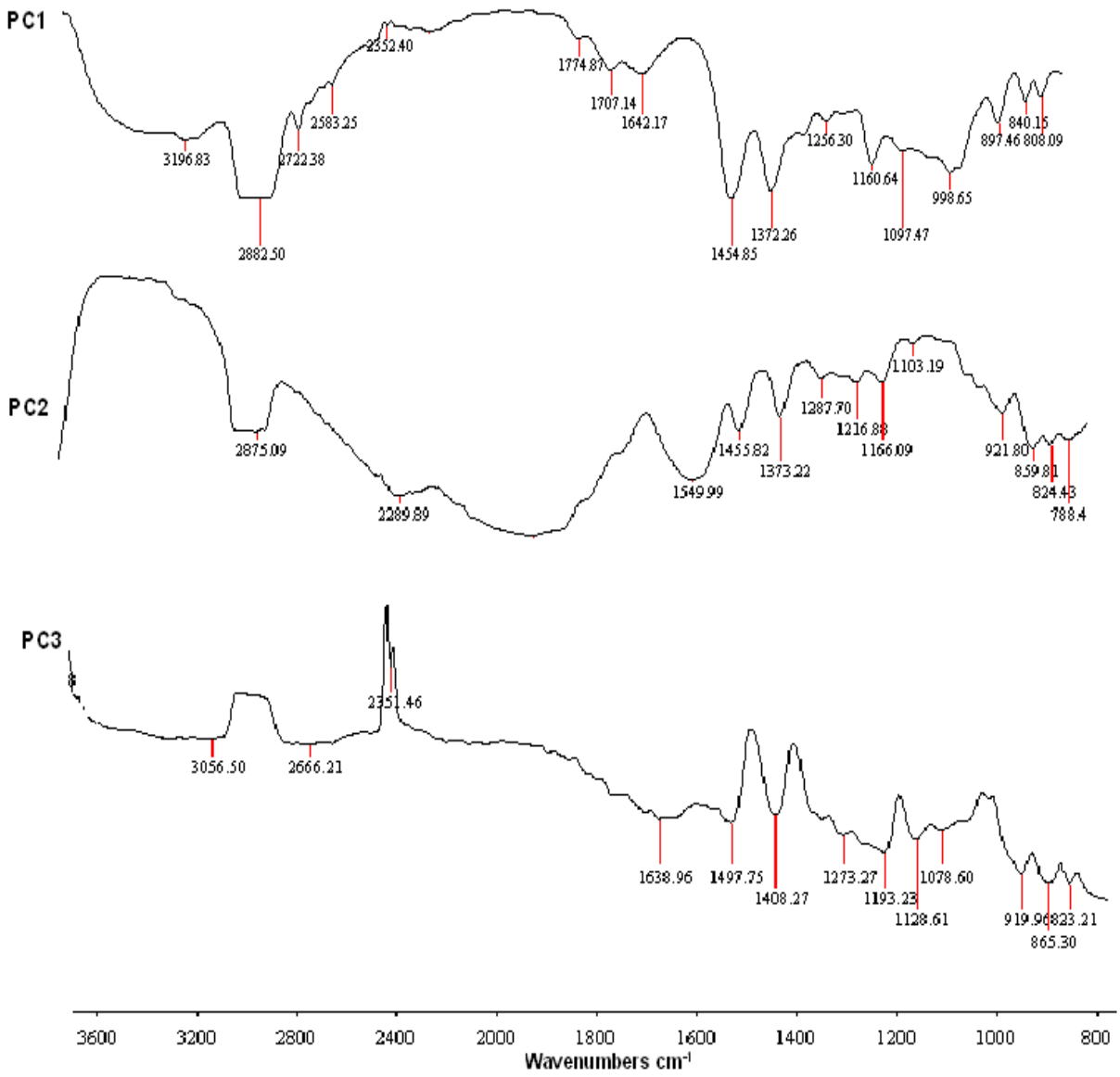

Figure 5.4. First three PCs or factors which contribute for major variations of 10% MAPP composites

The point spectra method of identifying specific functional group of a particular constituent such as fiber, matrix, and the interphase was almost impossible due to more or less band overlapping in fiber and matrix. Figure 5.5 shows AFM image showing the spacing of the fibers. The fibers were so close that it was impossible to identify specific functional group due to the limited resolution of FTIR imaging. The spatial resolution of FTIR imaging is 6.25 µm. The diameter of the fiber used in this experiment is 10 µm. So it was hard to distinguish between the fiber and matrix chemical groups. The results showed that the multivariate methods gave more satisfactory, interpretable results and were conclusive in showing that they can discriminate and classify differences between the functional groups of fiber, matrix and interphase.

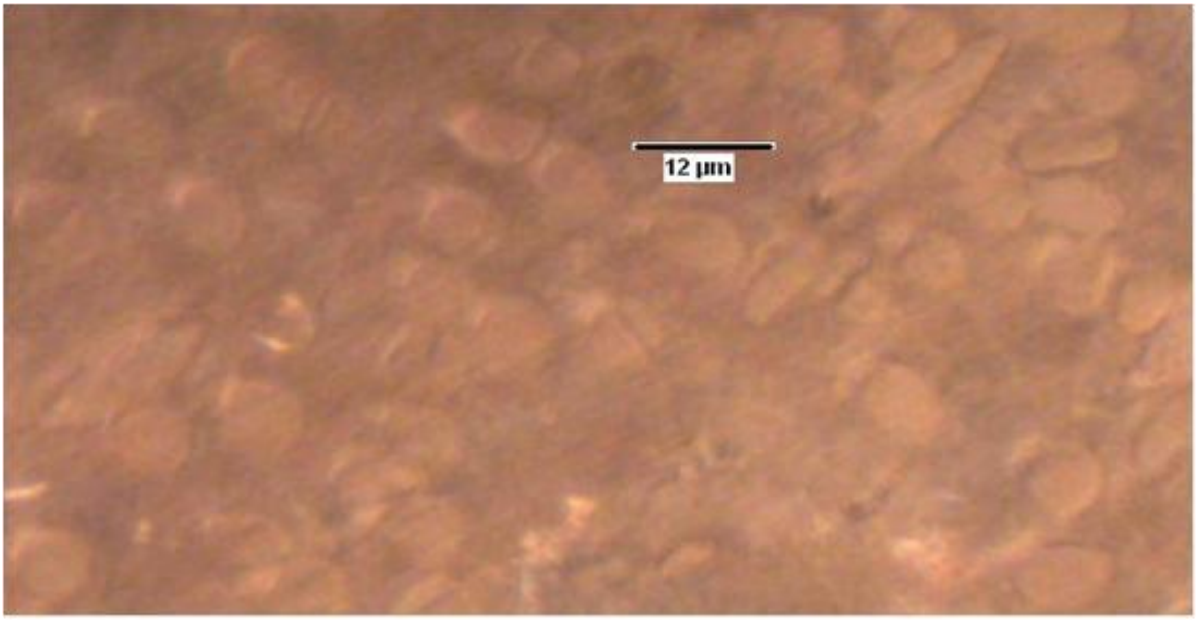

Figure 5.5. AFM image showing the spacing of the MAPP treated fibers

5.4.1.2. Bulk mechanical properties

5.4.1.2.1. Tensile and impact properties

Table 5.3 summarizes the mean and standard deviation of the mechanical properties of lyocell/PP composites with different MAPP concentration. The results are also presented in separate Figure 5.7 below. The average tensile modulus was found to increase with the addition of MAPP, but not statistically significant (one way analysis of variance at $P<0.05$). The addition of high modulus fillers to a polymer always increases the composite modulus. Coupling agent helps better disperse of high modulus fillers in the polymer, thus increasing the composite tensile modulus. However, the adhesion between the filler and polymer has little impact on the modulus (Borja, 2006). There was little increase in the average tensile modulus with the addition of 2.5 % MAPP. But with further addition, the modulus remained constant without much increase. Also, there was significant decrease in modulus with the addition of 10% MAPP compared to 2.5% MAPP (one way analysis of variance followed by Tukey's multiple comparison tests at $P<0.05$).

Table 5.3. Mean and standard deviation of the mechanical properties of lyocell/PP composites with different MAPP concentration

MAPP (%)	**Tensile modulus (GPa)**		**Tensile strength (MPa)**		**Impact strength (kJ/m^2)**	
	Average	Std Dev	Average	Std Dev	Average	Std Dev
0	4.05	0.58	40.96	1.58	3.94	0.16
2.5	4.67	0.36	54.46	1.65	3.26	0.30
5	4.62	0.55	50.76	2.54	2.82	0.24
7.5	4.60	0.29	49.41	1.26	2.80	0.29
10	3.57	0.60	47.19	2.05	2.70	0.22

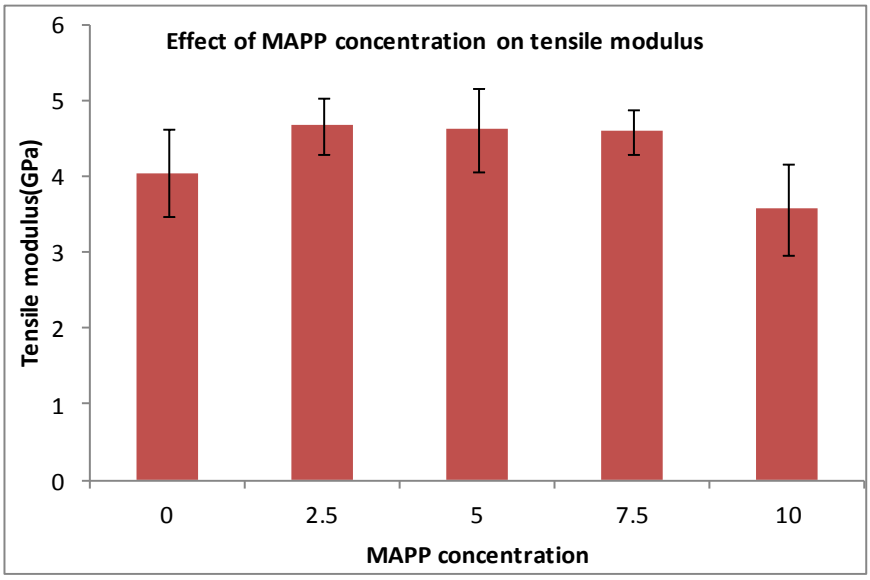

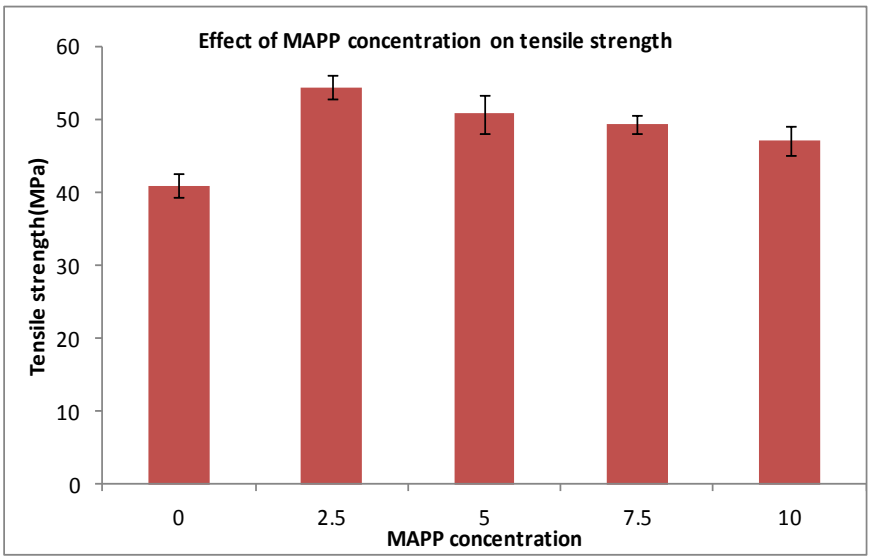

Figure 5.6. Effect of MAPP concentration on the tensile modulus (top) and tensile strength (bottom)

The decrease can be due to the change in the molecular morphology of the polymer near the fiber surface or due to the effect on the bulk polymer phase (Harper et al, 2009). Structural difference between MAPP and PP can cause chain interaction such as hydrogen bonding between the hydrolyzed maleic anhydride groups. This means that a small amount of MAPP can effect the crystallization of PP matrix and thereby affect the morphology of matrix and the final mechanical properties. From the CR-FM results, it is quite evident that addition of MAPP from 2.5% to 10% did not increase the interphase thickness. This means that more amount of MAPP is concentrated on the PP matrix for 10% MAPP composites than 2.5% composites. This was also confirmed from the FTIR results.

There was significant increase of tensile strength with the use of MAPP (one way analysis of variance at $P<0.05$). However, with further addition of MAPP from 2.5 % to 5%, 7.5% and 10 % showed a gradual decrease in tensile strength. The addition of coupling agents helps in better adhesion between the matrix and the fiber and thereby increases the tensile strength in the resultant composites. High tensile strength is a direct reflection of interfacial bonding resulting in better stress transfer between fiber and polymer in the composite (Figure 5.7). The tensile results can be compared to the CR-FM results. The average interphase thickness increased with the addition of 2.5 % MAPP and further addition to 10% MAPP decreased the average interphase thickness of the lyocell/PP composites. Thus an optimum amount of MAPP increase the interphase thickness to the maximum and further addition only decreased the interphase thickness. Figure 5.8 shows the strong correlation between the tensile strength and interphase width.

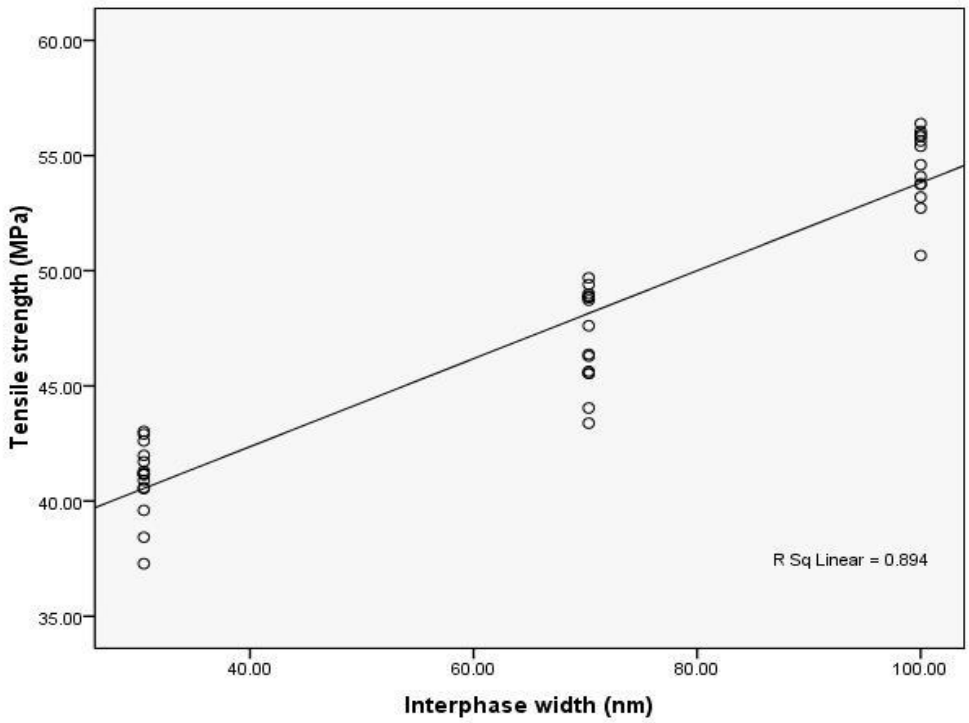

Figure 5.7. Correlation of interphase width with tensile strength

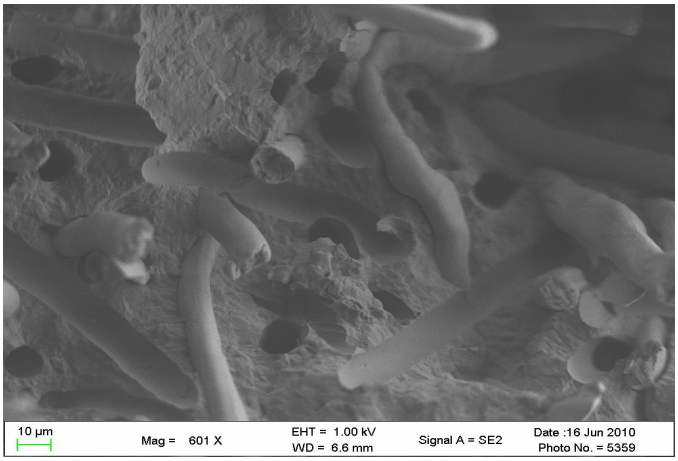

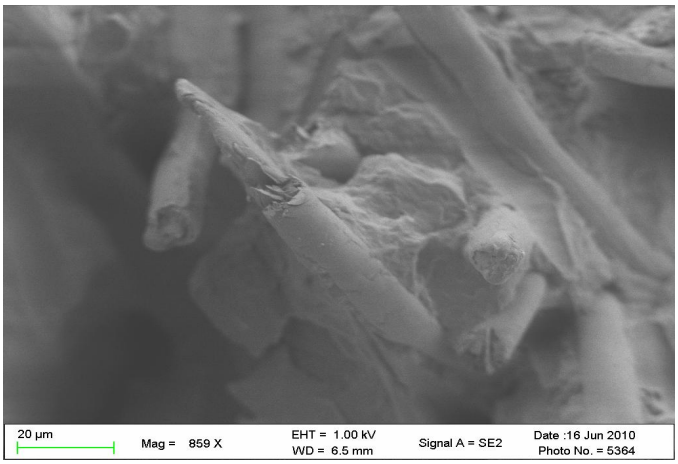

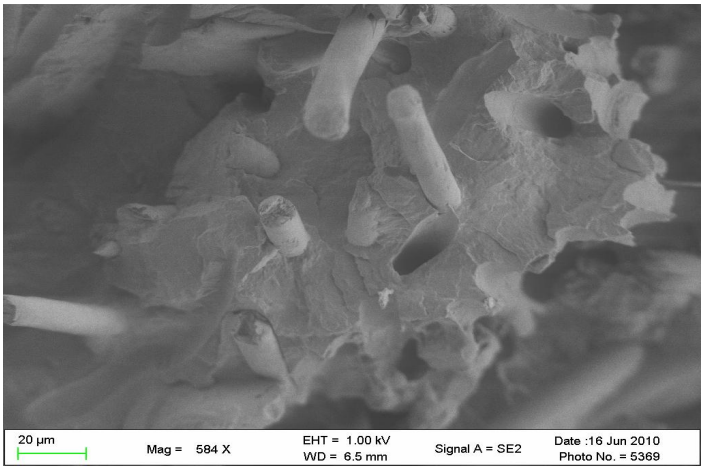

Figure 5.8. SEM images of the fracture surfaces of (top) lyocell/PP composites without MAPP, (middle) 2.5 % MAPP, (bottom) 10 % MAPP treatment

Figure 5.6 (top) and (bottom) shows cavities and easy fiber pull out, indicating weak adhesion while Figure 5.6 (middle) shows stronger bonding, evident from the short broken fiber ends and less number of cavities.

The impact strength significantly decreased with the addition of MAPP (one way analysis of variance at $P<0.05$). The average impact strength was found to decrease with the increasing concentration of MAPP (Figure 5.9). While for a continuous fiber reinforced composite, the fracture mode mainly depends on the interphase, the failure for a short fiber reinforced composite is mainly dependent on the fracture mode of matrix material, volume fraction of fiber, fiber aspect ratio and fiber orientation (Kim and Mai, 1998). Figure 5.9 shows the impact strength for different MAPP concentrations. The presence of fiber ends within the matrix can create considerable stress concentrations near the fiber ends where microcracks form and this can cause debonding of the fiber even from a ductile matrix (Sato et al., 1983).

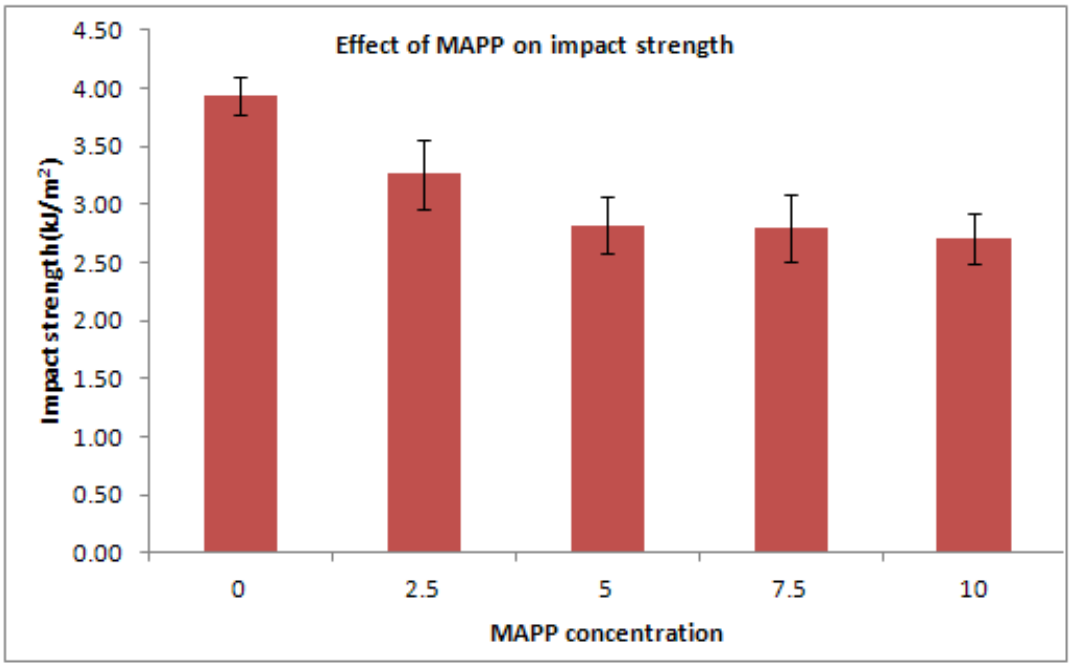

Figure 5.9. Effect of MAPP concentration on impact strength

In our samples, the composite with 2.5% MAPP showed the best adhesion with better interphase properties while the samples without MAPP showed the least adhesion. The highest impact strength of 0% MAPP composites indicates that impact strength was not highly dependent on the interphase. Also, the decrease in impact strength with increasing MAPP concentration can be due to the increased amount on maleic anhydride in the matrix polymer affecting the crystalline structure. The studies from other group (Myers et al., 1991a and b) have shown the positive effect of MAPP on tensile properties and the negative effect on the impact strength. They believed that the loss of impact strength was due to increased filler reinforcement

and filler brittleness. From our results we could conclude that the matrix properties were also a determinant factor on the impact strength.

5.4.1.2.2. Dynamic mechanical response

The storage modulus was found to decrease with the addition of MAPP (Figure 5.10). This could be due to the change in morphology of the bulk matrix caused by the MAPP, which was quite evident from the CR-FM and FTIR results. The tan δ curve of polypropylene is characterized by two relaxations. The α-relaxation around 100^0C is related to the relaxation of bound or restricted PP chains in the crystalline phase and the β-relaxation around 10^0C which is the unrestricted relaxation of the fully amorphous phase. Around the β transition the molecules in the amorphous component of the matrix begin to relax (Harper et al., 2009). Figure 5.11 and Table 5.4 Shows the temperature depends of damping (tan δ) and the glass transition temperature (T_g) for the Lyocell/PP composites with different MAPP concentration. The tan δ peak values were fairly consistent for all the treatments. However, the results clearly showed that T_g decreased with use of coupling agent. Poor packing density and blends with plasticizers can cause increased molecular mobility within the amorphous matrix. All of these can lead to decrease in T_g. (Harper et al., 2004).

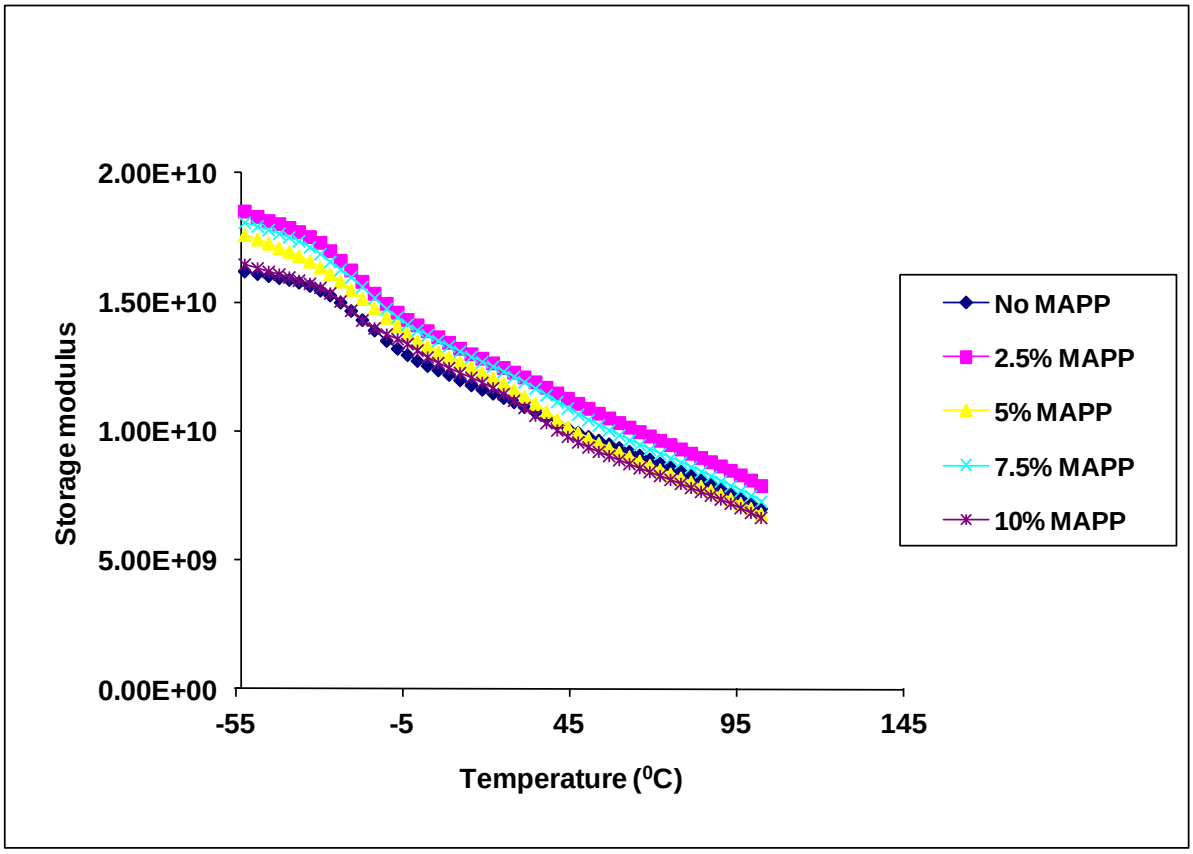

Figure 5.10. Dependence of storage modulus at different temperature for different MAPP concentration measured at 1 Hz

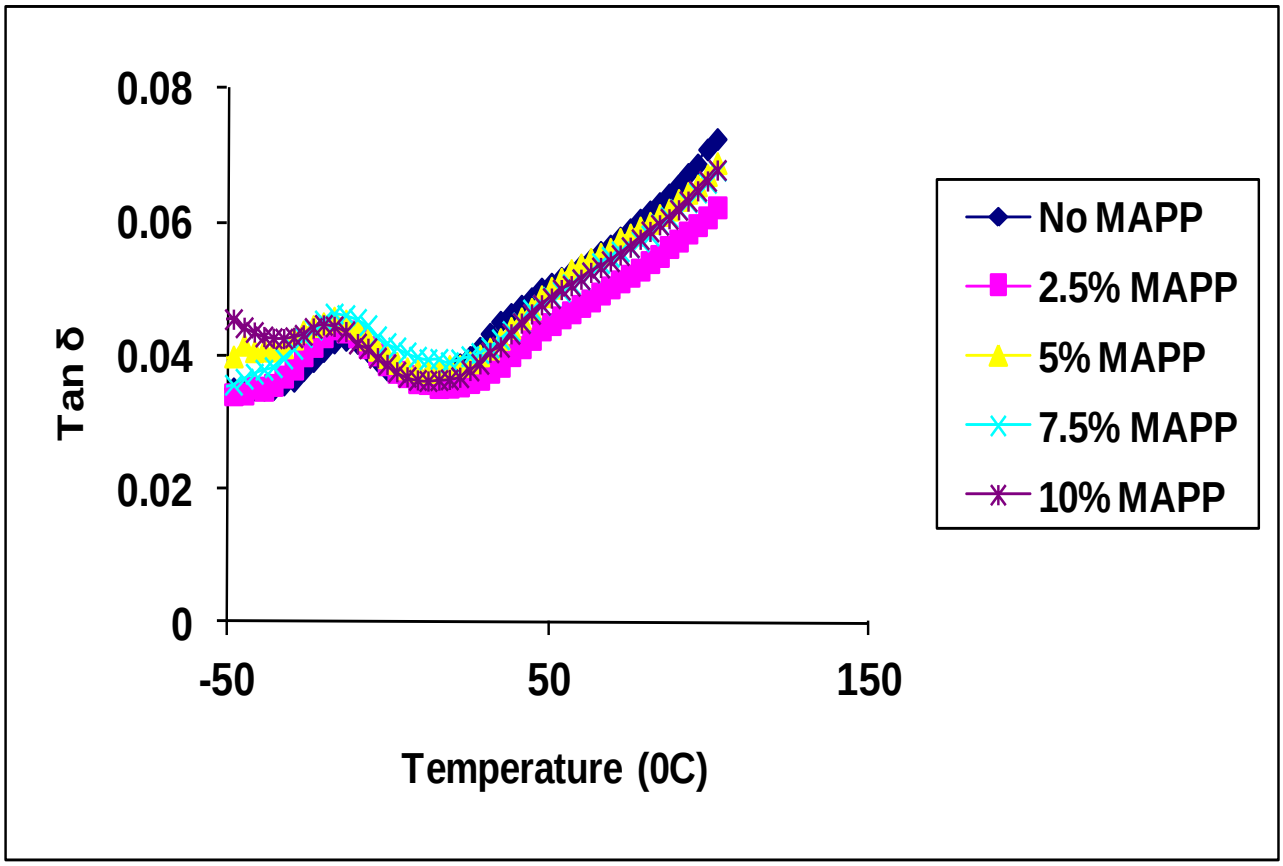

Figure 5.11. Temperature depends of damping (tan δ) and the glass transition temperature (T_g) for different MAPP concentration measured at 1 Hz

Table 5.4. Temperature depends of damping (tan δ) and the glass transition temperature (T_g) for different MAPP concentration measured at 1 Hz

Composite type	T_g(^{0}C)	Tan δ
Lyocell/PP/0% MAPP	-14.3	0.043
Lyocell/PP/2.5% MAPP	-18.0	0.044
Lyocell/PP/5% MAPP	-17.9	0.045
Lyocell/PP/7.5% MAPP	-17.9	0.046
Lyocell/PP/10% MAPP	-18.6	0.045

5.4.2. SEBS

5.4.2.1. Interphase characterization

5.4.2.1.1 CR-FM

Contact resonance frequency images were obtained at the interfacial region between the fiber and matrix for composites made with 5 % and 10 % SEBS. Figure 5.12 shows CR-FM modulus maps for each of the composite samples and corresponding line profile with different treatments.

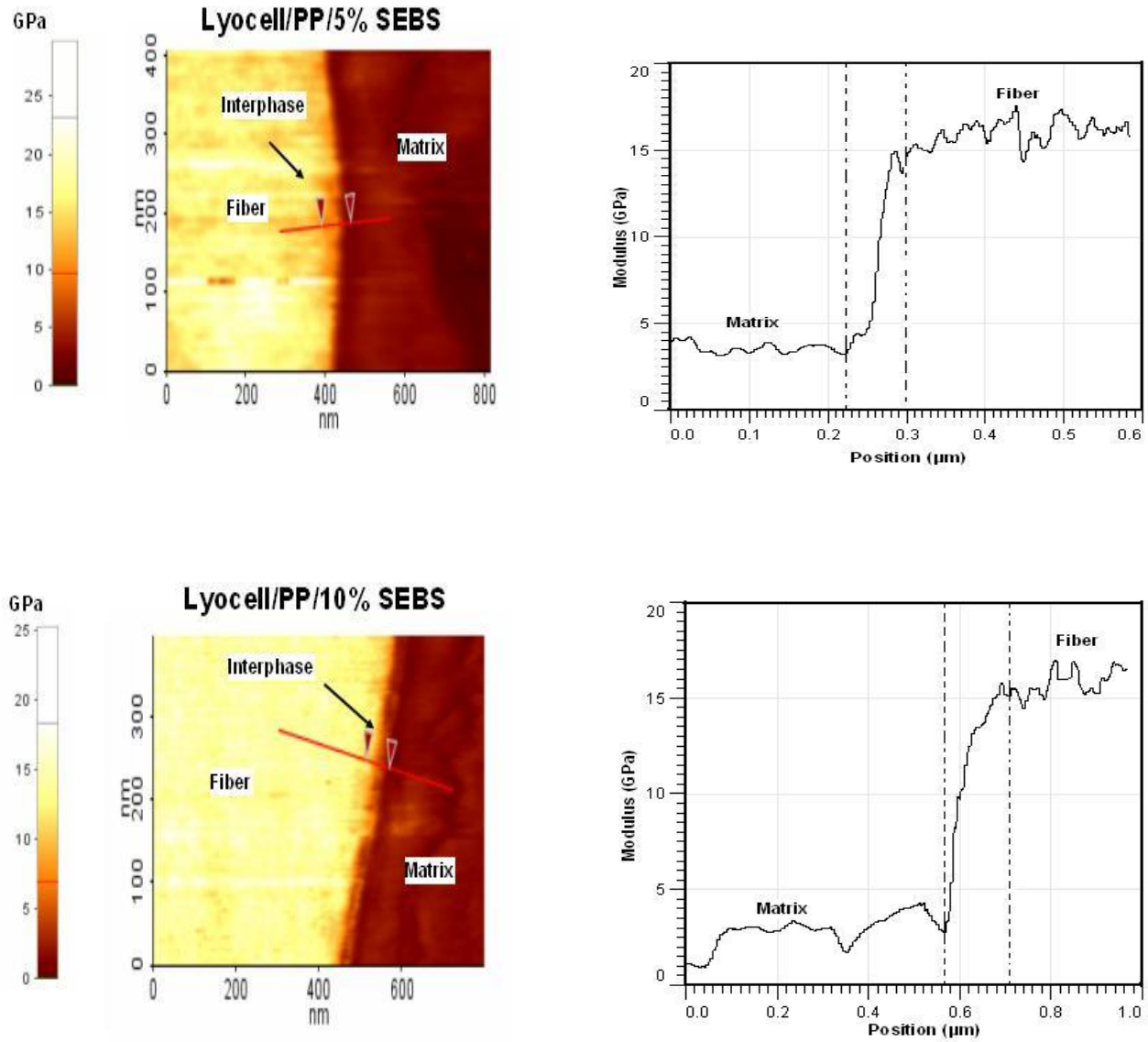

Figure 5.12. CR-FM modulus maps for each of the composite samples (left) and corresponding line profile (right) with different treatments

The images clearly show the interphase region with intermediate modulus exists between the matrix and the fiber. The average interphase thickness was obtained in the same statistical way as MAPP. Table 5.5 shows values for the average and uncertainty in interphase thickness for each treatment.

Table 5.5. Average and uncertainty in interphase thickness for each treatment

Composite type	**Estimated average interphase width (nm)**
Lyocell/PP/0% SEBS	**30.5 ± 2.6**
Lyocell/PP/5% SEBS	**79.1 ± 15.2**
Lyocell/PP/10% SEBS	**100.1 ± 34.7**

From the results, the interphase thickness was found to increase with use of SEBS and with increasing SEBS concentration from 5 % to 10 %. In order to further characterize the interphase, slope and coefficient of determination R^2 for each radial line scans were determined. Table 5.6 shows the average values for the slope and R^2 for each treatment.

Table 5.6. The average values for the slope and R^2 for each treatment

Composite type	**Coefficient of determination (R^2)**	**Slope**
Lyocell/PP/0% SEBS	0.95 ± 0.05	0.40 ± 0.10
Lyocell/PP/5% SEBS	0.89 ± 0.07	0.13 ± 0.06
Lyocell/PP/10% SEBS	0.85 ± 0.05	0.16± 0.05

The R^2 value for 5% SEBS was slightly lower than 2.5% MAPP and the slope was slightly higher than 2.5% MAPP. But 5% SEBS has higher interphase width than 2.5% MAPP. It was the same trend in the case of 10% SEBS and 10% MAPP. This could be due to presence of different blocks such as styrene on both sides of ethylene-co-butylenes blocks and maleic anhydride grafted to butylene block within the interphase of SEBS treated composites. While MAPP has only maleic anhydride grafted to polypropylene chains. PP in MAPP due to the similarity to the bulk PP permits the segmental crystallization and, thus the cohesive coupling happens between them. For SEBS, each line showed a gradient of modulus across the interphase region that ranged between the modulus values of the fiber and the matrix.

5.4.2.1.2 FTIR

Figure 5.13 shows the first three PC or factors which contribute major variations for samples containing 5% SEBS composites. The PC1 (94%), PC2, and PC3 showed very weak signals of ester bonds at 1744 cm^{-1} of the total variation. The rest of PCs did not show any signs on maleic anhydride bands. However, for 10% SEBS (Figure 5.14), PC1 (93%) and PC3 showed weak bands at 1744 cm^{-1} showing that esterification occurred between fiber and SEBS (Kazayawoko et al., 1997).

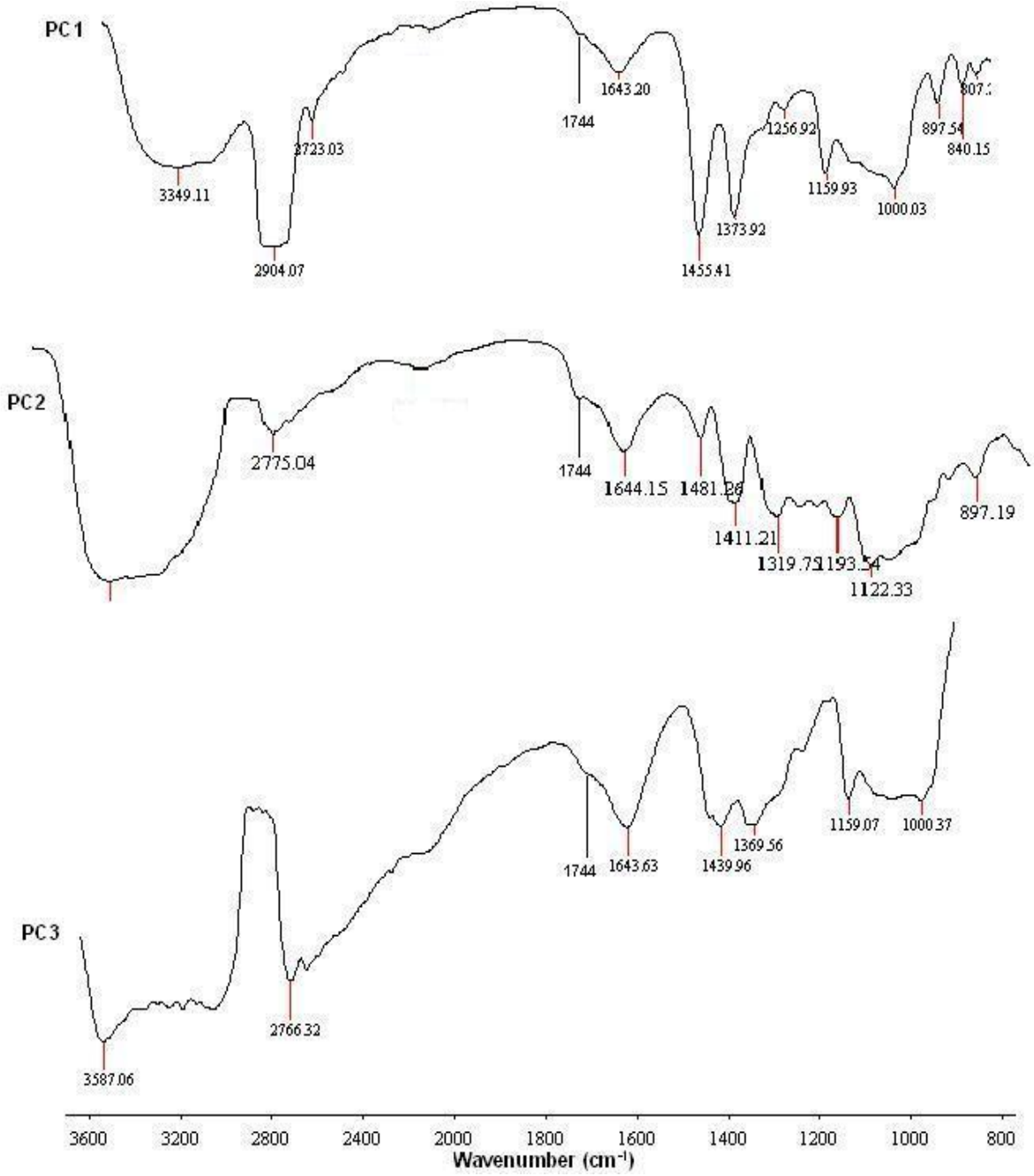

Figure 5.13. PC or factors which contribute major variations for samples containing 5% SEBS composites

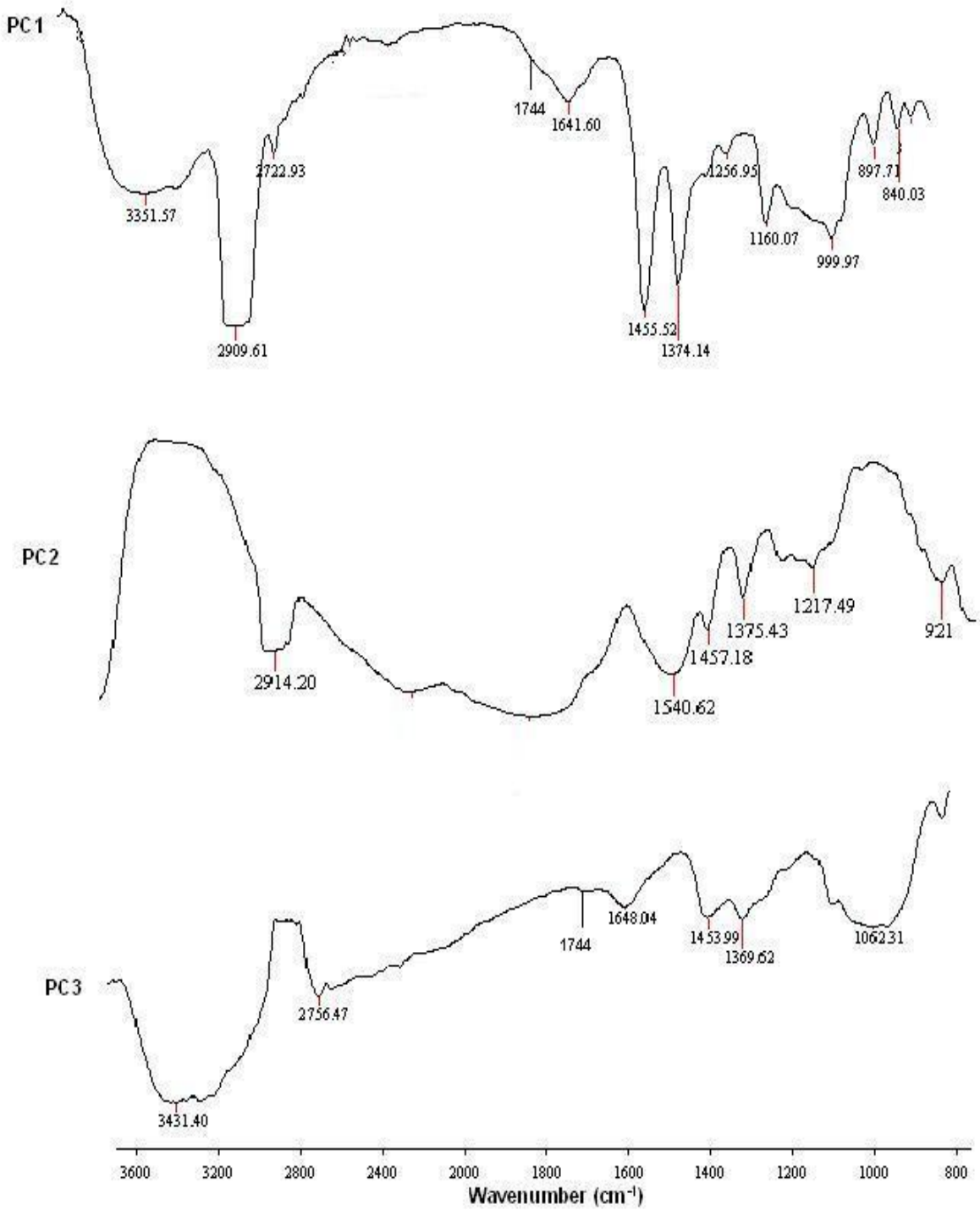

Figure 5.14. PC or factors which contribute major variations for samples containing 10% SEBS composites

5.4.2.2. Mechanical properties

5.4.2.2.1 Tensile and impact properties

Table 5.7 summarizes the mean and standard deviation of the mechanical properties of lyocell/PP composites with different MA-SEBS concentrations. The results are also summarized in Figure 5.17. The average tensile modulus was found to decrease with addition of MA-SEBS. This was expected because the low E-modulus of elastomers in the impact modifiers always decreases the stiffness of the composites. The average tensile modulus was found to significantly decrease with addition of 5 % MA-SEBS (one way analysis of variance at $P<0.05$). However, with further addition of MA-SEBS to 10% increased the modulus.

Table 5.7. Mean and standard deviation of the mechanical properties of composites with different
MA-SEBS concentrations

SEBS (%)	**Tensile modulus (GPa)**		**Tensile strength (MPa)**		**Impact strength (kJ/m^2)**	
	Average	Std Dev	Average	Std Dev	Average	Std Dev
0	4.05	0.58	40.96	1.58	3.94	0.16
5	3.24	0.35	51.03	1.93	4.73	0.50
10	3.79	0.29	47.09	3.82	5.61	0.36

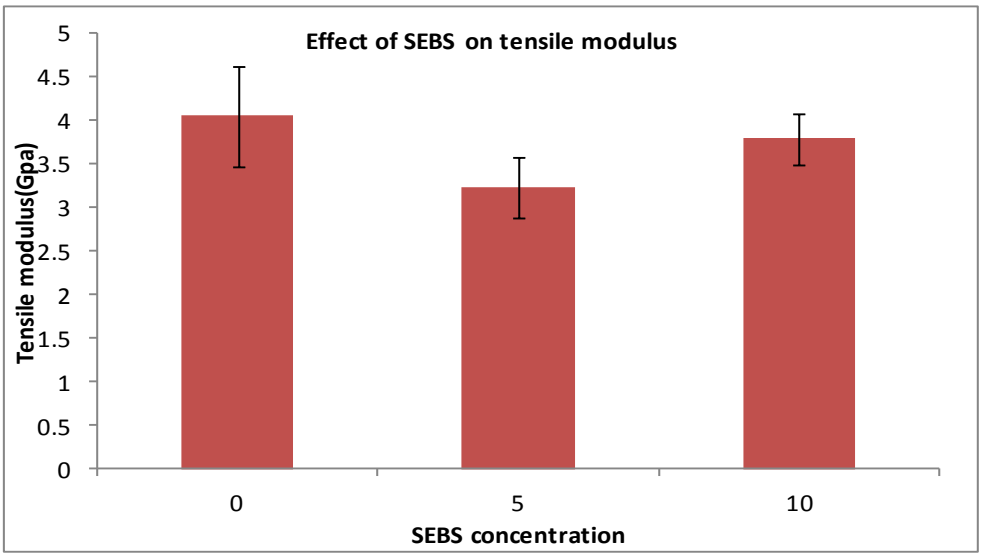

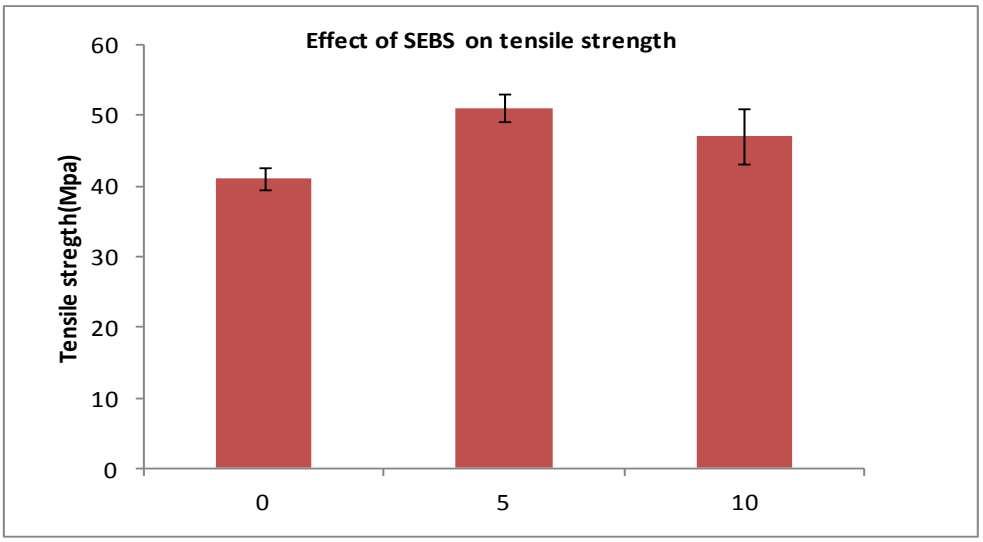

Figure 5.15. Effect of different MA-SEBS concentrations on the tensile modulus (top) and tensile strength (bottom)

From our CR-FM, FTIR and SEM results, it is quite evident that MA-SEBS forms an interphase around the fibers. At the same, the elastomers also exist as separate domains in the matrix. Several studies have proved that the formation of interphase around fibers can cause a greater reduction in modulus than a morphology where elastomers exist as separate domains in the matrix (Oksman and Clemons, 1997).

There was significant increase in the tensile strength with the use of MA-SEBS (one way analysis of variance at $P<0.05$). However, with the further addition of coupling agent from 5% to 10% decreased the strength. We have found from the CR-FM results that 10% MA-SEBS had the best adhesion properties with the highest average interphase thickness. So, we can say that in these composites tensile strength is not a direct reflection of interfacial bonding. One of the reasons could be the matrix effect, due to the formation of separate morphology where elastomers exists as separate domains in the matrix. Thus with the addition of MA-SEBS helps in better adhesion between the matrix and the fiber and thereby increases the tensile strength in the resultant composites.

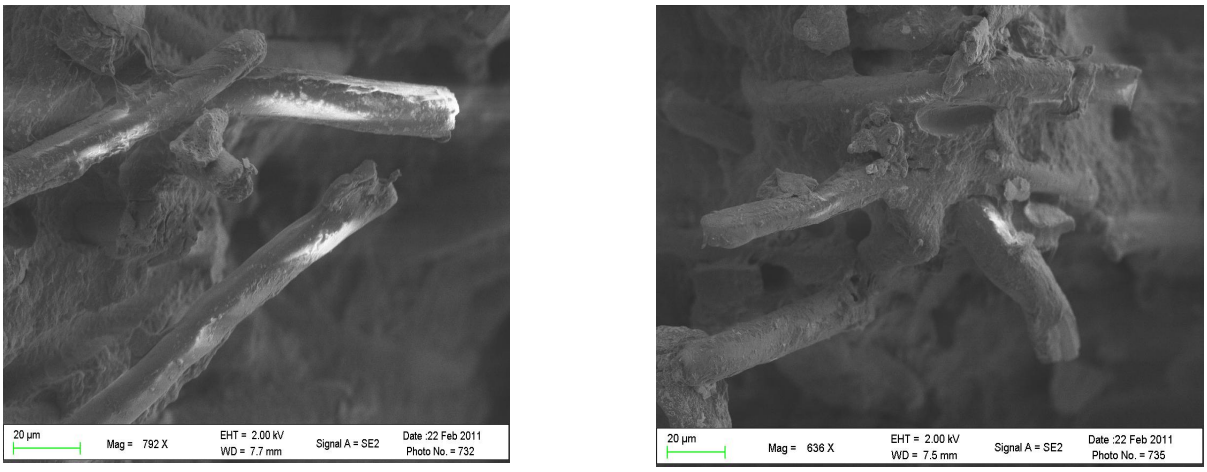

Figure 5.16. SEM images of the fracture surfaces of (left) 5 % SEBS, (right) 10 % SEBS treatment

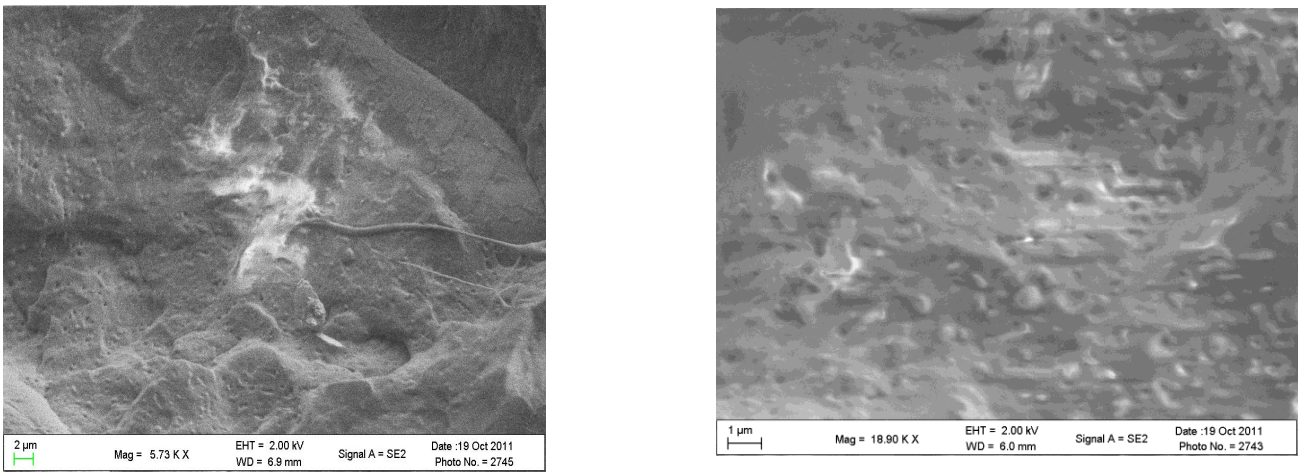

Figure 5.17. SEM images of the matrix fracture surfaces of (left) 5 % SEBS, (right) 10 % SEBS treatment

Compared to 0% SEBS composites, addition of 5% SEBS showed better adhesion properties (Figure 5.16). This is quite evident from the presence of polymer on the fiber surface on the fracture surfaces. However with the addition of SEBS, there was a separate dispersion of elastomer on the matrix (Figure 5.17).

Figure 5.18 shows the dependence of impact strength with the MA-SEBS concentration. The impact strength was found to increase with addition of MA-SEBS (one way analysis of variance at $P<0.05$). Also there was a significant increase with further addition of MA-SEBS from 5% to 10% (one way analysis of variance followed by Tukey's multiple comparison tests at $P<0.05$). The encapsulation of MA-SEBS around the fiber reduces the stress concentrations at the fiber-polymer interphase, leading to a better impact performance (Oksman and Clemons, 1997).

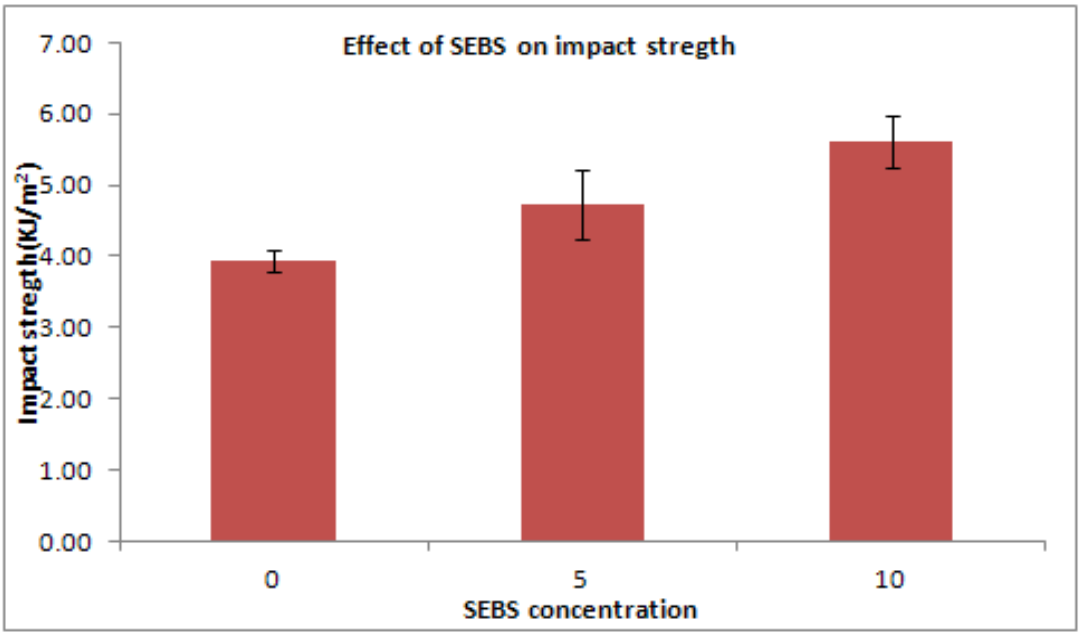

Figure 5.18. Effect of different MA-SEBS concentrations on the impact strength

5.4.2.2.2 Dynamic mechanical response

The storage modulus was found to decrease with the addition of MA-SEBS (5.19). This was expected because the low E-modulus of elastomers in the impact modifiers always decreases the stiffness of the composites. Figure 5.20 and Table 5.9 shows the temperature depends of damping (tan δ) and the glass transition temperature (T_g) for the Lyocell/PP composites with different SEBS concentration. The tan δ peak values were fairly consistent for all the treatments. However, the results clearly showed that T_g increased with use of coupling agent. These results are fairly consistent with the CR-FM results because the addition SEBS forms better adhesion properties with increase interphase width around the fillers. However the activation energies showed that β transition is not a strong indicator of filler–matrix interaction because the highest energy does not occur in composite with the highest matrix-filler interaction (Table 5.10).

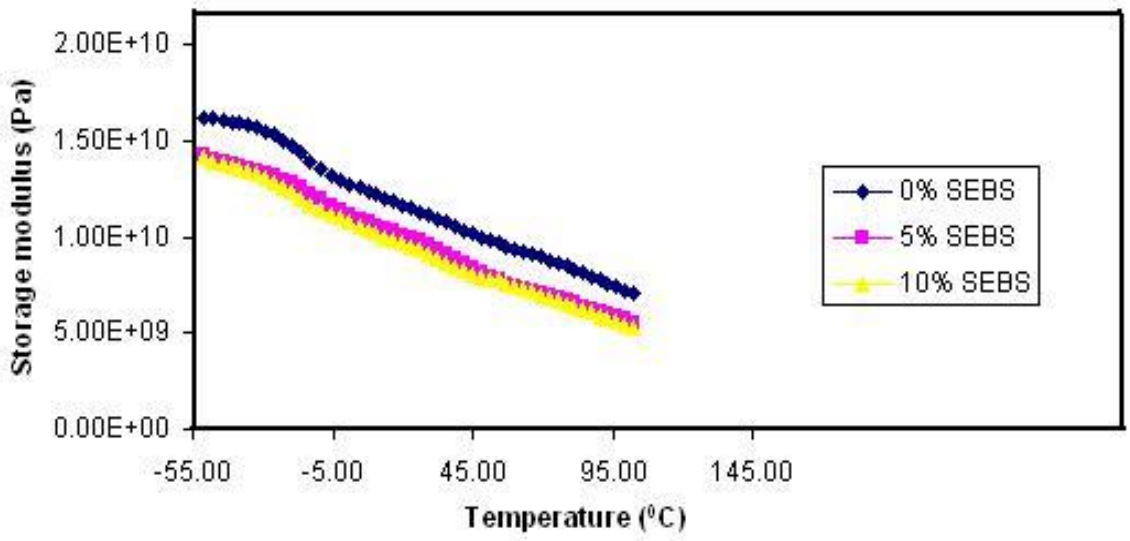

Figure 5.19. Dependence of storage modulus on different concentrations of MA-SEBS measured at 1 Hz

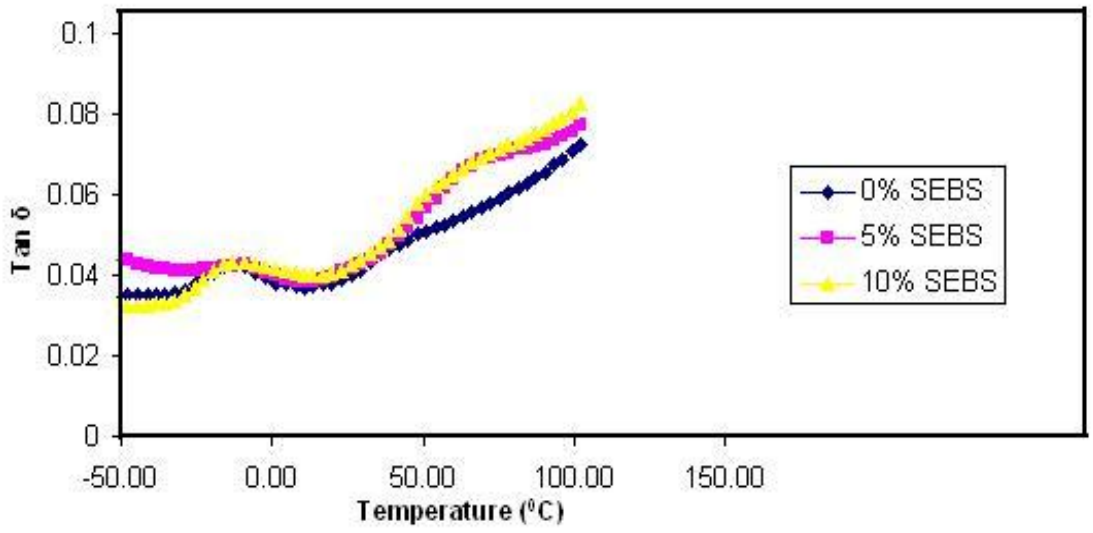

Figure 5.20. Temperature depends of damping (tan δ) and the glass transition temperature (T_g) for different MA-SEBS concentration

Table 5.8. Temperature depends of damping (tan δ) and the glass transition temperature (T_g) for different MA-SEBS concentration measured at 1 Hz

Composite type	**T_g(^{0}C)**	**Tan δ**
Lyocell/PP/0% SEBS	-14.3	0.043
Lyocell/PP/5% SEBS	-9.22	0.42
Lyocell/PP/10% SEBS	-8.28	0.43

5.5. Conclusions

Contact-resonance force microscopy proved to be a valuable technique for evaluating the interphase of NFRPCs. We were able to investigate the mechanical properties of interphases as narrow as 30.5 nm. Multivariate analysis using FTIR gave more satisfactory, interpretable results and was conclusive in showing that they can discriminate and classify differences between the functional groups of fiber, matrix and interphase. The nanoscale characterization of interphase and its effects on the bulk mechanical properties in this study shows that an increased interphase thickness is very essential for the improved tensile strength in lyocell/PP/MAPP composites. A very thin interfacial zone with an abrupt change in the modulus from pure fiber to pure matrix can easily debond the fiber from matrix under a little amount of stress and can have an adverse effect on the final mechanical properties of the composite. Care should be taken to avoid the overuse of MAPP in composites. An optimum amount of MAPP increase the interphase thickness to the maximum and further addition only decreased the interphase thickness and can adverse effect on the strength properties. The average impact strength was found to decrease with the increasing concentration of MAPP and our results showed that matrix properties were

also a determinant factor on the impact strength. For lyocell/PP/MA-SEBS composites, tensile strength was not a direct reflection of interfacial bonding. One of the reasons could be the matrix effect, due to the formation of separate morphology where elastomers exists as separate domains in the matrix. The impact strength was found to increase with addition of MA-SEBS. Interphase region showed gradient of modulus values that ranged between the modulus values of the fiber and the matrix for both lyocell/PP/MAPP and lyocell/PP/MA-SEBS composites. The interphase region showed a gradient in modulus that could be described to first order by a linear fit, with a gradual decrease in modulus from fiber to matrix. Also, it is quite evident that the interphase thickness accounts for the majority of property variations within the interphase for different treatments. This result defies the earlier perception of a flexible interphase with low modulus than the matrix formed by the elastomers in composites.

5.6. References

Borja Y, Rie G, Lederer K. Synthesis and characterizations of polypropylene reinforced with cellulose 1 and 11 Fibers. J Appl Polym Sci 2006;101:364-369.

Drzal LT, Rich MJ, Koenig MF, Lloyd PF. Adhesion of graphite fibers to epoxy matrices. 2. The effect of fiber finish. J Adhesion 1983;16(2):133-152.

Drzal LT. The interphase in epoxy composites. Adv Polym Sci 1986;75:1-32.

Duvall J, Sellitti C, Myers C, Hiltner A, Baer E. Interfacial effects produced by crystallization of polypropylene with polypropylene-g-maleic anhydride compatibilizers. J Appl Polym Sci 1994;52:207-216.

Felix JM, Gateholm P. Formation of entanglements at brushlike interfaces in cellulose- polymer

composite. J Appl Polym Sci 1993;50:699-708.

Griswold C, Cross WM, Kjerengtroen L, Kellar JJ. Interphase variation in silane-treated glass-fiber-reinforced epoxy composites. J Adhesion Sci Technol 2005;19(3-5):279-290.

Grozdanov A, Buzarovska A, Bogoeva-Gaceva G, Avella M, Errico ME, Gentile G. Nonisothermal crystallization kinetics of Kenaf fiber/polypropylene composites. Polymer Engineering and Science 2007;47:745–749.

Harper DP, Laborie MP, Wolcott MP. Molecular relaxations in wood-polypropylene composites. 32nd Annual Conference on Thermal Analysis and Applications, Williamsburg, VA, 2004.

Harper DP, Pierre M, Laborie G, Wolcott MP. The impact of polypropylene –graft- maleic anhydride on the crystallization and dynamic mechanical properties of isotactic polypropylene. J Appl Polym Sci 2009;111:753-58.

Hodzic A, Stachurski ZH, Kim JK. Nano-indentation of polymer-glass interfaces. Part I. Experimental and mechanical analysis. Polymer 2000;41:6895-6905.

Hurley DC, Shen K, Jennett NM, Turner JA. Atomic force microscopy methods to determine thin film elastic properties. J App Phy 2003;94:2347-2354.

Hurley DC, Kopycinska-Müller M, Kos AB. Mapping mechanical properties on the nanoscale with atomic force acoustic microscopy. JOM 2007;59**:** 23-29.

Hurley DC. Contact Resonance Force Microscopy Techniques for Nanomechanical Measurements. Applied Scanning Probe Methods Vol. XI, eds. Bhushan B, Fuchs H. Springer-Verlag, Berlin, 2009; 5: 97-138.

Hurley DC. Measuring mechanical properties on the nanoscale with contact resonance force microscopy methods: Scanning probe microscopy of functional materials. Nanoscale

imaging and spectroscopy, eds. Kalinin S, Gruverman A. Springer-Verlag, Berlin 2009 .

Joffe R, Andersons J, Wallstrom L. Strength and adhesion characteristics of elementary flax fibers with different surface treatments. Composites Part A; applied science and manufacturing 2003;34:603-612.

Karnani, R., Krishnan, M., Narayan, R. Biofiber-reinforced polypropylene composites. Polym. Eng. Sci 1997;37(2): 476–483.

Kazayawoko M, Balatinecz JJ, Woodhams RT. Diffuse reflectance fourier transform infrared spectra of wood fibers treated with maleated polypropylene. J Appl Polym Sci 1997;66:1163-1173.

Kim JK, Sham ML, Wu J. Nanoscale characterization of interphase in silane treated glass fibre composites. Compos Part A: Appl Sci Manfact 2001;32:607-618.

Kim JW, Harper DP, Taylor AM. Effect of wood species on the mechanical and thermal properties of wood plastic composites. J Appl Polym Sci 2009;112:1378-1385.

Kim J-K, and Mai Y-W. Engineered Interfaces in Fiber Reinforced Composites, Elsevier, Oxford, UK 1998:401 pp.

Klien N, Selivansky D, Marom G. The effects of a nucleating agent and of fibers on the crystallization of nylon 66 matrices. Polymer Composites 1995;16:189-197.

Kopycinska-Muller M, Geiss RH, Muller J, Hurley DC. Elastic property measurements of ultra thin films using atomic force acoustic microscopy. Nanotechnology 2005;16:703-709.

Lane R, Hayes SA, Jones FR. Modelling the efficiency of strain transfer across an interphase region in fibre reinforced composites. Composite Interfaces 1999;6(5);425-440.

Lee SH, Wang S, Takashi E, Kim NH. Visualization of interfacial zones in lyocell fiber-reinforced polypropylene composite by AFM contrast imaging based on phase and

thermal conductivity measurements. Holzforschung 2009;63:240-247.

Lu JZ, Wu Q, Negulescu II. Wood-fiber/high density-polyethylene composites: Coupling agent performance. J Appl Polym Sci 2005;96:93-102.

Munz M, Sturm H, Schulz E, Hinrichsen G. The scanning force microscope as a tool for the detection of local mechanical properties within the interphase of fiber reinforced polymers. Compos Part A1998;29:1251-1259.

Myers GE, Chahyadi IS, Coberly CA, Ermer DS. Wood flour polypropylene composites-Influence of maleated polypropylene and process and composition variables on mechanical properties. Journal of polymeric materials 1991;15:21-44.

Myers GE, Chahyadi IS, Gonzalez C, Coberly CA, Ermer DS. Wood flour and polypropylene or high density polyethylene composites-Influence of maleated polypropylene concentration and extrusion temperature on properties. Journal of polymeric materials 1991;15:171-186.

Nair SS, Wang S, Hurley DC. Nanoscale characterization of natural fiber and its composite using contact resonance force microscopy. Compos Part A 2010;41:624-631.

Nair SS, Hurley DC, Wang S, Young TM. Nanoscale characterization of interphase properties in maleated polypropylene-treated natural–fiber reinforced polymer composites. Polym. Eng. Sci (In revision).

Oliver WC, Pharr GM. An improved technique for determining hardness and elastic modulus using load and displacement sensing indentation experiments. J Mater Res 1997;7(6):1564-1583.

Rabe U, Amelio S, Kester E, Scherer V, Hirsekorn S, Arnold W. Quantitative determination of contact stiffness using atomic force acoustic microscopy. Ultrasonics 2000;38:430-43.

Sato N, Kurauchi T, Sato S, Kamigaito. SEM observation of the initiation and propagation cracks in a short fiber reinforced thermoplastic composite under stress. J. Mater. Sci Lett 1983;2:188-190.

Seo Y, Kim J, Kim KU, Kim YC. Study of the crystallization of polypropylene and maleic anhydride grafted polypropylene. Polymer 1999;41:2639-46.

Stamboulis A, Baillie C, Schulz E. Interfacial characterization of flax fibre-thermoplastic polymer composites by the pull out test. Die Angewandte Makromolekulare Chemie 1999;272:117-120.

Torres FG, Cubillas ML. Study of the interfacial properties of natural fibre reinforced polyethylene. Polymer Testing 2005;24:694-698.

Williams JG, Donnellan ME, James MR, Morris WL. Properties of the Interphase in organic matrix composites. Mater Sci Eng A 1990;126:305-312.

Wu J, Yu D, Chan C M, Kim J, Mai Y W. Effect of fiber pretreatment condition on the interfacial strength and mechanical properties of wood fiber/pp composites. J of Appl Poly Sci 1999;76:1000-1010.

CHAPTER 6. CONCLUSIONS AND RECOMMENDATIONS

6.1. Conclusions

This dissertation was focused on the nanoscale characterization of fiber/matrix interphase and its impact on the performance of natural fiber reinforced polymer composites.

The results of the first experiment in the research demonstrated that contact resonance force microscopy is a valuable technique for evaluating the interphase of natural fiber-reinforced polymer composites and for characterizing the elastic properties of cell wall layers of natural fibers. The nanoscale spatial resolution of CR-FM, combined with its ability to provide quantitative modulus images, makes it possible to investigate the mechanical properties of interphases as narrow as 50 nm in NFRPCs and thin cell wall layers in natural fibers. The use of extremely low loads and small tip radius characteristic of CR-FM enables *in-situ* elastic property information with significantly higher spatial resolution than other, destructive methods like nanoindentation. The use of a reference material with similar modulus values removes much of the uncertainty arising in the final modulus values from tip wear and tear, which is very common with other AFM methods. One of the major limitations of CR-FM technique used here is that the elastic properties of the reference samples were obtained using nanoindentation. The indentation modulus obtained by these methods can be different. One way to avoid this is to obtain the reference values using nanoindentation techniques using AFM tips having similar tip radius and using low forces similar to those used in CR-FM technique. However, experimental uncertainties such as depth of penetration, tip wear and tear, piezo creep, and hysteresis effects limit the utility of AFM based nanoindentation measurements. Also, proper care has to be taken to protect the test sample and reference sample from the formation of any oxides or adsorbed water on the surface. These can prevent the tip from pure elastic contact with sample.

The results of second experiment described property variation within the interphase region as well as the variation in interphase thickness with maleic anhydride grafted polypropylene (MAPP) concentration by quantitative imaging using CR-FM and qualitative images obtained by noncontact AFM phase imaging. The modulus distribution within the interphase region as well as the variation in interphase thickness with MAPP concentration was confirmed by these advanced AFM techniques. The average interphase thickness was found to increase with increasing MAPP concentration. The interphase region showed a gradient in modulus that could be described to first order by a linear fit, with a gradual decrease in modulus from fiber to matrix. The results of this study provide valuable information to improve the design of NFRPC products that use MAPP as coupling agent.

The final experiment evaluated the effect of various coupling agents such as MAPP and MA-SEBS on the NFRPCs and finally correlated the interfacial effects created by these coupling agents on the macroscale performance of the composites. The nanoscale characterization of interphase and its effects on the bulk mechanical properties in this study shows that an increased interphase thickness is very essential for the improved tensile strength in lyocell/PP/MAPP composites. An optimum amount of MAPP increase the interphase thickness to the maximum and further addition only decreased the interphase thickness and can adverse effect on the strength properties. The average impact strength was found to decrease with the increasing concentration of MAPP and our results showed that matrix properties were also a determinant factor on the impact strength. For lyocell/PP/MA-SEBS composites, tensile strength was not a direct reflection of interfacial bonding. One of the reasons could be the matrix effect, due to the formation of separate morphology where elastomers exists as separate domains in the matrix. The impact strength was found to increase with addition of MA-SEBS. Interphase region showed

gradient of modulus values that ranged between the modulus values of the fiber and the matrix for both lyocell/PP/MAPP and lyocell/PP/MA-SEBS composites. The study of the interphase region showed a gradient in modulus that could be described by a first order linear model, with a gradual decrease in modulus from fiber to matrix. Also, it is quite evident that the interphase thickness accounted for the majority of property variations within the interphase for different treatments. This result contradicts earlier perceptions of a flexible interphase with low modulus than the matrix formed by the elastomers in composites.

6.2. Recommendations for Future Work

One of the major limitations of CR-FM technique used here is that the elastic properties of the reference samples were obtained using nanoindentation. The indentation modulus obtained by these methods is different from that obtained using CR-FM mainly due to difference in tip and forces used to create indentation on the sample. In future, we have to come up with a technique to obtain the reference values using indentation techniques using tips having similar tip radius and using low forces similar to those used in CR-FM technique. This would avoid any disagreement in final quantitative modulus values obtained using CR-FM and would help in establishing more confidence in CR-FM methods. In all our experiments, we tried to treat the coupling agents with the matrix, so one of the interesting things to look in future is to see how these different concentrations of coupling agents affect the interphase when they are directly treated to the fiber and then mixed with the polymer matrix. Also, we had only limited access to the CR-FM. So we had to choose the samples with treatments which showed the extreme mechanical properties. If we have more time and more access to CR-FM, we could have done quantitative imaging on all samples. This research has shown for the first time to characterize

mechanical properties within narrow interphases with nanoscale spatial resolution. So this technique should be used for characterizing interphase for different types of fiber/matrix composites. This will enable researchers to get much more information about the nanoscale properties of interphase and fibers, and correlate these information to macroscale performance provides an interesting direction for future work, which is very important for optimum design of final composite products.

APPENDIXES

APPENDIX A. Accomplishments from This Work

A.1. Publications

Nair SS, Hurley DC, Wang S, Harper DP. Influence of fiber/matrix nano-interphase on the mechanical properties of natural fiber reinforced polymer composites (In preparation).

Nair SS, Hurley DC, Harper DP, Wang S. Characterization of interfacial chemistry of interphase in cellulose fiber reinforced polymer composites using CR-FM and FTIR imaging (In preparation).

Nair SS, Hurley DC, Wang S, Young TM. Nanoscale characterization of interphase properties in maleated polypropylene-treated natural-fiber reinforced polymer composites. Polym Eng Sci, (In revision).

Nair SS, Wang S, Hurley DC. Nanoscale characterization of natural fibers and their composites using contact-resonance force microscopy. Compos Part A: Appl Sci Manfact 2010; 41: 624-631.

Wang S**, Nair SS**, Hurley DC, Lee S-H. Characterizing interphase properties in fiber reinforced polymer composite with advanced AFM based tools. Advanced Materials Research 2010; 123-125: 403-406.

Nair SS, Wang S, Hurley DC. Evaluation of interphase properties in fiber reinforced polymer composite using contact resonance force microscopy. In: Proceedings of the 51st annual meeting of the society of wood science and technology (Concepción, Chile, 10–12 November 2008).

A.2. Awards and Recognitions

Jerry Saeman Award for Student Achievement in Wood Plastic Composites Research, for the poster presentation and talk "Importance of nanostructured interphases on the mechanical properties of cellulose fiber reinforced polypropylene composites" at the 11th International Wood and Biofiber Plastic Composites Conference, Madison, WI, USA- May 2011.

First-place Award in the poster competition at the Forest Products Society 64th International Convention, Madison, WI, USA- June 2010. Presentation titled "Influence of fiber/matrix nano-interphase on the mechanical properties of natural fiber reinforced polymer composites".

Second-place Award in the poster competition at the 51st Annual Convention of Society of Wood Science and Technology, Concepción, Chile – November 2008. Presentation titled "Evaluation of interphase properties in fiber reinforced polymer composite using contact resonance force microscopy".

Travel Award ($500) awarded by Society of Wood Science and Technology for attending the 51st Annual Convention at Concepción, Chile – November 2008.

A.3. Conference Presentations

Nair SS, Wang S, Hurley DC, and Harper DP. Effects of interphase properties on the mechanical behavior of natural fiber reinforced polypropylene composites. 11th International Conference on Wood & Biofiber Plastic Composites**,** Madison, WI, USA- May 2011 (Oral presentation).

Nair SS, Wang S, and Hurley DC. Importance of nanostructured interphases on the mechanical properties of cellulose fiber reinforced polypropylene composites. 11th International Conference on Wood & Biofiber Plastic Composites**,** Madison, WI, USA- May 2011 (Poster presentation).

Wang S, **Nair SS**, Hurley DC, and Lee SH. Advanced AFM-based techniques for characterizing composite interphases. TAPPI International Conference on Nanotechnology for the Forest Product Industry, Espoo, Finland - September 2010 (Oral presentation).

Wang S, **Nair SS**, Hurley DC, and Lee SH. Characterizing Interphase properties in fiber reinforced polymer composites with advanced AFM based tools. 3rd International Conference on Multi-Functional Materials and Structures. Jeoju, Korea – September 2010 (Oral presentation).

Nair SS, Wang S, and Hurley DC. Nanoscale characterization of interphase and their impact on the performance of natural fiber reinforced polymer composites. FPS 64th International Convention, Madison, WI, USA- June 2010 (Oral presentation).

Nair SS. Influence of fiber/matrix nano-interphase on the mechanical properties of natural fiber reinforced polymer composites. FPS 64th International Convention, Madison, WI, USA- June 2010 (Poster presentation).

Hurley DC, **Nair SS**, and Wang S. Nanomechanical mapping of composite interphases with contact resonance AFM. Nanotech Conference & Expo Houston, TX, USA - May 2009 (Oral presentation).

Nair SS, Wang S, and Hurley DC. Evaluation of interphase properties in fiber reinforced polymer composite using contact resonance force microscopy. Society of Wood Science and Technology 51st Annual Convention, Concepción, Chile – November 2008 (Poster

presentation).

Nair SS and Wang S. Characterizing wood cell wall using microthermal analysis and atomic force microscopy. FPS 61st International Convention, Knoxville, TN, USA- June 2007 (Oral presentation).

APPENDIX B. Qualitative Imaging of Natural Fiber Cell Walls Using Advanced AFM Based Techniques

B.1. Abstract

Advanced atomic force techniques such as noncontact mode phase imaging, and scanning thermal microscopy have been used to characterize different cell wall layers in natural fiber. Non contact phase images showed difference in phase shifts between the different layers showing the difference in mechanical properties among cell wall layers. This was further confirmed with the thermal conductivity image. It was clear that S_2 layer showed a clear difference from other layers, while the other layers did not show much variation among themselves. This is mainly due to the difference in mechanical properties of S_2 layer compared other layers. Also the thermal conductivity images showed a wide range of conductivities within S_2 layer. The S_2 layer showed lower conductivities towards the outer edges of the S_2 layer.

Keywords: **a**tomic force microscopy, phase image, thermal conductivity, modulus

B.2. Introduction

Characterization of different fiber layers is necessary to improve the utilization of natural fibers as reinforcements in composites. Each wood fiber consists of different layers. The primary cell walls of adjoining fibers, together with the middle lamellae in between, form the compound middle lamellae (CML). The secondary wall is divided into the S_1, S_2 and S_3 layers. The orientation of the cellulose microfibrils within each cell wall layer strongly influences the

mechanical properties of natural fibers in their longitudinal direction (Bergander and Salmen, 2002). The orientation of the cellulose microfibrils is nearly perpendicular (flat helix) to the fiber axis in the S_1 and S_3 layers, while it is almost parallel (steep helix) to the fiber axis in the S_2 layer (Brandstrom, 2001; Donaldson and Xu, 2005). Characterization of mechanical properties within different layers of cell wall is very important to improve the utilization of natural fibers as reinforcements in composites. Due to limitation of proper technique with nanoscale resolution, much of the studies have been confined to the S_2 layer which is the largest layer within cell wall (Nair et al., 2010).

With the advent of scanning probe microscopy techniques, particularly atomic force microscopy (AFM), it became possible to probe materials with nanoscale spatial resolution. In the present study, we used different advanced AFM techniques such as noncontact mode phase imaging (AFM-PI), and scanning thermal microscopy (SThM) to characterize different cell wall layers in natural fiber.

B.3. Experimental

B.3.1. Materials and sample preparation

The experiments involved samples collected from a 14-year-old loblolly pine. A latewood portion of the 14th annual ring was cut with dimensions of 2 mm X 5 mm X 5 mm in the radial, tangential and longitudinal directions, respectively. The samples were embedded in an epoxy medium under vacuum and cured by heating and drying for 8 h at 70^{0}C (Spur, 1969). A cross section of the sample was prepared by use of an ultramicrotome with a diamond knife. The microtome process yielded sufficiently smooth surfaces for the AFM-PI and SThM experiments.

B.3.2. AFM-PI

Phase images were obtained with True Noncontact AFM mode (XE-100, Park Systems, Suwon, Korea). Noncontact AFM (NC-AFM) is one of several AFM methods in which the cantilever is oscillated near the surface of a sample. In NC-AFM, the spacing between the tip and the sample is on the order of one to ten nanometers. NC-AFM monitors the phase shift data obtained from the images. Phase shift is defined as the phase lag between the sinusoidal excitation signal and the resulting cantilever oscillation signal. Changes in phase angle reveal differences in the surface properties of the material (Lee et al., 2009). The AFM cantilevers used in these experiments had nominal dimensions L = 225 µm and w = 40 µm, tip radius of curvature 10 nm or less, and k_c = 48 N/m. The resonant frequency of the cantilever was approximately 190 kHz.

B.3.3. SThM

Scanning Thermal Microscopy is operated with a nanofabricated thermoprobe with tip of radius of curvature 100 nm**.** SThM uses the CCM (conductivity contrast mode) for getting the thermal images. During scanning the thermal tip is at first equilibrium with the sample surface. When tip starts scanning, heat flows from tip to sample due to change in thermal conductibility of the sample. This causes the change in equilibrium. The feedback circuit senses the change in equilibrium and then increases or decreases the energy supplied to the tip in order to maintain a constant temperature.

B.4. Results and Discussion

Noncontact phase images were obtained for different fibers within the growth ring. Figure B.1 shows the phase images of cell walls. Contrasts in phase shifts between the different layers are clearly visible. It is quite clear that S_2 layer showed lower phase shifts when compared to other layers. Phase shifts are obtained due to changes in the tip-sample force caused by differing mechanical properties of the sample surface and are a particularly sensitive way to detect qualitative local stiffness variations in the surface (Lee et al., 2009). The higher modulus values of S_2 layer might have contributed to these lower phase shifts. The higher modulus values of the S_2 layer compared to other layers are consistent with previous results in the literature (Clair et al., 2003; Nair et al., 2010; Wimmer and Lucas, 1997).

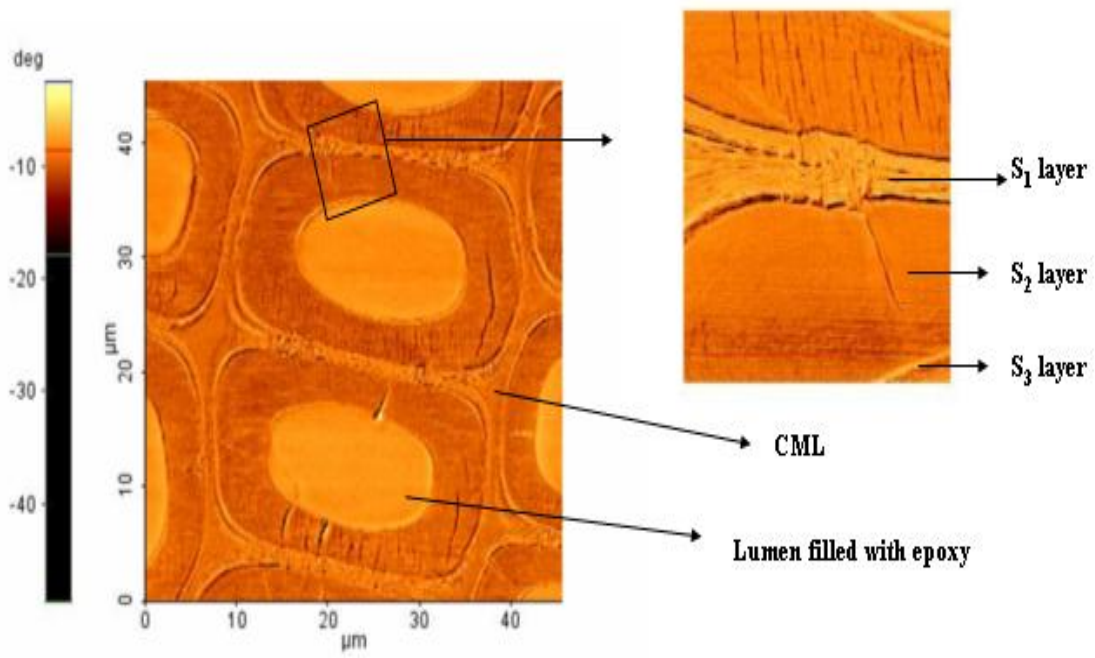

Figure B.1. Phase image of different cell wall layers

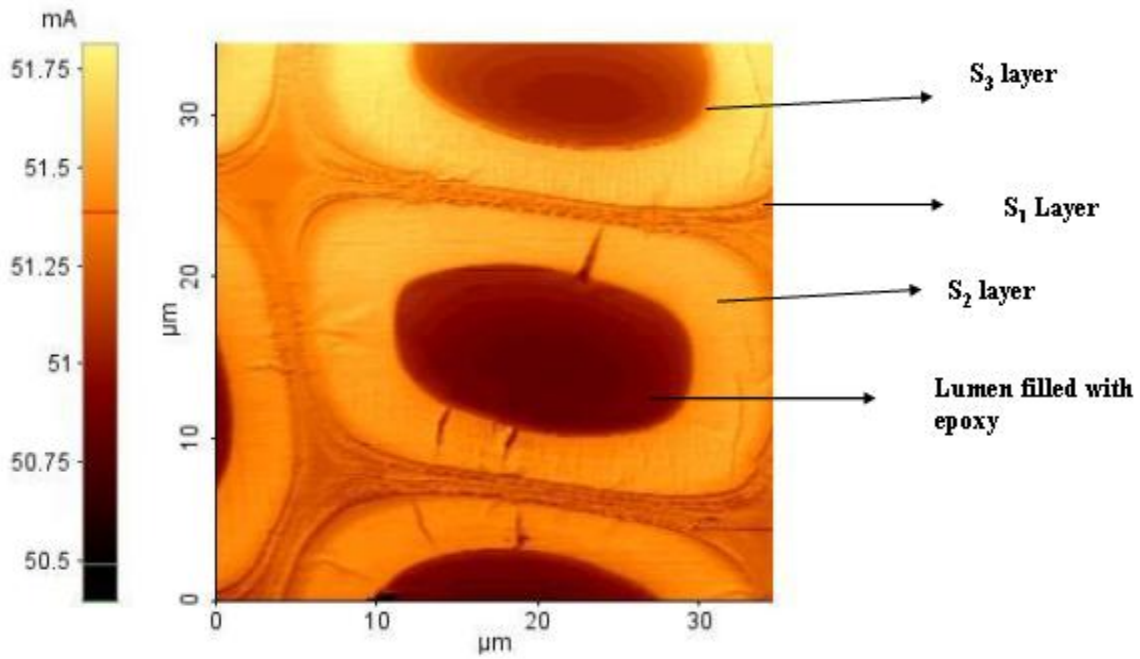

Figure B.2. Thermal conductivity image of cell wall layers

Table B.1 Average phase shift and thermal conductivity for different cell wall layers

Different cell wall layers	**Average phase shift (deg)**	**Average Thermal conductivity (mA)**
S1	-9.1	51.3
S2	-11.1	51.8
S3	-9.0	51.5
CML	-9.5	51.4

This was further confirmed with the thermal conductivity image obtained from SThM (Figure B.2). S_2 layer showed higher thermal conductivity compared to other layers. Lee et al. (2009) has shown with his experiments with SThM that higher modulus region show high thermal conductivity than the lesser modulus regions. Thus the higher modulus values of S_2 layer might have contributed to these higher thermal conductivities.

Average phase shifts and thermal conductivities for different layers were obtained using similar method used in Chapter 3, from the area enclosed within box plots for different layers. Table B.1 shows the average phase shifts and thermal conductivities. It is quite clear from the figures and table that S_2 layer showed a clear difference from other layers, while the other layers did not show much variation among themselves. This is mainly due to the high modulus of S_2 layer compared other layers (Nair et al., 2010). Also, the thermal conductivity images showed a wide range of conductivities within S_2 layer (Figure B.3). The corresponding line profile of the selected region in the S_2 layer shows that the conductivity decreases towards the outer edges of the S_2 layer.

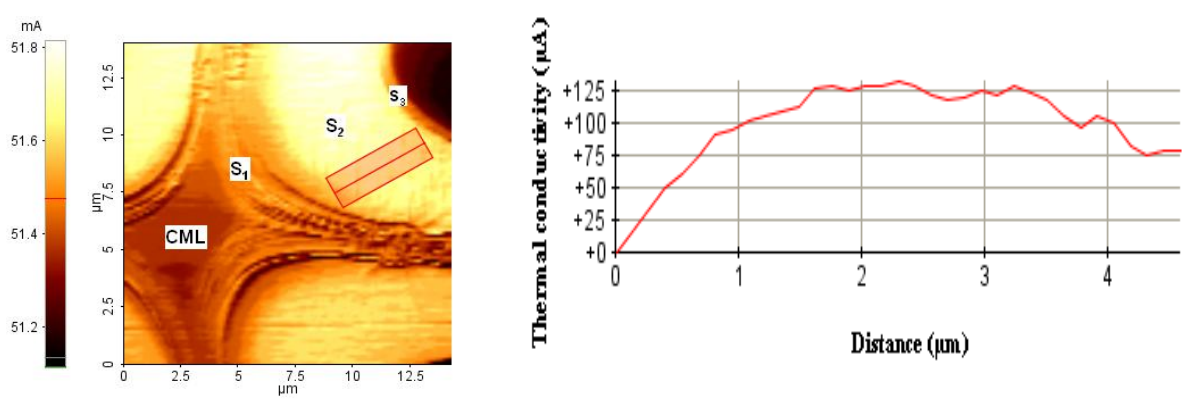

Figure B.3. Thermal conductivity image (left) and the line profile (right) of the selected region

Although the S_2 layer has a steeper helix and the S_1 layer has a flatter helix of microfibril orientation with respect to the fiber axis, various studies have shown that there is a shift of microfibril orientation from the outer S_1 layer to the inner S_2 layer and from the outer S_2 layer to the inner S_3 layer. Xing et al. (2008) examined the cell wall layers of refined fibers of loblolly pine by use of nanoindentation and showed that there exists a clear interphase between S_2 and S_1 and between S_2 and S_3. The wider range of indentation modulus values obtained in this study for each of the secondary layers can be explained partly by differences in the cellulose microfibril angle within each layer (Bergander and Salmen, 2002; Watanabe and Norimoto, 2000).

B.5. Conclusions

The results of our experiments prove that advanced AFM-based tools such as AFM-PI and SThM are valuable techniques for characterizing the cell wall layers of natural fibers. While AFM noncontact mode characterizes the cell wall layers based on the phase shifts between the components, SThM uses the thermal conductivity to characterize the layers.

B.6. References

Bergander A, Salmen L. Cell wall properties and their effects on the mechanical properties of fibers. Journal of Materials Science 2002;37:151-156.

Brandstrom J. Micro- and ultrastructural aspects of Norway spruce tracheids: A review. IAWA 2001;22(4):333-353.

Clair B, Arinero R, Lévesque G, Ramonda M, Thibaut. Imaging the mechanical properties of wood cell wall layers by atomic force modulation microscopy. IAWA 2003;24(3):223–30.

Donaldson L, Xu P. Microfibril orientation across the secondary cell wall of radiate pine tracheids. Trees 2005;19:644-653.

Lee SH, Wang S, Takashi E, Kim NH. Visualization of interfacial zones in lyocell fiber-reinforced polypropylene composite by AFM contrast imaging based on phase and thermal conductivity measurements. Holzforschung 2009;63:240-247.

Nair SS, Wang S, DC Hurley. Nanoscale characterization of natural fibers and their composites using contact-resonance force microscopy. Compos Part A: Appl Sci Manfact 2010; 41: 624-631.

Spur AR. A low-viscosity epoxy resin embedding medium for electron microscope. J Ultrastruct Res 1969;26:31-43.

Watanabe U, Norimoto M. Three dimensional analysis of elastic constants of the wood cell wall. Wood Research 2000;87:1-7.

Wimmer R, Lucas BN, Tsui TY, Oliver WC. Longitudinal hardness and Young's modulus of spruce tracheid secondary walls using nanoindentation. Wood Science and Technology 1997;31:131-141.

Xing C, Wang S, Pharr GM, Groom LH. Effect of thermo-mechanical refining pressure on the properties of wood fiber cell walls: measured by nanoindentation and atomic force microscopy. Holzforschung 2008;62(2): 230-236.

APPENDIX C. Score Maps for Different Treatments

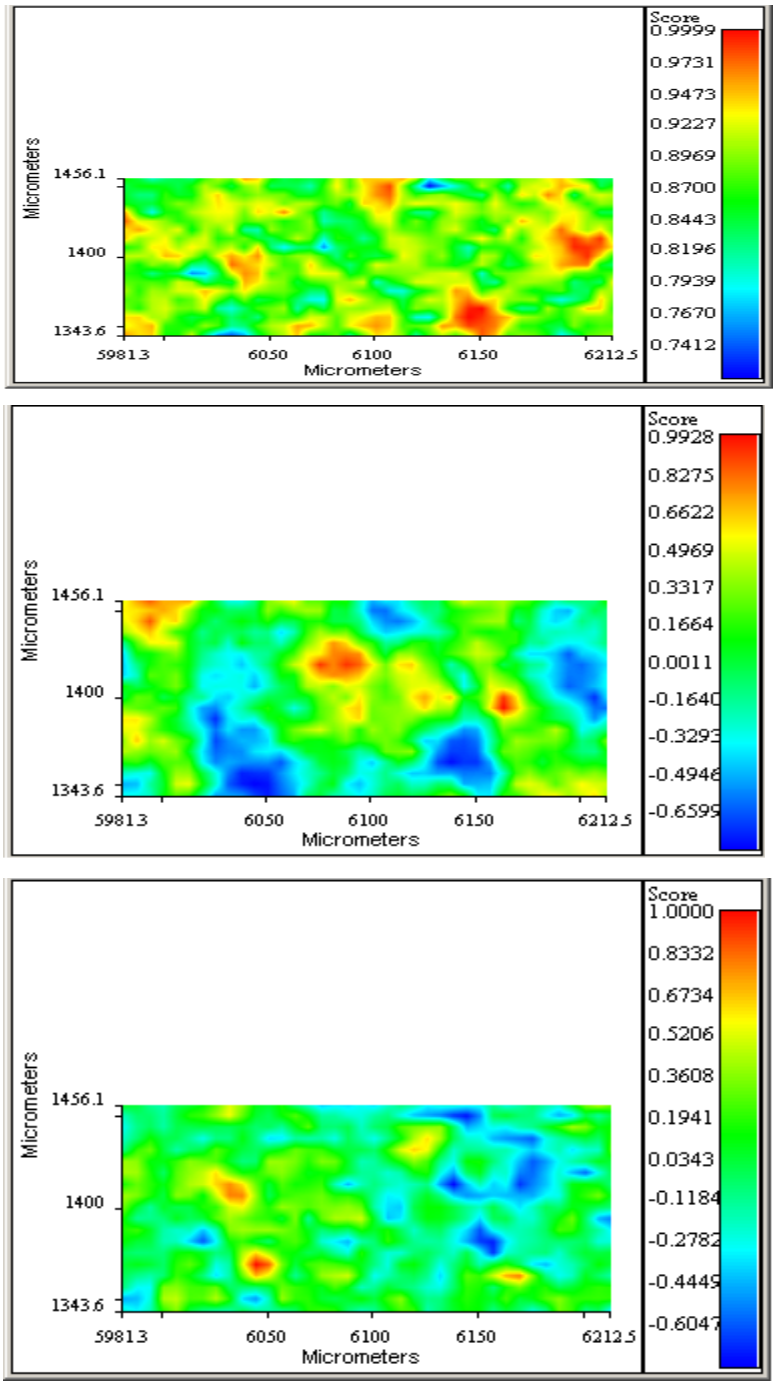

Figure C.1. Score maps for PC1 (top), PC2 (middle), PC3 (bottom) for 0% MAPP composites

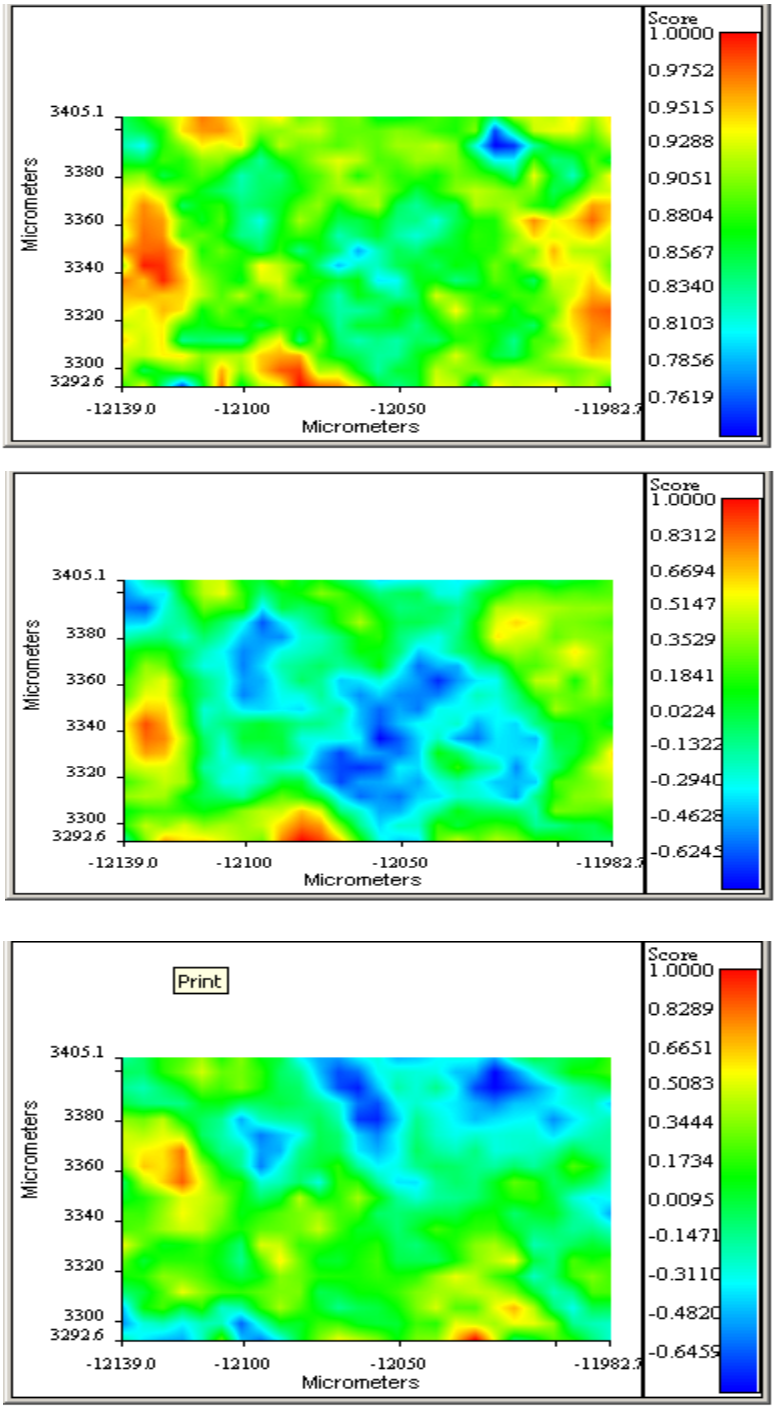

Figure C.2. Score maps for PC1 (top), PC2 (middle), PC3 (bottom) for 2.5% MAPP composites

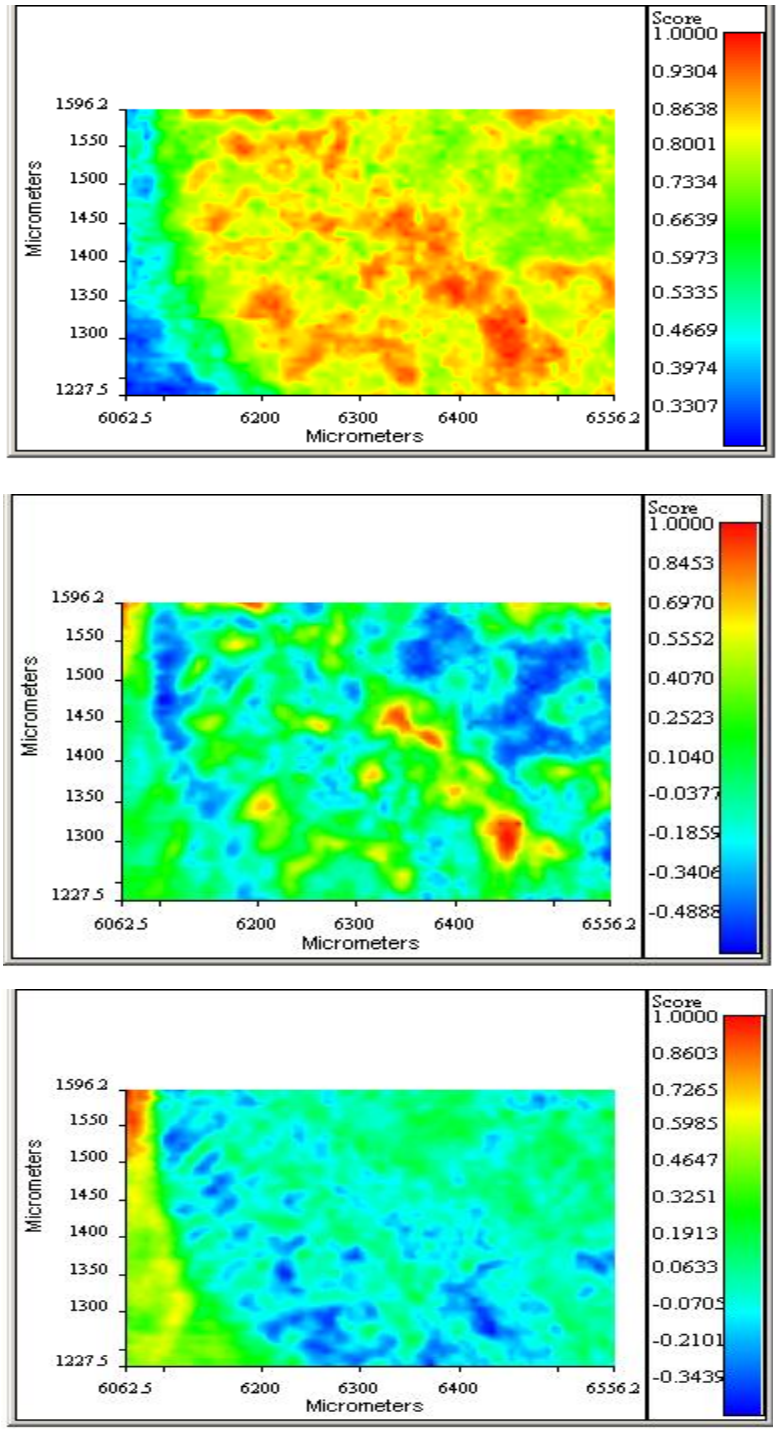

Figure C.3. Score maps for PC1 (top), PC2 (middle), PC3 (bottom) for 10% MAPP composites

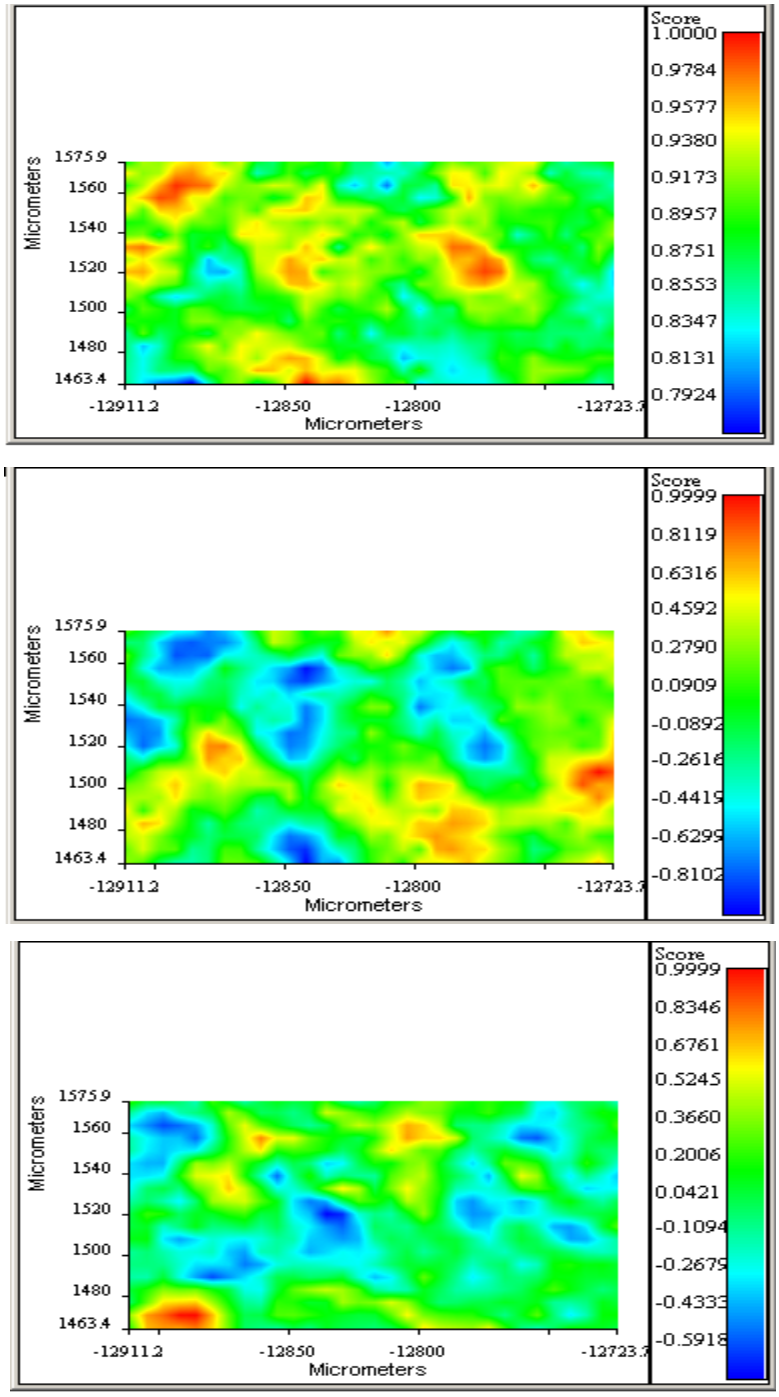

Figure C.4. Score maps for PC1 (top), PC2 (middle), PC3 (bottom) for 5% SEBS composites

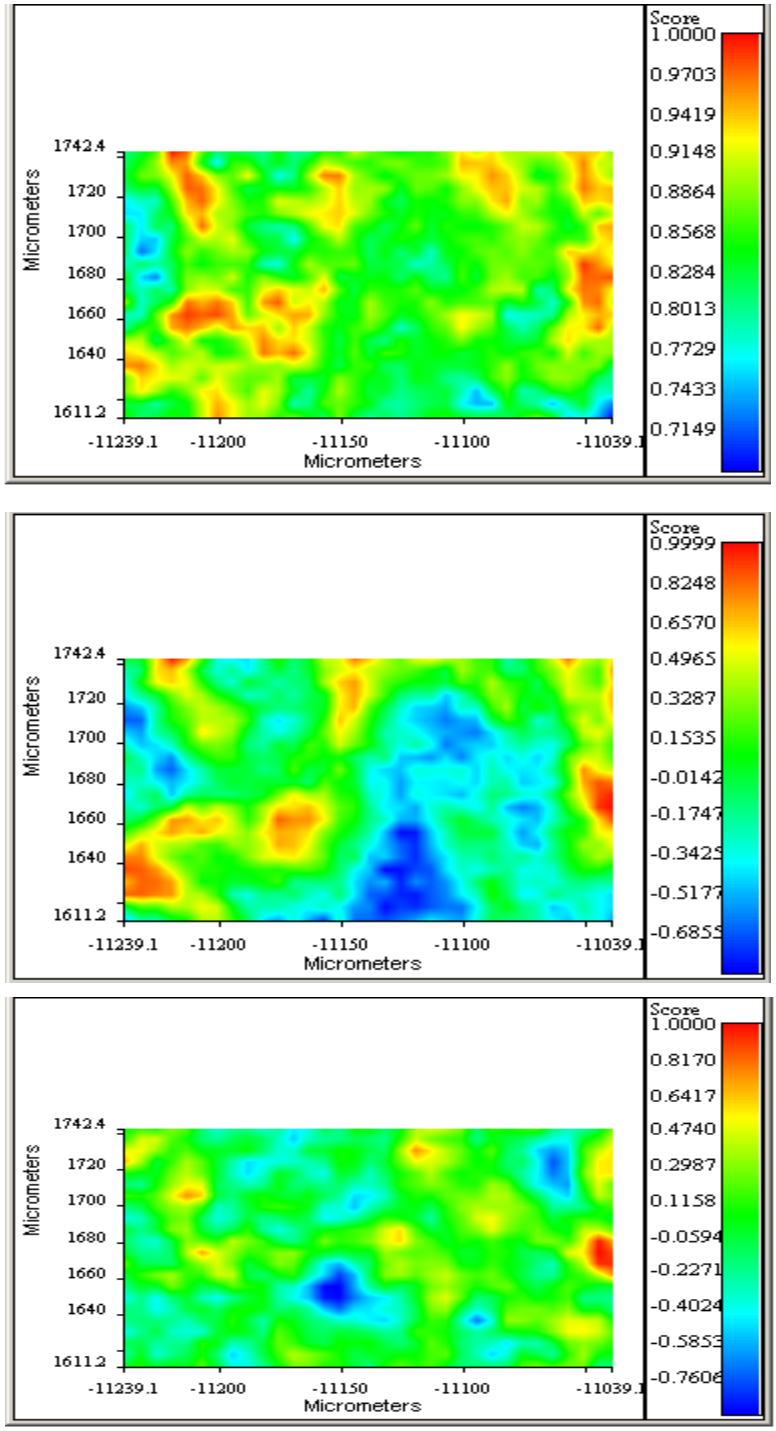

Figure C.5. Score maps for PC1 (top), PC2 (middle), PC3 (bottom) for 10% SEBS composites

VITA

Sandeep Sudhakaran Nair was born in Cochin, India on May 25, 1978. He was raised in Cochin where he underwent schooling. He completed a Bachelors Degree from College of Forestry (Kerala Agricultural University) in December 2002. After working for 2 years, he attended University of Idaho, Moscow where he obtained a Masters degree in Forest Products in August 2006. In the year 2006, he pursued a Doctor of Philosophy degree in Natural Resources in the Department of Forestry, Wildlife, and Fisheries at the University of Tennessee. He graduated with this degree in May 2012. He has accepted a position as a post-doctoral research fellow in the School of Chemistry and Biochemistry at the Georgia Institute of Technology, Atlanta.